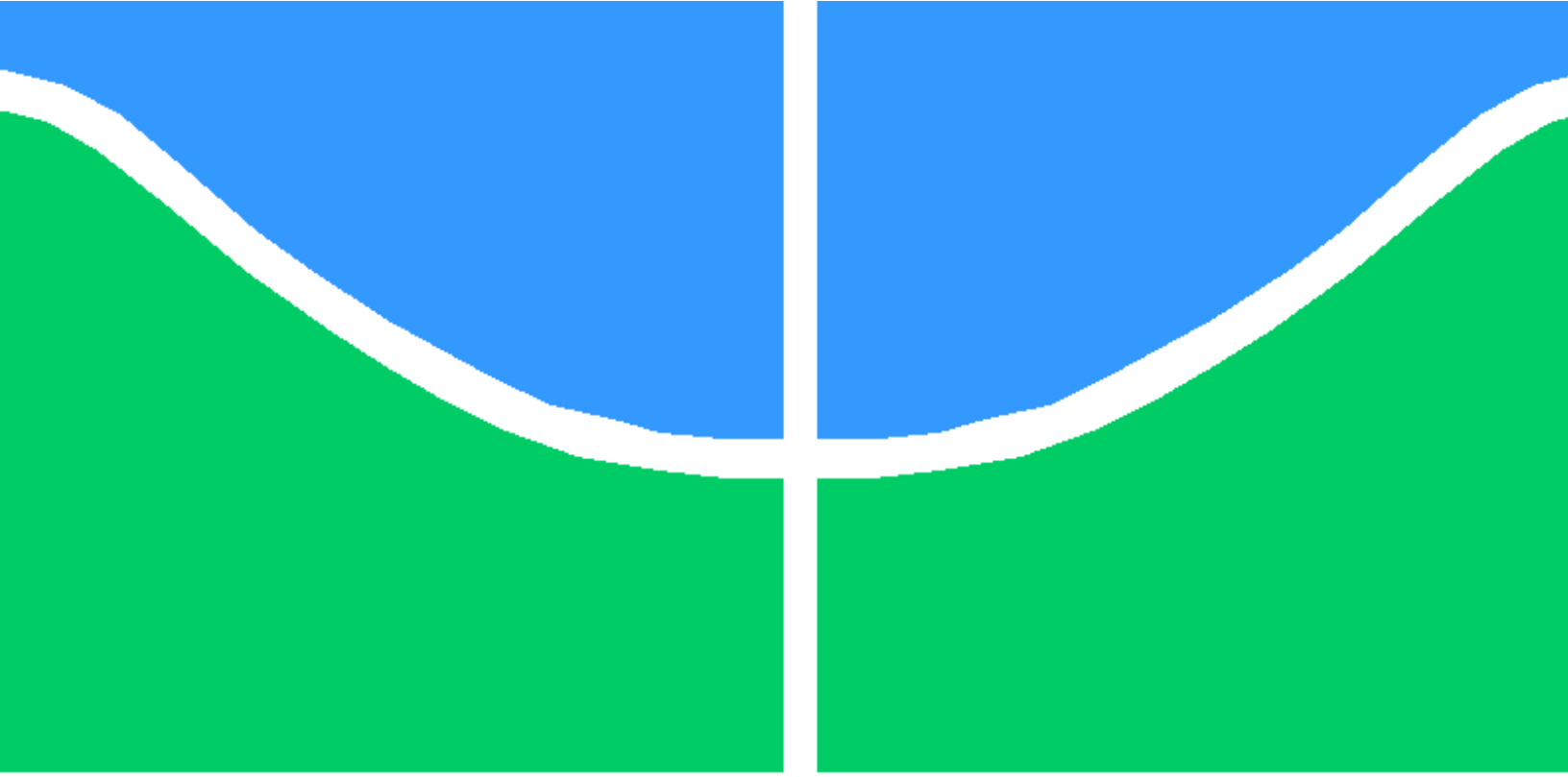

Doctoral Exam

EFFECTS OF THE VOLTAGE UNBALANCE ON POWER FACTORS CONSIDERING THE FAIRNESS PERSPECTIVE FOR BILLING PURPOSES

Victor do Prado Brasil

Brasília, December 2023

UNIVERSIDADE DE BRASÍLIA

FACULDADE DE TECNOLOGIA

UNIVERSIDADE DE BRASÍLIA
FACULDADE DE TECNOLOGIA
DEPARTAMENTO DE ENGENHARIA ELÉTRICA

Effects of the Voltage Unbalance on Power Factors Considering the Fairness Perspective for Billing Purposes

VICTOR DO PRADO BRASIL

SUPERVISOR: JOÃO YOSHIYUKI ISHIHARA
CO-SUPERVISOR: ANÉSIO DE LELES FERREIRA FILHO

DOCTORAL EXAM

PUBLICATION: PPGEE.TD 203/23
BRASÍLIA/DF: December- 2023.

UNIVERSIDADE DE BRASILIA
Faculdade de Tecnologia

Doctoral Exam

Effects of the Voltage Unbalance on Power Factors Considering the Fairness Perspective for Billing Purposes

Victor do Prado Brasil

Thesis presented to the Department of Electrical Engineering as a partial requirement to obtain the degree of Philosophy Doctor in Electrical Engineering

Jury

Prof. João Yoshiyuki Ishihara, UnB _____
Supervisor

Prof. Ivan Nunes Santos, UFU _____
External Examiner

Prof. Kleber Melo e Silva, UnB _____
Internal Examiner

Prof. Rodrigo Andrade Ramos, USP _____
External Examiner

FICHA CATALOGRÁFICA

BRASIL, VICTOR DO PRADO
Effects of the Voltage Unbalance on Power Factors
Considering the Fairness Perspective
for Billing Purposes. [Distrito Federal] 2023.
xiv, 134p., 210x297 mm (ENE/FT/UnB, Doutor, Electrical Engineering)
Tese (doutorado) - Universidade de Brasília.
Faculdade de Tecnologia.
Departamento de Engenharia Elétrica.

1. Power Factor	2. Billing Policies
3. Harmonic Distortion	4. Voltage Unbalance
I. ENE/FT/UnB	II. Título

BIBLIOGRAPHY

BRASIL, V. P. (2023). Effects of the Voltage Unbalance on Power Factors Considering the Fairness Perspective for Billing Purposes. Tese de Doutorado em Engenharia Elétrica, Publicação PPGEE.TD-203/23 Departamento de Engenharia Elétrica, Universidade de Brasília, Brasília, DF, 134p.

CESSÃO DE DIREITOS

AUTOR: Victor do Prado Brasil.

TÍTULO: Effects of the Voltage Unbalance on Power Factors Considering the Fairness Perspective for Billing Purposes.

GRAU: Doutor ANO: 2023

Victor do Prado Brasil
SQN 212 bloco J, asa norte, Brasília.
70.864-100 Brasília - DF - Brasil.

To the Creator of all things.

Acknowledgments

This thesis, though entitled to me, has come to exist by the efforts and dedication of many. This section therefore is an attempt to acknowledge most of those who contributed with this work.

As a thesis reveals the existence of its author, all the creation reveals the existence of its Creator. To God the Father, the Son and the Holy Spirit I am thankful for the life and meaning put into the creation. I thank Him for being the light in the valleys of darkness, the truth in the midst of confusion, and the solid way in which we can stand and walk.

I thank my dad, Joaquim, and my mom, Ana, for their encouragement and for always believing in my potential even before the beginning of my academic journey. I thank my brother, Marcelo, for keeping things light and being playful with me even in the most stressful moments. I am also grateful to my wife, Julyana, and her family for all their loving support throughout this PhD. It is worth emphasizing how much I am thankful for the patience and endurance offered by my beloved wife during all the everlasting hours of study. Thank you, my love, for collecting all my tears and for never giving up on me. I am very proud of you all and I hope you feel the same way about me.

I would like to express my gratitude for the faculty of electrical engineering from the University of Brasília (UnB). All the faculty, professors, technicians and the administrative staff have been very attentive and patient with me. My special thanks to Professor João Ishihara for accepting the challenge of being my supervisor and for patiently checking my progress and developments. Professor Anésio Leles, thank you for being my co-supervisor and for always encouraging me in my journey.

As one once said, "true friends are great riches" and I must acknowledge my dear friends and colleagues for enriching not only this work but also my life. In particular, I thank Alexandre Willik Neto for the precious lifelong friendship. I thank Lucio Sidney, Marcos Diego, Pedro Franco and Ronaldo Chacon for the daily life in the laboratory, the countless shared meals and all discussions, both technical and personal during most of my studies.

It is interesting to note that this thesis is nothing more than several words organized in a very specific way to convey ideas and information which are the results of a thoughtful experience aiming to contribute to a better understanding of PF definitions and their measurement methods. The only value of this thesis is due to the fact that there are readers who can read it and, hopefully, understand it. As we read, write and give feedbacks to each other, we improve our communication and can advance in our purposes and goals. To all of the brave readers, I am very thankful. I hope you all enjoy and find valuable insights in your reading.

Victor do Prado Brasil

ABSTRACT

Name: Victor do Prado Brasil
Title: Effects of the Voltage Unbalance on Power Factors Considering the Fairness Perspective for Billing Purposes
Name of Program: Graduate Program in Electrical Engineering
Date of Defense: Brasília, December 21st, 2023
Supervisor: João Yoshiyuki Ishihara
Co-supervisor: Anésio de Leles Ferreira Filho

Keywords: Power Factor, Billing Policies, Harmonic Distortion, Voltage Unbalance.

The expected growth of distributed photovoltaic generators and electric vehicles in the coming years brings challenges to power quality in distribution networks, such as potential increase of harmonic distortion and voltage unbalance. These phenomena have several undesired effects on the grid-connected equipment, especially induction motors. However, there is not yet a consensus regarding the correct power-related definitions, such as reactive power and power factor (PF), as well as their appropriate measurement methods when the voltage is unbalanced or nonsinusoidal. As a result, commercial meters can give different measurements for the same load and supply conditions, potentially leading to unfair PF charges.

This work evaluates existing PF definitions and their measurement methods, considering the fairness perspective for billing purposes under unbalanced nonsinusoidal voltage conditions. Here, the fairness notion is in the sense that the meter (built based on a particular definition and measurement method) under a nonideal supply should lead to very close values as if it was submitted to ideal balanced sinusoidal voltages. In other words, a fair PF definition should depend exclusively on the load's parameters, not supply quality. The fairness investigation considered computational simulations with the application of different voltage conditions at the point of connection of two constant impedance loads, a three-phase induction motor (TIM), and an unbalanced set of light-emitting diode (LED) lamps. In the sequel, the simulations' findings were experimentally examined employing a controlled voltage source, a three-phase induction motor, a mechanical load (DC generator and a variable resistor), a computer, and a speed sensor. Lastly, an analytical investigation was performed with a constant impedance load.

The simulations and experimental results show that a PF definition leading to a fair billing for a balanced constant impedance (the main load investigated in the literature) may not provide a fair billing for a TIM or a set of LED lamps when supplied with poor quality voltages. Additionally, this work has determined the fairest PF definitions and characterized the class of their corresponding measurement algorithms for metering the PF of a balanced constant impedance and a TIM submitted to a wide range of unbalanced nonsinusoidal voltages. For the LED lamps, none of the existing definitions were shown to be independent of the voltage supply. Notably, despite being recommended by IEEE Standard 1459-2010, the effective power factor was not an adequate definition for the investigated supply conditions applied to the TIM.

The results of the analytical investigation reveals that all the investigated definitions are actually non-linear

functions of the voltage unbalance factor (VUF) and the load's admittances. In other words, utilizing these five PF definitions in the presence of voltage and load unbalances may lead to unfair billing scenarios for both the utility or the customer. It is also proposed new admittance factors that can be employed for billing purposes because they do not depend on the voltage unbalance but solely on the load's characteristics.

RESUMO

Name: Victor do Prado Brasil
Título: Efeitos do Desequilíbrio de Tensão nos Fatores de Potência Considerando a Perspectiva de Justiça para Fins de Cobrança
Nome do Programa: Programa de Pós-Graduação em Engenharia Elétrica
Data da Defesa: Brasília, 21 de Dezembro de 2023
Orientador: João Yoshiyuki Ishihara
Co-Orientador: Anésio de Leles Ferreira Filho

Palavras-chave: Fator de Potência, Políticas de Cobrança, Distorção Harmônica, Desequilíbrio de Tensão.

O esperado crescimento de geradores fotovoltaicos distribuídos e veículos elétricos nos próximos anos traz desafios para a qualidade da energia em redes de distribuição, como o aumento potencial da distorção harmônica e desequilíbrio de tensão. Esses fenômenos têm vários efeitos indesejados nos equipamentos conectados à rede, especialmente motores de indução. No entanto, ainda não há um consenso sobre as definições corretas relacionadas à potência, como potência reativa e fator de potência (FP), bem como seus métodos de medição apropriados quando a tensão é desequilibrada ou não senoidal. Como resultado, medidores comerciais podem fornecer medidas diferentes para a mesma carga e condições de fornecimento, potencialmente levando a cobranças injustas de FP.

Este trabalho avalia definições de FP existentes e seus métodos de medição, considerando a perspectiva de justiça para fins de faturamento em condições de tensão não senoidal e desequilibrada. Aqui, a noção de justiça é no sentido de que o medidor (construído com base em uma definição e método de medição específicos) sob um fornecimento não ideal deve levar a valores muito próximos aos obtidos caso estivesse submetido a tensões senoidais equilibradas ideais. Em outras palavras, uma definição justa de FP deve depender exclusivamente dos parâmetros da carga, não da qualidade do fornecimento. A investigação de justiça considerou simulações computacionais com a aplicação de diferentes condições de tensão no ponto de conexão de duas cargas de impedância constante, um motor de indução trifásico (MIT) e um conjunto desequilibrado de lâmpadas de diodo emissor de luz (LED). Em seguida, os resultados das simulações foram examinados experimentalmente usando uma fonte de tensão controlada, um motor de indução trifásico, uma carga mecânica (gerador DC e um resistor configurável), um computador e um sensor de velocidade. Por fim, uma investigação analítica foi realizada com uma carga de impedância constante.

Os resultados das simulações e experimentos mostram que uma definição de FP que leva a uma cobrança justa para uma impedância constante equilibrada pode não proporcionar uma cobrança justa para um MIT ou um conjunto de lâmpadas LED quando alimentado com tensões de qualidade inferior. Além disso, este trabalho determinou as definições mais justas de FP e caracterizou a classe de seus algoritmos de medição correspondentes para medir o FP de uma impedância constante equilibrada e um MIT submetido a uma ampla gama de tensões desequilibradas não senoidais. Para as lâmpadas LED, nenhuma das definições existentes mostrou-se independente do fornecimento de tensão. Notavelmente, apesar de ser recomendado pelo IEEE Standard 1459-2010, o fator de potência efetivo não foi uma definição adequada para as condições de

fornecimento investigadas aplicadas ao MIT.

Os resultados da investigação analítica revelam que todas as definições investigadas são, na verdade, funções não lineares do fator de desequilíbrio de tensão (VUF) e das admitâncias da carga. Em outras palavras, utilizar essas cinco definições de FP na presença de desequilíbrios de tensão e carga pode levar a cenários de cobrança injusta tanto para a concessionária quanto para o cliente. Também são propostos novos fatores de admitância que podem ser utilizados para fins de faturamento, pois não dependem do desequilíbrio de tensão, mas apenas das características da carga.

Contents

List of Tables

List of Figures

List of Symbols

Latin Symbols

D_B	Budeanu's distortion power	[VA]
f	Electrical frequency	[Hz]
G	Conductance	[℧]
H	Set of nonfundamental components	
I	Single-Phase RMS current	[A]
I^+	Positive sequence RMS current	[A]
I^-	Negative sequence RMS current	[A]
I^0	Zero sequence RMS current	[A]
I^e	Effective current	[I]
I_1	Single-Phase fundamental RMS current	[A]
I_A	Fryze's RMS active current component	[A]
I_h	Single-Phase RMS current of order h	[A]
I_x	RMS current of phase $x \in [a, b, c]$	[A]
I_N	Fryze's RMS nonactive current component	[A]
$I_{1,x}$	Fundamental RMS current of phase $x \in [a, b, c]$	[A]
$I_{h,x}$	RMS current of order h and phase $x \in [a, b, c]$	[A]
$i(t)$	Single-Phase instantaneous current	[A]
$i_1(t)$	Single-Phase instantaneous fundamental current	[A]
$i_A(t)$	Fryze's instantaneous active current component	[A]
$i_h(t)$	Single-Phase instantaneous current of order h	[A]
$i_N(t)$	Fryze's instantaneous nonactive current component	[A]
$i_x(t)$	Instantaneous current of phase $x \in [a, b, c]$	[A]
$i_{1,x}(t)$	Instantaneous fundamental current of phase $x \in [a, b, c]$	[A]
$i_{h,x}(t)$	Instantaneous current of order h and phase $x \in [a, b, c]$	[A]
k	Multiplier that defines window of calculation	
n_m	Three-phase induction speed	

n_s	Three-phase induction synchronous speed	
P	Single-phase active power	[W]
P^+	Positive sequence active power	[W]
P_1	Single-phase fundamental active power	[W]
P_H	Single-phase nonfundamental active power	[W]
$P_{1,3\phi}$	Three-phase fundamental active power	[W]
$P_{3\phi}$	Three-phase active power	[W]
P_x	Active power of phase $x \in [a, b, c]$	[W]
P_1^+	Fundamental positive sequence active power	[W]
$P_{1,x}^+$	Fundamental positive sequence active power $x \in [a, b, c]$	[W]
$p(t)$	Single Phase instantaneous power	[W]
$p_1(t)$	Single Phase instantaneous fundamental power	[W]
$p_{1p}(t)$	Instantaneous fundamental active power	[W]
$p_{1q}(t)$	Instantaneous fundamental reactive power	[W]
$p_{3\phi}(t)$	Three-phase instantaneous power	[W]
$p_H(t)$	Single Phase instantaneous distortion power	[W]
$p_{ii}(t)$	Single Phase instantaneous distortion intrinsic power	[W]
$p_{1,x}(t)$	Instantaneous fundamental power of phase $x \in [a, b, c]$	[W]
$p_x(t)$	Instantaneous power of phase $x \in [a, b, c]$	[W]
PF_1	Fundamental power factor	
PF_1^{+a}	Fundamental positive sequence arithmetical power factor	
PF_1^{+g}	Fundamental positive sequence geometrical power factor	
PF_1^a	Arithmetic fundamental power factor	
PF_1^g	Geometric fundamental power factor	
PF_B	Budeanu's power factor	
PF_B^+	Positive Sequence Budeanu's power factor	
PF_B^a	Arithmetic Budeanu's power factor	
PF_B^g	Geometric Budeanu's power factor	
PF_N^+	Positive Sequence nonactive power factor	
PF_N^a	Arithmetic nonactive power factor	
PF_N^g	Geometric nonactive power factor	
PF_R	Fryze's power factor	
PF^e	Effective power factor	
Q_1	Single-phase fundamental reactive power	[VAr]
$Q_{1,3\phi}$	Three-phase fundamental reactive power	[VAr]
$Q_{1,x}$	Fundamental reactive power of phase $x \in [a, b, c]$	[VAr]
Q_1^+	Fundamental positive sequence reactive power	[VAr]
$Q_{1,x}^+$	Fundamental positive sequence reactive power of phase $x \in [a, b, c]$	[VAr]
Q_B	Budeanu's reactive power	[VAr]
Q_N	Fryze's reactive power (or nonactive power)	[VAr]
R_L	Transmission system equivalent resistance	[Ω]
R_r	Motor rotor resistance	[Ω]

R_s	Motor stator resistance	[Ω]
s_h	Three-phase induction motor slip at frequency of order h	
S_1	Single-phase fundamental apparent power	[VA]
$S_{1,x}$	Fundamental apparent power of phase $x \in [a, b, c]$	[VA]
S_1^+	Fundamental positive sequence apparent power of phase $x \in [a, b, c]$	[VA]
$S_{1,x}^+$	Fundamental apparent power of phase $x \in [a, b, c]$	[VA]
S_1^{+a}	Fundamental positive sequence arithmetic apparent power	[VA]
S_1^{+g}	Fundamental positive sequence geometric apparent power	[VA]
S_1^a	Arithmetic fundamental apparent power	[VA]
S_1^g	Geometric fundamental apparent power	[VA]
S_N	Buchholz' apparent power	[VA]
S^e	Effective apparent power	[VA]
T	Period of the sinusoidal fundamental voltage	[s]
t	Time variable	[s]
V	Single-Phase RMS voltage	[V]
V^+	Positive sequence RMS voltage	[V]
V^-	Negative sequence RMS voltage	[V]
V^0	Zero sequence RMS voltage	[V]
V^e	Effective voltage	[V]
V_1	Single-Phase fundamental RMS voltage	[V]
V_1^+	Fundamental positive sequence RMS voltage	[V]
V_h^+	Positive sequence RMS voltage of order h	[V]
V_h	Single-Phase RMS voltage of order h	[V]
V_x	RMS voltage of phase $x \in [a, b, c]$	[V]
$V_{1,x}$	Fundamental RMS voltage of phase $x \in [a, b, c]$	[V]
$V_{h,x}$	RMS voltage of order h and phase $x \in [a, b, c]$	[V]
$v(t)$	Single-Phase instantaneous voltage	[V]
$v_1(t)$	Single-Phase instantaneous fundamental voltage	[V]
$v_h(t)$	Single-Phase instantaneous voltage of order h	[V]
$v_{1,x}(t)$	Instantaneous fundamental voltage of phase $x \in [a, b, c]$	[V]
$v_{h,x}(t)$	Instantaneous voltage of order h and phase $x \in [a, b, c]$	[V]
$v_x(t)$	Instantaneous voltage of phase $x \in [a, b, c]$	[V]
$v_{xy}(t)$	Instantaneous phase-to-phase voltages, having $x, y \in [a, b, c]$	[rad]
X_m	Motor shunt reactance	[Ω]
X_r	Motor rotor reactance	[Ω]
X_s	Motor stator reactance	[Ω]
Z_{xy}	Impedance connected between phases x and y, having $x, y \in [a, b, c]$	[Ω]

Greek Symbols

α_h	Phase shift between $v_{h,a}(t)$ and $v_{1,a}(t)$	[rad]

ΔP	Transmission loss	[W]
$\gamma_{1,xy}$	Phase shift between $v_{1,x}(t)$ and $v_{1,y}(t)$, having $x, y \in [a, b, c]$	[rad]
$\gamma_{h,xy}$	Phase shift between $v_{h,x}(t)$ and $v_{h,y}(t)$, having $x, y \in [a, b, c]$	[rad]
ω	Angular electrical frequency	[rad/s]
τ	Moment that measurement started	[s]
θ_1	Phase shift between $i_1(t)$ and $v_1(t)$	[rad]
$\theta_{1,x}$	Phase shift between $i_{1,x}(t)$ and $v_{1,x}(t)$, having $x \in [a, b, c]$	[rad]
$\theta_{h,x}$	Phase shift between $i_{h,x}(t)$ and $v_{h,x}(t)$, having $x \in [a, b, c]$	[rad]

Subscripts

1	Fundamental frequency
h	Frequency of order h
$x \in [a, b, c]$	Component of phase “a”, “b” or “c”
B	Budeanu’s PT-related definition
N	Fryze’s PT-related definition

Superscript

$+$	Positive sequence
$-$	Negative sequence
0	Zero sequence
a	Arithmetic aggregation
g	Geometric aggregation
e	Effective aggregation

Abbreviations

LED	Light-emitting diode
MM	Measurement method
PF	Power factor
TIM	Three-phase induction motor
THD	Total harmonic distortion
UN	United Nations
UNVC	Unbalanced nonsinusoidal voltage conditions
VUF	Voltage unbalance factor

CHAPTER 1

Introduction

1.1 Background

The 7^{th} objective of the 2030 Agenda of the United Nations (UN), which is to ensure "access to affordable, reliable, sustainable, and modern energy for all", has been driving the development of renewable technologies, such as solar photovoltaic (PV) generation and electric vehicles (EVs). The analysis performed by [2] projected that distributed solar PV is likely to more than double in capacity in the period of 2020 - 2024, accounting for almost half of all solar PV growth. According to [3]: "The expansion of solar PV capacity in the next five years is expected to be almost double that of the previous five years."[1] The deployment of electric vehicles (EVs) is growing as well, being driven also by zero emission policies. According to [4], sales of EVs doubled in 2021 to a new record of 6.6 million. Nonetheless, integration of PV and EVs in distribution grids poses a challenge to power quality. The grid voltage unbalance, quantified by the voltage unbalance factor (VUF), can be increased due to irregular charging/generation periods and random geographically distribution of single-phase EVs [5] and PV systems [6]. Also, harmonic injections of the inverters (used in both EV charging stations and PV systems) contribute to the total harmonic distortion (THD) [5, 7, 8]. In the ongoing scenario, there is an expectation of a steep increase of distributed solar PV and EVs, which can further degrade the electric grid VUF and THD.

PV generators, EVs, as well as other new technologies are mostly based on the advancements of power electronics, particularly of switching-based devices. If for one hand, these non-linear devices have allowed the development of several new technologies, on the other hand, they increased the distortion in the currents and voltages. In this context, concerns regarding the quality of power were raised and have since being a field of much attention [1, 9–81]. The power quality can be divided in two major categories: the quality of the service

[1] Reference [3] is from 2021, so the next five years period mentioned refers to 2022 - 2026, whereas the previous five refers to 2017 - 2021.

and the quality of the product [82]. Studies regarding the quality of the service usually focus on how well utilities can manage the problems related to the supply of energy (for example preventing or shortening the duration of outages). Studies regarding the quality of the product usually focus on phenomena that affect the voltage delivered by utilities at the customer's point of common connection (PCC). Any phenomenon that contributes to the voltages and currents not being balanced and sinusoidal anymore is the subject of such studies. According to [61], "The development of efficient, high-power, semi-conductor switching devices and their application to the control of large electrical machines and industrial processes has imposed severe problems on the electrical utilities, particularly with respect to the measurement of energy flow and the optimum use of transmission networks. Not only is it necessary to know accurately the active power being delivered to the load under highly nonsinusoidal conditions, means must also be provided to determine and control the reactive current so that losses in the network can be minimized."

Reference [83] reported that approximately 32% of the distribution systems in the United States have VUF between 1% and 3%. According to [11], a survey conducted by CIGRE showed that the THD is greater than 3.5% in medium-voltage networks. It is worth mentioning that voltage unbalance can cause overheating, vibration, reduction in efficiency, and derating of three-phase induction motors (TIM) and transformers [83–87]. Harmonic distortion can also cause derating and torque pulsation of TIMs [87, 88]. According to [87], the combined effect of voltage unbalance and harmonic distortion can lead to unacceptable TIM vibrations even when the VUF and the THD are within acceptable levels.

The voltage unbalance and distortion not only impact the end-user's equipment connected to the grid [83–88] but they also negatively affect the transmission of power [31, 35, 44, 45, 55, 61, 65, 68, 89–93]. In balanced sinusoidal conditions the efficient usage of the transmission can be characterized solely by the reactive power caused by the phase-shift between voltage and current. If the current is in-phase with the voltage, the reactive power is zero and the load is utilizing the transmission system with the maximum efficiency. In unbalanced or nonsinusoidal conditions, however, there are other components which can reduce the transmission efficiency. Researchers have long been proposing new power theories as an attempt to explain what are these power components and how they affect the transmission of power [13, 14, 20, 31–33, 35, 44, 45]. Usually, there are four main aspects which are addressed by these studies, they are:

i) energy billing

ii) evaluation of power quality,

iii) detection of the sources of unbalance and distortion, and

iv) design of power quality enhancement equipment such as active filters or dynamic compensators.

Although several power-related definitions have been proposed in the literature, none of them has yet been proved to successful and jointly address these four topics [1, 9–81]. The present work focuses mainly on the power factor (PF) billing. It is worth mentioning that the four topics mentioned above are somehow connected to each other. For example, utilities apply PF billing policies based on the assumption that the customers' loads are the source/cause of the low measured PF [9, 11, 94], see also Section 1.2. In addition to discussing power-related definitions, it is important to discuss the applicable measurement methods (MMs), otherwise the definitions will remain in the theoretical world and will not be effectively applied in the real world.

Power-related definitions and MMs are applied to quantify and price the energy consumption and the usage of the electrical system world-wide [9, 11, 94]. Although some tariffs account for the grid utilization within the energy price, there are some situations where the usage of the system exceeds the energy consumption. In other words, two loads can consume the same amount of electrical energy but with different grid utilizations. In an extreme situation, a load may not consume any energy but still draw currents from the grid. In balanced sinusoidal systems, this phenomenon is explained by the transmission of reactive power caused by the phase shift between voltage and current. Since, in such conditions, it can be shown that the load is the solely responsible for this phase-shift, some utilities apply a reactive power (or PF) charge to control the system utilization [9, 11, 94]. Nonetheless, it is difficult to establish general rules for the reactive power because it depends on the customer's size (or equivalently on the amount of active power being drawn). The PF, on the other hand, has a well-defined range of $[0, 1]$, which does not depend on the customer's size. As a matter of fact, it should depend only on how efficiently the customer draws energy from the source. It can be noted that although the PF definitions and MMs discussed in IEEE Standard 1459 [1] give the same value in balanced sinusoidal conditions, they may provide different values in unbalanced nonsinusoidal conditions. It is noteworthy that most countries studied by [11] "have not yet established rules for reactive power billing under nonsinusoidal conditions and keep applying old regulation to systems where voltage and current are not sinusoidal anymore." This can potentially lead to a situation where commercial meters may give unexpected results under unbalanced or nonsinusoidal conditions.

Reference [39] reports an experience in which an industry's PF dropped from 0.95 to approximately 0.88 after the meter replacement. The new meter would have led to a 4% surcharge in the customer's bill had the technician not noticed this discrepancy. One thing that stands out is that these meters were approved for commercialization and usage. According to [19], the discrepancies shown in [39] were due to different PF definitions and MMs implemented in the commercial meters. As pointed out by [39], "Utilities must be able to install any meter in any electrical environment (sinusoidal or nonsinusoidal[2]) with full confidence that they will all give the same readings for the same load. Anything less is unacceptable". Recent studies [9] have shown that the same PF definition applied to the same load under the same VUF and THD can have different results since there are different voltage conditions which have the same VUF and THD. Such lack of reliability, regarding the measured PF, leads to an uncomfortable situation for both the utility and the customer where they may feel suspicious that the measured PF may be benefitting the other in detriment of them.

As field research, reference [41] investigated the arithmetic, geometric, effective, fundamental, and modified fundamental PF applied to an arc furnace of a real industry in Taiwan. The authors showed that the selection of different definitions could cause an impact up to 1% in the customer's bill. Although this percentage may seem small, it represents a huge impact for large customers with expensive monthly revenues. It is worth mentioning that the study of [41] is restricted to industries that use arc furnaces, and it does not consider different supply conditions and measurement methods.

Reference [11] compared the application of the fundamental reactive power (Q_1) and the non-active power (N) for billing purposes. They computed Q_1 and N employing several nonsinusoidal voltages and a current signal (measured from a residential load) by means of digital simulations. They have shown that in single-phase nonsinusoidal conditions some PF definitions are affected by voltage variations and their usage in billing policies

[2]We should also add balanced or unbalanced.

may lead to unfair charges of end-customers. However, the study was restricted to single-phase systems.

Among all PF definitions, the most important seems to be the effective PF (PF^e). In fact, it has been investigated by several researchers [1, 10, 12–14, 18, 23, 31–33, 35–38, 40, 43–45, 52, 54–57, 59, 91, 95–97] and it is recommended by IEEE Standard 1459-2010 [1] for unbalanced sinusoidal conditions. For nonsinusoidal conditions, references [13, 37, 44, 45] ratify PF^e as a measure of the energy transmission efficiency in the sense of [37]. Furthermore, reference [31] showed that the PF^e values of balanced constant impedance loads are not significantly affected by voltage unbalance.

In three-phase three-wire systems, reference [95] analytically showed that the effective PF (PF^e) of an unbalanced constant impedance load can be rewritten solely in terms of the load's admittances when the voltage is balanced and sinusoidal. This implies that in this case, the PF^e is a characteristic of the load and it does not depend on any voltage parameter. Also, this allows a clear attribution of responsibility to the customer to improve its PF. This result was then extended to four-wire systems by [14]. Nonetheless, the analytical results of both [14,95] are restricted to constant impedance loads under balanced sinusoidal voltages.

In three-phase three-wire systems having balanced nonsinusoidal voltages, reference [12] showed that the apparent power of an unbalanced constant impedance load can be decomposed into five power components associated with distinctive phenomena. Each power component is shown to be strictly related to a component of the Currents Physical Components (CPC) power theory. As a result, reference [12] was able to express the load's effective PF in terms of the distinct current components. However, the authors could not provide an expression for the effective PF solely in terms of the load's admittances as it was done in [14, 95].

Based on the foregoing discussion, it can be noticed that an evaluation of one significant load has not been done yet. According to [98]: "there are 85 million large electrical motors in the community market. These consume 65–70% of the energy used within industry." Additionally, voltage unbalance and harmonic distortion have harmful (individual and combined) effects on three-phase induction motors (TIMs) [83–87]. Considering the 7^{th} objective of the UN's 2030 Agenda, an increasing integration of nonlinear and geographically distributed grid elements, such as PV systems and EVs, is expected to take place. As a result, voltage unbalance and harmonic distortion can be further degraded [5–8], potentially leading to unfair PF billing of customers whose main load is the three-phase induction motor (TIM).

1.2 Prospect of PF Charging Policies

It is a common practice for utilities to adopt mechanisms to encourage customers to control their reactive energy consumption. One of these mechanisms is the PF charging, which consists of financially penalising customers with PF below the established limit. In order to provide a basic overview of the existing charging policies, this section presents the investigation results of grid codes taken from 6 utilities, 9 states, and 5 countries, considering the four different types of policies adopted worldwide, as presented in [11] and [99]. Table 1.1 show the results.

Table 1.1: PF legal and regulatory aspects in selected utility companies.

Policy	**Country**	**States**	**Utility**	**Minimum Demand or Average Consumption**	**Minimum Lagging**	**Minimum Leading**	**References**
Surcharge over the total bill	Canada	British Columbia	BC-Hydro	35 kW	0.9	Not regulated	[100]
Charge "maximum power demand"		Quebec	Hydro-Quebec	65 kW	0.9 (0.95 for large customers with 5 MW or more)	Not allowed	[101]
Charge reactive power	Australia	Victoria	All	150 kVA	[0.75; 0.95] depending on demand and voltage level	[0.8; 0.98] depending on demand and voltage level	[102]
		Queensland	Ergon Energy's	4 GWh per year	0.8	Allowed only in specific cases	[103, 104]
		Western Australia	Synergy	1285 kWh per day	0.8	Not allowed	[105, 106]
Charge reactive energy	England	Southern Electric	Southern Electric Power Distribution	100 kW	0.95		[107–109]
	Scotland	Merseyside, North Wales, South Scotland	Scottish Power				[109–111]
Charge reactive energy or power	Brasil	All	All	112.5 kVA	0.92		[112–114]

The four types of charging policies are detailed next.

1. BC-Hydro applies a surcharge percentage proportional to the PF deviation from the minimum accepted value [100]. Table 1.2, taken from [100], shows the PF range with the respective surcharge applied to the customer's bill. For instance, if the load PF is lagging and lower than 0.9 but greater than or equal to 0.88, then a 2% surcharge is applied to the customer's bill. If the load PF is lagging and lower than 0.88 but greater than or equal to 0.85, then the surcharge increases to 4% of the customer's bill, and so on.

2. Hydro-Quebec charges the maximum power demand, defined as the greatest value between the maximum real power (that is the active power) and 90% of the maximum apparent power [101].

3. The third policy, employed in the Australian standards investigated, is the charging of exceeding reactive power. The Brazilian regulation allows the usage of this policy.

4. The fourth policy, employed in the Scottish and English standards investigated, is the charging of exceeding reactive energy. This policy is also allowed in the Brazilian regulation.

Table 1.2: BC-Hydro power factor surcharge policy.

Lagging Power Factor	Power Factor Surcharge (%)
90% or more	nil
Less than 90% but 88% or more	2%
Less than 88% but 85% or more	4%
Less than 85% but 80% or more	9%
Less than 80% but 75% or more	16%
Less than 75% but 70% or more	24%
Less than 70% but 65% or more	34%
Less than 65% but 60% or more	44%
Less than 60% but 55% or more	57%
Less than 55% but 50% or more	72%
Less than 50%	80%

From Table 1.1, it can be noticed that there is a PF limit/threshold below which charges are applicable, regardless of the policy adopted. In the case of BC-Hydro [100] and Brazilian utility companies [113], the PF should also be used to compute the financial charge that will be applied.

In all investigated standards, residential customers are not chargeable [100–114]. This can also be inferred from Table 1.1 based on the minimum demand[3] above which PF evaluation is applied. The minimum demand threshold (among the investigated standards) found in this investigation was 35 kW, which is not compatible with residential and small customers. Such demand level is typical of medium and large units (in general, industries) supplied by three-phase voltages. Therefore, a three-phase PF definition compatible with the characteristics of TIMs (industries main load [98]) might be more adequate for billing. Nonetheless, it was not found an explicit statement in the investigated documents about which of the existing PF definitions should be used.

Considering the foregoing discussion, it can be concluded that the PF is used as a trigger in all four policies and, in some of them, it is also used in the computation of the financial charge. This initial analysis highlights that only medium and large customers are subjected to PF billing, in the investigated standards. For this reason, the usage of TIMs for evaluating different PFs may be more adequate than the constant impedance load model usually adopted in PF studies. Additionally, it is pointed out the lack of an explicit standardization of which definition should be used for revenue purposes in the investigated standards.

[3]Some standards adopt the average consumption over given periods instead of the instantaneous demand.

1.3 Objectives and Contributions

Based on the foregoing discussion, it can be observed that evaluation of PF definitions and measurement methods for the three-phase induction motor when the voltages are unbalanced and nonsinusoidal had not yet been done to the best of our knowledge. Additionally, evaluation of PF definitions when both the load and the source are unbalanced were also missing. So, the objective of this study is to evaluate the existing PF definitions and their measurement methods considering the fairness perspective for billing purposes under unbalanced nonsinusoidal voltage conditions (UNVC).

When both sources and loads are balanced and provide/consume power only at the fundamental frequency, the load PF has a unique value that depends entirely on the load's characteristics, that is, based on its capacitance or inductance [9,14,95]. In real circumstances, however, the voltages and the load are not perfectly balanced and sinusoidal/linear [11, 83].

Considering that utilities often apply PF billing policies, it is reasonable that the customers should be charged only for what they are accountable for. Since the load's admittances are a property of the load, it is expected that the customer should be responsible for improving the load's admittances if its susceptances are too high. The voltage quality, on the other hand, cannot be solely attributed to the customer as there are other factors that contribute to worsening the voltages (for example, the transmission lines are not perfectly transposed, single-phase loads are not uniformly distributed between phases throughout the grid, uneven aging of the grid equipment, etc). Additionally, the load is designed mainly to operate under balanced sinusoidal nominal voltages. For these reasons, the measured value for each PF definition under balanced sinusoidal nominal voltages (at the point of connection of the load) is adopted as the reference value for that definition. Each PF definition may have its own reference value, which may differ from others. It is expected that, if the load remains constant, a fair PF definition should retain its reference value even when the voltages are not balanced and sinusoidal anymore. With this viewpoint, the fairest PF definition to be applied in billing purposes is the one that changes only when the load changes.

The discussion of the relation between the PF of a balanced load and an unbalanced load is related to whether the PF should measure the load unbalance. But we need to emphasize that this analyzes could be extended to what the PF should actually measure and whether it should consider other power quality phenomena. These aspects are beyond the scope of this work, which is focused on the effects of the voltages on the PF definitions with the viewpoint of accountability and PF billing.

More specifically, this work aims to

i) Evaluate the value of PF definitions for different loads submitted to several UNVC by means of computational simulation.

ii) Evaluate the value of PF definitions for different loads submitted to several UNVC by means of experimental tests.

iii) Obtain analytical expressions for PF definitions as a function of the VUF and the load's admittances for a constant impedance load.

iv) Evaluate the metering of the fairest PF definitions with different measurement algorithms for different

loads submitted to several UNVC by means of computational simulation.

In [9], we have evaluated some PF definitions concerning voltage unbalance and distortion for a balanced constant impedance load and a three-phase induction motor (TIM) employing digital simulations and experimental tests. The effect of the measurement algorithm on the final value of the fairest PF definitions has also been assessed by means of digital simulations. The obtained results have been published by IEEE Access in [9], which has the following contributions:

i) The paper shows that a PF definition that leads to a fair billing for a constant impedance load may not provide a fair billing for a TIM in unbalanced and nonsinusoidal voltage conditions (UNVC). In other words, it shows that the selected load affects the performance of the PF definition.

ii) The paper determines the fairest power factor (PF) definitions and their corresponding measurement algorithms for metering the PF of any of the two loads, a balanced constant impedance and a TIM, submitted to a wide range of UNVC.

1.4 Document Outline

This work is organized as follows. Chapter 2 presents some power-related definitions and measurement methods. It is divided in three sections. The first one, Section 2.1, provides a brief historical overview of the development of power theories. The second one, Section 2.2, gives some definitions for single and three-phase systems. The third one, Section 2.3, lists some measurement methods. Chapter 3 presents the methodology employed in the simulations and the experimental tests. Section 3.1 details how the computational simulations of PF definitions from the fairness perspective were performed. Section 3.2 shows how the measurement algorithms were simulated. Section 3.3 explains how the experimental tests of PF definitions from the fairness perspective were conducted. Chapter 4 presents the results from the computational simulation of PF definitions and measurement methods. Section 4.1 shows the results of different PF definitions from the fairness perspective. In Section 4.2, measurement techniques for the fairest definitions are evaluated under several unbalanced and nonsinusoidal voltage conditions. The results of the experimental tests of different PF definitions are shown in Chapter 5. Chapter 6 obtains, for a constant impedance load, analytical expressions for each PF definition as a function of the load's admittances and the VUF. At last, Chapter 7 summarizes the main findings of this work.

CHAPTER 2

Power-Related Definitions and Measurement Methods

2.1 Brief Historical Overview of the Development of Power Theories

This section provides a concise historical overview of the development of power theories (PTs). It contextualizes our research within the wider domain of PTs while highlighting the inherent complexities associated with understanding and working with power phenomena. Our objective is to offer a broad perspective, rather than an exhaustive examination of individual theories or an in-depth discussion of their physical foundations. For those seeking more detailed insights, comprehensive references such as [37, 115, 116] are recommended.

As the reader will notice, some papers address PTs considering only single-phase systems, some consider only three-phase systems, and a few others consider more than one type of system. Although it is possible to present an state of the art for each of these types, such approach may prejudice the notion of time in the historical development of PTs. So, it seems that considering a unique timeline is the most appropriate way to present the state-of-the-art as it follows next.

The origins of PTs can be traced back to the classic work of Steinmetz [81] first published in 1892 in German and recently translated to English by [117]. Steinmetz noticed that the apparent power of a single-phase arc bulb was higher than the active power and that there was no phase-shift between the currents and voltages. This experiment raised a fundamental question for the field of PTs: what phenomena in the load are responsible for the apparent power being higher than the active power?

Shortly after, the increase of three-phase systems drew the attention of researchers to the phenomenon of unbalance in the voltages and currents. In 1908, reference [79] discussed the issue of defining PF for unbalanced sinusoidal systems considering that each phase may have a different phase-shift between its current and voltage. Aiming to combine all-phase shifts in a single-number, reference [79] proposed a three-phase PF definition as

an average of each phase PF weighted by its apparent power, that is

$$PF^a = \frac{PF_a S_a + PF_b S_b + PF_c S_c}{S_a + S_b + S_c}. \tag{2.1}$$

The proposed PF was later named as the arithmetic PF, since it can be rewritten as the total active power divided by the arithmetic apparent power (given by the sum of the absolute values of each phase apparent power),

$$PF^a = \frac{P}{S_a + S_b + S_c}. \tag{2.2}$$

Reference [79] claims that the arithmetic PF combines the phase-shifts of the different phases in a single number which has practical importance. He also developed a measurement method for the proposed definition which could be realized with the wattmeters and VAR meters available at that time. This might be one of the reasons why such a simple definition remained in the context of PTs, being cited even in the recent version of IEEE Std 1459-2010 [1].

In 1920, a special joint committee, composed by the American Institute of Electrical Engineers (AIEE) and the Technical Section of the National Electric Light Association (NELA), discussed the correct PF definition for poly-phase systems [72]. Fueled by various sets of papers [71, 73–78], the committee thoroughly discussed two main existing definitions, the arithmetic and the vector (or geometric) PF definitions. As the problem proved to be very intricate, the committee concluded that "no agreement has yet been reached upon a definition of the term as applied to polyphase circuits, nor even upon the underlying purpose which a definition should serve to express" [72].

It is worth mentioning that one of the papers [77] submitted to the committee had been written by Fortescue, in which he proposed the positive and negative-sequence PFs. Later on, the decomposition of active, reactive and apparent powers in the sequence-domain was incorporated in other PTs.

Two years later, in 1922, Buchholz [70] proposed a new apparent power definition based on the concepts of collective voltage and current for unbalanced three-phase systems with three-wires. The main objective was that the apparent power should reflect the total losses in the transmission system. For this purpose, the unbalanced load is compared with a balanced load causing the same transmission losses and drawing balanced currents equal to the collective current and the voltages supplied being equal to the collective voltage. From this moment on, several author's adopted Buchholz apparent power and tried to decompose it in terms of different power components related to different phenomena [56, 61, 63, 91].

According to Emanuel [37], at about the same time, the proliferation of mercury rectifiers to transportation and electrochemical processes drew back the attention of researchers to the issue of nonsinusoidal conditions. In this context, Budeanu proposed a new PT in 1927 [118]. The reactive power was redefined to account for the harmonics and also a distortion power was proposed to represent the effects of nonsinusoidal voltages and currents in the transmission of power. Budeanu's PT was adopted by several engineers and researchers who tried to design and provide effective measurement methods for the usage in meters [119–121]. Only after approximately 60 years the flaws of this theory became severe questioned [21, 57, 65, 68]. For more details regarding Budeanu's PT, see Appendix II.2

In 1932, considering single-phase nonsinusoidal systems, Fryze [69] proposed a novel viewpoint in the development of PTs. Instead of decomposing the apparent power in the frequency domain, Fryze proposed

that the decomposition of power components should start from the analysis of instantaneous quantities. In this context, he decomposed the instantaneous current into two orthogonal (in the sense of function space) components, the active and the non-active currents. Fryze showed that the RMS values of these components multiplied by the voltage RMS value leads to the active (P) and non-active (Q_F) power, respectively. Following this novel viewpoint, other PTs were developed using the instantaneous current as the starting point [20, 51, 56, 60, 115].

In 1935, at the request of the A.I.E.E Institute's Committee on Instruments and Measurements, Curtis and Silsbee [90] collected the most common definitions at that time considering the following situations:

- single-phase circuits when the currents and potential differences are sinusoidal,
- single-phase circuits with nonsinusoidal currents and potential differences,
- balanced polyphase circuit under sinusoidal conditions,
- balanced polyphase circuit under nonsinusoidal conditions,
- unbalanced polyphase circuit under sinusoidal conditions,
- unbalanced polyphase circuit under nonsinusoidal conditions,
- circuits in which the effective values of the currents and potential differences vary with time.

The objective was to systematically discuss the existing definitions in a way that general acceptance could be obtained. According to Curtis and Silsbee [90], "To discuss generalizations to more general situations (periodic but nonsinusoidal polyphase currents and voltages) one should reflect on the questions of which properties of the concepts of active power, apparent power, and power factor are fundamental and which properties are rather **coincidental**, and which features are due to the sinusoidal single-phase situation and should not be expected to be true in more general cases. A second point of thought is the question of whether several fundamental features can be generalized to more general situations by a single concept." With this viewpoint, the authors discuss the properties of each power definition for each situation and compare them with the properties observed in single-phase circuit with sinusoidal currents and voltages. Under non-sinusoidal conditions, the authors evaluate Fryze's non-active power and Budeanu's reactive and distortion powers. Considering the unbalance, the authors evaluate the following aggregating definitions for the apparent power: i) the limiting, ii) the arithmetic, iii) the vector (or geometric), and iv) the algebraic (or Lyon-Lienard) apparent power. Under more general conditions, the authors evaluate the possible combinations of non-sinusoidal definitions (Budeanu's and Fryze) with the aggregating methods for unbalanced powers (*e.g.* arithmetic, geometric, etc). The work of [90] was then used as basis for the formulation of standards.

According to [115], in 1950 Buchholz [122] extended to polyphase systems the collective voltages and currents proposed previously in [70] for three wire systems. Later on, contributions on Buchholz apparent power when harmonics are present led to the effective apparent power as defined in [1].

Shortly after, in 1962, Depenbrock building upon the concepts of Fryze and Buchholz proposed, in his PhD thesis [123], novel instantaneous current components which would be associated with distinct physical

phenomena in unbalanced nonsinusoidal three-phase systems. However, few papers addressed this theory until its publication in 1993 in [51], named as the Fryze-Buchholz-Depenbrock (FBD) method.

In 1972, considering single-phase systems, Shepherd and Zakikhani [68] concluded that Budenau's reactive power (Q_B) does not represent any real physical quantity, and that circuit compensation of Q_B does not lead to maximum power factor operation. Then, the authors of [68] proposed a novel resolution (based on the frequency domain) to the apparent power employing new definitions for active (S_R), reactive (S_X), and distortion (S_D) powers in nonsinusoidal systems. According to the authors, the proposed reactive power allows assessing how much of the apparent power can be compensated with passive elements. Shortly after the publication, Shepherd and Zakikhani PT was strongly criticized by three following discussion papers [64,66,67] mainly because of the lack of physical interpretations and the difficulties of implementation in meters. Further details of the proposed decomposition can be found in Appendix II.3.

In 1973, reference [65] discussed reactive power definitions and PF improvement based on single-phase generic current and voltage nonsinusoidal signals. He defined the PF as the ratio between the actual active power consumed by the load and the maximum average active power that could be obtained with the same economic effort, i.e., with the same values of RMS voltage and current. He showed that compensation of Budenau's reactive power (Q_B) does not always lead to the minimization of the apparent power. Reference [65] also examined the "true reactive apparent power" (S_X) as defined by [68] and proposed an alternative reactive power (S_Q) to address the impacts of harmonics that may appear in the voltage signal. The author also proposed a "complimentary reactive power" (S_C). He showed that shunt compensation leads to the minimization of S_Q while not affecting the active power P and S_C; leading therefore to a better power factor. At last, the author commented that defining reactive power is not indispensable for power factor improvement, since the value of the capacitor (C) for shunt compensation can be obtained through the minimization of the apparent power with respect to C. It is worth mentioning that the paper is restricted to single-phase (or balanced) systems.

In 1980, building upon the new viewpoint introduced by Fryze in [69] and considering nonsinusoidal single-phase systems, Kusters and Moore [61] proposed the decomposition of the instantaneous current into four components, having the source voltage waveform as a reference. The inductive/capacitive reactive current (I_{QL}/I_{QC}) components are equivalent currents that would flow through an inductor/capacitor submitted to the reference voltage. The residual inductive/capacitive reactive current (I_{QLr}/I_{QCr}) are the components that remain of the current after the active current and I_{QL}/I_{QC} components have been extracted. The multiplication of these components by the voltage RMS value leads to the inductive reactive power (Q_L), the capacitive reactive power (Q_C), the residual inductive reactive power (Q_{Lr}), and the residual capacitive reactive power (Q_{Cr}). Kusters and Moore also employed Q_L and Q_C to design an LC compensator. The method proposed by Kusters and Moore was also investigated by [62], which showed that in some nonsinusoidal voltage situations, the best compensation of the reactive current may require the simultaneous use of shunt capacitors and shunt inductors. Later on, the method for designing the LC compensator was incorporated in [54].

In 1984, following fryze's approach to the decomposition of the current into instantaneous components, Akagi, Kanazawa and Nabae [60] proposed the p-q theory for single-phase nonsinusoidal systems. Although Fryze introduced the concept of instantaneous current components, the p-q theory goes farther by proposing instantaneous power components, such as the instantaneous active power and instantaneous reactive power.

The authors employed the method to provide reference signals so that active power filters (APFs) can compensate the instantaneous reactive power without energy storage components. This theory inaugurated the so-called instantaneous PTs.

It is worth recalling that so far there are three different approaches to defining power components. In the first one, currents, voltages and powers are described in the frequency domain. This is the approach adopted in [65, 68, 70–79, 118]. In the second approach, adopted by [61, 69, 123], instantaneous current components are obtained and employed to describe powers in the frequency domain. In the third, inaugurated by the p-q theory [60], instantaneous current components are employed to derive instantaneous power components.

In 1985, considering single-phase nonsinusoidal conditions, Czarnecki [59] discussed the power definitions proposed in [61, 62, 68]. Then, he proposes the scattering power (D_S) and the Czanercki's reactive power (Q_Z) to decompose the apparent power and shows their relation to the components provided by Fryze [69] and Shepherd [68]. In the proposed decomposition, D_S is caused by the different values of each harmonic conductance in relation to the equivalent conductance, which accounts for the total active power. The scattering power does not contribute to the total active power and cannot be compensated by passive devices. Czarnecki's reactive power on the other hand, refers to the apparent power component caused only by the phase shift between voltage and current at each harmonic order. It was shown that Q_Z can be compensated by passive devices.

After approximately 60 years of Budeanu's PT, in 1987 Czarnecki [57] severely questioned Budeanu's PT and proposed that it should be abandoned. After thoroughly examining Budeanu's concepts of reactive power (Q_B) and distortion power (D_B), he concluded that D_B may actually have nothing to do with waveform distortion in absolute terms (meaning that the waveform is not sinusoidal) or even in relative terms (current distortion with respect to the voltage). It is also shown that there is no clear interpretation for Q_B, particularly due to the fact that in Budeanu's definition the harmonic reactive components are added and may result in zero reactive power even when the current is not in-phase with the voltage. This was one of the most severe critics Budeanu's PT have received.

In 1988, Czarnecki [56] extended the proposed definitions of [59] to three-phase unbalanced nonlinear loads. In this case, the load current can be decomposed into active, reactive, scattered, unbalanced and harmonic generated current components. It is shown that these components are orthogonal to each other and when multiplied by the voltage RMS value results in the active, reactive, scattered, unbalanced and harmonic generated powers. It should be noticed that the authors consider only a symmetrical source with nonsinusoidal voltages supplying unbalanced and non-linear or periodically variant loads. They do not consider unbalanced voltage sources neither source impedances greater that zero. As a result the harmonics generated by the load are present only at the current signal.

In 1990, Emanuel [91] provided a review of power definitions and their physical interpretation in single-phase nonsinusoidal situations. In the review, Emanuel corroborates that Budeanu's model lacks physical meaning, particularly due to the algebraic sum of harmonic reactive power components.

Also in 1990, Czarnecki [55] analyzed and discussed the active, reactive and scattering powers in single-phase nonsinusoidal situations. According to Czarnecki, the sign of the active power at each harmonic order indicates the direction of the flow of active power at that given frequency, thus allowing to identify who is

acting as source and as load. Both works [91] and [55] considered only single-phase nonsinusoidal conditions.

In 1991, Czarnecki [54] addressed the relative nature of the CPC in single-phase nonsinusoidal conditions. It is shown that the reference point for the voltage measurement affects the value of the reactive and scattered currents. Then, it is shown that this relative nature can actually be employed to design series and shunt passive compensators.

In 1992, Willems [53] proposed a novel interpretation of the p-q theory. For this purpose, Willems derived the instantaneous active and reactive powers using only phase currents and voltages without Clarke's transformation. According to Willems, the novel equations allow to extend the concepts to systems with more than three phases. Additionally, Willems also accounted for zero-sequence components.

In 1993, Depenbrock [51] published the Fryze-Buchholz-Depenbrock PT formulated earlier in 1962 as his PhD thesis [123].

Also in 1993, Emanuel [52] proposed that Buchholz apparent power can be decomposed as a function of the positive-sequence active, positive-sequence reactive and unbalanced powers. The unbalanced power is proposed as being the power associated with either negative or zero-sequence voltages or currents. Using the symmetrical-sequence components, Emanuel also proposes the usage of the positive-sequence PF.

In 1994, reference [93] addressed the problem of power definitions for PF correction under single-phase nonsinusoidal conditions, especially considering the effects of non-negligible Thévenin grid equivalent impedance, which had not yet been considered. Existing power definitions at that time did not consider the effects of the equivalent source impedance. As a result, the PF compensation derived from such power definitions could lead to harmonic resonance and to the increase of the current RMS value, instead of its reduction. It is worth highlighting that the current increase due to harmonic resonance can be hazardous to the system components. With this viewpoint, the paper proposes some power components to account for the effects of such impedance. The paper concludes that evaluation of the grid equivalent harmonic impedance is required before implementing PF correction.

In 1995, Czarnecki [95] addressed the power properties of three-phase circuits with three wires supplying unbalanced loads. Czarnecki shows that the unbalanced power does not occur due to power oscillations and then explains why this power occurs. To support his argument he shows the presence of unbalanced power in DC circuits, where certainly there is no oscillations of power. At last, Czarnecki analytically shows that the PF can be rewritten as a function of the load's admittances. Thus, the PF is not affected by the source supplier but only by the load's characteristics when the the source voltages are balanced and the load is unbalanced. Additionally, Czarnecki did not consider the effects of non-neglible Thévenin grid impedance.

In 1996, Sharon [49] examined the apparent power and PF definitions and proposed new power transfer quality factors for single-phase nonsinusoidal situations. According to Sharon, interpreting the PF as a measure of the degree of utilization of the source power capacity is misleading in nonsinusoidal situations especially when using conventional capacitive PF compensation. The argument is that capacitive PF compensation may increase the current RMS value instead of reducing it due to harmonic resonance. To address that, the paper suggests a quality factor calculated as an weighted average of the fundamental PF, the voltage harmonic distortion (VHD), and the current harmonic distortion (IHD). The use of this quality factor is illustrated in relation to PF compensation in nonsinusoidal situations for two source/load configurations. The first is

a balanced nonsinusoidal voltage source supplying a balanced (linear) constant impedance load (inductive). The second is a balanced sinusoidal voltage source feeding a six-pulse converter which provides dc voltage to a constant load (resistor). The paper shows that resonance can occur when shunt compensation is employed without any filters. One advantage of the proposed quality factor is that the separate measurable components allow the identification of the specific cause for a low-quality power, and thus one can increase the quality factor by addressing its lower component. For instance, if the voltage distortion is the lower component in the quality factor, one may employ dedicated techniques to deal with voltage distortion, instead of trying to raise the PF with capacitor compensation. It is worth mentioning that the proposed method identifies which component is contributing to the low quality factor, but without assigning the responsible for that. For instance, the proposed methodology does not identify when a harmonic producing load causes high voltage distortion, reducing the quality factor, at another location of the grid. Also, the paper is limited to balanced systems.

In 1998, Emmanuel [45] examines Buchholz apparent power in unbalanced nonsinusoidal conditions. To the best of our knowledge, this is the first paper that refers to Buchholz apparent power as the effective apparent power (S^e). Emanuel shows that the losses in the transmission of power are a function of the effective apparent power. It is also provided a decomposition of S^e in terms of the fundamental positive-sequence apparent power, the unbalanced fundamental apparent power, and the non-60Hz equivalent apparent power. According to Emmanuel [45], the unbalanced fundamental apparent power is "The recommended quantity to be measured, that helps to find load unbalance".

In 1999, Emanuel [44] evaluates apparent power definitions in unbalanced nonsinusoidal conditions. Comparing the arithmetic, geometric (or vectorial), and effective apparent power, Emanuel concludes that the effective apparent power is the definition the most closely related to the transmission losses. For this reason, Emanuel advocates that the effective apparent power should be employed for the "estimation of the utilization of distribution lines and equipment supplying systems that are unbalanced and sinusoidal, balanced and nonsinusoidal and, unbalanced and nonsinusoidal." It is worth mentioning that Emanuel does not discuss if the utility has any responsibility over the effective apparent power.

In 2005, reference [32] discussed the effective apparent power in a poly-phase unbalanced nonsinusoidal system. Since the effective apparent power considers transmission lines with equal resistances, it is not proportional to transmission losses. For this reason, reference [32] proposed a modification of the effective voltages and currents so that the resulting apparent power accounts for unequal resistances of the transmission lines. As in most transmission systems, the phases usually have very close resistances. Usually, only the neutral wire has a different resistance value. The different resistance of the neutral wire was incorporated in the definition of the effective current provided in the recent version of IEEE Std 1459-2010 [1].

In 2010, IEEE Std 1459-2010 was published collecting the most common power definitions [1]. It is proposed that the arithmetic and geometric PFs should be replaced by the effective PF.

In 2012, Czarnecki [18] discussed the billing of the active power for unbalanced constant impedance loads and for induction motors. It is noteworthy that until this moment there was no significant publications questioning the active power, which was the only quantity that researchers seemed to agree in the field of power theories. In this innovative approach, Czarnecki decomposes the active power into working, reflected and detrimental powers, considering the perspectives of the utility and the customer as both of them can

contribute to a low power quality. Czarnecki concludes that "switching accounts between the energy provider and its user from that based on the cost of the active energy to the accounts based on the cost of the working energy creates natural financial incentives for improving the supply quality and the loading quality." The author acknowledges, however, that switching to the working energy/power is not simple and further studies are recommended.

In 2015, Czarnecki [14] addressed the powers and the currents physical components (CPC) of unbalanced linear loads with a neutral conductor supplied by balanced sinusoidal voltages. The paper is an extension of [56] to four-wire systems. In such systems, there are zero-sequence currents which lead to the definition of the unbalanced zero-sequence power (D_u^z). The paper shows that all proposed power definitions can be expressed in terms of the load parameters. As a result, the load PF is rewritten only in terms of the load's impedances, without any dependence on the voltages, currents, nor power. Thus, the authors claim that the load PF is a property of the load [14]. The paper also presents a method of calculation of LC parameters for delta and wye passive compensators. The proposed method is validated by a numerical example. The paper however assumes that the source and the transmission lines have zero impedance, and that the voltages are balanced sinusoidal.

One year later, Czarnecki [13] addressed the powers and the currents physical components (CPC) of unbalanced linear loads with a neutral conductor supplied by balanced nonsinusoidal voltages. The paper is an extension of [14] to systems with non-sinusoidal voltages. In such systems, the total active current is not equal to the sum of the active currents for each harmonic, because there are different harmonic conductances for different frequencies. The difference between these two currents is the scattered current, named due to the scattering of the harmonic conductances ($G_{e,h}$) around the total equivalent conductance (G_e). The paper shows that all proposed power definitions can be expressed in terms of the proposed current components. As a result, the load PF is rewritten only in terms of the load's currents. It is worth noting that, differently from [14], the obtained PF expression is not expressed solely in terms of the load's admittances without any dependence on the voltages, currents, nor power. Thus, the authors previous claim that the load PF is a property of the load [14] could not be confirmed in [13] when the voltages are nonsinusoidal. The paper assumes that the grid Thévenin impedance is zero and that the voltages are balanced.

Reference [124] addresses 4 different PTs (PTs) and assesses whether they can be easily measured, if they allow correct quantification of powers and PF for a fair charge, and if they provide the necessary information for the design of compensation techniques. The first PT addressed is the the Budeanu's extension to three-phase systems, despite the previous critics of Budeanu's theory [21, 57, 91]. Then, the decomposition of the effective apparent power in terms of harmonic and sequence components, as provided by IEEE Standard 1459-2010, is analyzed as a PT. The next is based on wavelet transformations, and the last one is the pq-theory. The authors concluded that Budeanu's extension to three-phase systems and the wavelet based PTs fully fulfill the 3 basic requirements desired for PTs. The authors also claim that the power definitions provided by the IEEE Standard 1459-2010 does not provide a fair charging. Also, the PQ-theory can be employed for compensation purposes, but cannot be easily measured nor allow correct quantification of powers and PF for a fair charge, though the definition for fairness is not provided.

In 2022, we [9] have evaluated five different PF definitions applied for both a balanced constant impedance load and for a three-phase induction motor (TIM) supplied by several unbalanced nonsinusoidal conditions by

means of digital simulations and experimental tests. We have shown that, under unbalanced nonsinusoidal voltages, the effective PF and the fundamental arithmetic PF of a three-phase induction motor (TIM) are significantly affected by the voltage unbalance. Moreover, PF definitions were affected by the voltage unbalance only when applied to the TIM, but not when applied to a balanced constant impedance load, showing that the behavior of PF definitions depends on the load under analysis. We concluded that it is necessary to investigate PF definitions with more loads to attempt a proposition that may be applicable to most of the loads subjected to PF billing. The methodology employed and the obtained results are part of this PhD thesis and will be detailed in the following chapters.

Table 2.1 summarizes the works described in this section.

Table 2.1: Historical Summary of Works Discussing Power-Related Definitions.

Reference	Authors	Title	Year
[81]	Steinmetz, C. P.	Does Phase Displacement Occur in the Current Of Electric Arcs?	1892
[79]	Burt, A.	Three-Phase Power-Factor	1908
[125]	Fortescue, C. L.	Method of symmetrical co-ordinates applied to the solution of polyphase networks	1918
[77]	Fortescue, C. L.	Polyphase Power Representation by Means of Symmetrical Coordinates	1920
[72]	Special Joint Committee	Power Factor in Polyphase Circuits	1920
[70]	Buchholz, F	The Three-Phase Apparent Power with Uneven Load on the Three Branches	1922
[118]	Budeanu, C I	Reactive and fictitious powers	1927
[69]	Fryze, S	Active, Reactive and Apparent Power in Circuits with Non-sinusoidal Voltage and Current	1932
[90]	Curtis, H. L. Silsbee, F. B.	Definitions of Power and Related Quantities	1935
[122]	Buchholz, F.	*Das Begriffssystem Rechtleistung, Wirkleistung, totale Blindleistung*	1950
[123]	Depenbrock, M.	Investigations of the Voltage and Power Conditions at Converters Without Energy Storage	1962
[68]	Shepherd, W. Zakikhani, P.	Suggested Definition of Reactive Power for Nonsinusoidal Systems	1972
[65]	Sharon, D.	Reactive-Power Definitions and Power-Factor Improvement in Nonlinear Systems	1973
[61]	Kusters, N.L. Moore, W.J.M.	On the Definition of Reactive Power Under Non-Sinusoidal Conditions	1980

Table 2.1: Historical Summary of Works Discussing Power-Related Definitions.

Reference	Authors	Title	Year
[60]	Akagi, H. Kanazawa, Y. Nabae, A.	Instantaneous Reactive Power Compensators Comprising Switching Devices Without Energy Storage Components	1984
[59]	Czarnecki, L. S.	Considerations on the Reactive Power in Nonsinusoidal Situations	1985
[57]	Czarnecki, L. S.	What is Wrong with the Budeanu Concept of Reactive and Distortion Power and Why It Should be Abandoned	1987
[56]	Czarnecki, L. S.	Orthogonal Decomposition of the Currents in a 3-phase Nonlinear Asymmetrical Circuit with a Nonsinusoidal Voltage Source	1988
[91]	Emanuel, A. E.	Powers in nonsinusoidal situations-a review of definitions and physical meaning	1990
[55]	Czarnecki, L. S. Swietlicki, T.	Powers in Nonsinusoidal Networks : Their Interpretation, Analysis, and Measurement	1990
[54]	Czarnecki, L. S.	Scattered and Reactive Current, Voltage, and Power in Circuits with Nonsinusoidal Waveforms and Their Compensation	1991
[53]	Willems, J. L.	A New Interpretation of the Akagi-Nabae Power Components for Nonsinusoidal Three-Phase Situations	1992
[51]	Depenbrock, M.	The FBD-Method, a generally applicable tool for analyzing power relations	1993
[52]	Emanuel, A. E.	On the Definition of Power Factor and Apparent Power in Unbalanced Polyphase Circuits with Sinusoidal Voltage and Currents	1993
[93]	Sasdelli, R. Menchetti, A. Montanari, G. C.	Power Definitions for Power-Factor Correction Under Nonsinusoidal Conditions	1994
[95]	Czarnecki, L. S.	Power related phenomena in three-phase unbalanced systems	1995
[49]	Sharon, D.	Power Factor Definitions and Power Transfer Quality in Nonsinusoidal Situations	1996
[45]	Emanuel, A. E.	The Buchholz-Goodhue Apparent Power Definition: The Practical Approach For Nonsinusoidal And Unbalanced Systems	1998
[44]	Emanuel, A. E.	Apparent Power Definitions For Three-Phase Systems	1999
[32]	Jeon, S.	Definitions Of Apparent Power And Power Factor In A Power System Having Transmission Lines With Unequal Resistances	2005

Table 2.1: Historical Summary of Works Discussing Power-Related Definitions.

Reference	Authors	Title	Year
[1]	IEEE	IEEE Standard 1459-2010 - Definitions for the Measurement of Electric Power Quantities Under Sinusoidal, Nonsinusoidal, Balanced, or Unbalanced Conditions	2010
[18]	Czarnecki, L. S.	Working, Reflected and Detrimental Active Powers	2012
[14]	Czarnecki, L. S. Haley, P. M.	Unbalanced Power in Four-Wire Systems and its Reactive Compensation	2015
[13]	Czarnecki, L. S. Haley, P. M.	Power Properties of Four-Wire Systems at Nonsinusoidal Supply Voltage	2016
[124]	Nicolae, P. M. Nicolae, I. D. Nicolae, M. S.	Powers and Power Factor in Non-Sinusoidal and Non-Symmetrical Regimes in Three-Phase Systems	2022
[9]	Brasil, V. P. Ishihara, J. Y. Ferreira Filho, A. d. L.	Fair Power Factor Billing Under Unbalanced and Nonsinusoidal Voltage Supply	2022

2.2 Power Factor Definitions

2.2.1 Single-Phase Systems

In single-phase systems, the instantaneous voltage is given by

$$v(t) = v_1(t) + \sum_{h \in H} v_h(t) \tag{2.3}$$

in which $v_1(t)$ is the instantaneous fundamental voltage, $v_h(t)$ is the instantaneous voltage of order h, and H is the set of nonfundamental components (which may include harmonics, interharmonics and subharmonics). If $v_h(t)$ is nil for all values of h and t, then the voltage is considered sinusoidal. If $v_h(t)$ is not nil for some value of h and t, then the voltage is distorted. The fundamental instantaneous voltage is given by

$$v_1(t) = \sqrt{2} V_1 \sin(\omega t) \tag{2.4}$$

where V_1 is the fundamental voltage RMS value and ω is the angular frequency of the system. The voltages $v_h(t)$ are given by

$$v_h(t) = \sqrt{2} V_h \sin(h\omega t + \beta_h) \tag{2.5}$$

where V_h is the RMS value of the voltage $v_h(t)$, and β_h is the phase shift of $v_h(t)$ with respect to $v_1(t)$. The voltage RMS value is given by the square root of the sum of the squared components of V_1 and V_h, that is,

$$V = \sqrt{V_1^2 + \sum_{h \in H} V_h^2}. \tag{2.6}$$

From (2.6), it can be observed that $V \geq V_1$ and $V \geq V_h$ for any value of h.

Similarly to the voltage, the instantaneous current is given by

$$i(t) = i_1(t) + \sum_{h \in H} i_h(t) \tag{2.7}$$

in which $i_1(t)$ is the instantaneous fundamental current, and $i_h(t)$ is the instantaneous current of order h. The fundamental instantaneous current is given by

$$i_1(t) = \sqrt{2} I_1 \sin(\omega t + \theta_1) \tag{2.8}$$

in which I_1 is the fundamental current RMS value and θ_1 is the phase shift between $i_1(t)$ and $v_1(t)$. Positive values of θ_1 indicate that $i_1(t)$ leads $v_1(t)$, whereas negative values indicate that $i_1(t)$ lags $v_1(t)$. The currents $i_h(t)$ are given by

$$i_h(t) = \sqrt{2} I_h \sin(h\omega t + \alpha_h + \theta_h) \tag{2.9}$$

where I_h is the RMS value of $i_h(t)$, β_h is the same as in (2.5) and θ_h is the phase shift between $i_h(t)$ and $v_h(t)$. The current RMS is equal to

$$I = \sqrt{I_1^2 + \sum_{h \in H} I_h^2}, \tag{2.10}$$

and it is always greater than or equal to the components I_1 or I_h, for any value of h.

The instantaneous voltage and current are the foundation for all other concepts in power systems. These basic quantities are often measured and used to calculate further complex quantities. With the foundation laid, it is possible to represent the instantaneous power $p(t)$ in terms of $v(t)$ and $i(t)$. The scientific community agrees on the definition and meaning of $p(t)$, differently from the other power-related definitions such as PF, apparent and reactive power. The instantaneous power is defined as the product of $v(t)$ and $i(t)$, that is

$$p(t) = \left(v_1(t) + \sum_{h \in H} v_h(t) \right) \left(i_1(t) + \sum_{h \in H} i_h(t) \right). \tag{2.11}$$

In terms of its physical meaning, it is the instantaneous rate of energy flow in the system, being commonly measured in units of W. The instantaneous power can be decomposed into

$$p(t) = p_1(t) + p_H(t) + p_{ii}(t) \tag{2.12}$$

in which

$$p_1(t) = v_1(t) i_1(t) \tag{2.13}$$

is the instantaneous fundamental power,

$$p_H(t) = \left(\sum_{h \in H} v_h(t) \right) \left(\sum_{h \in H} i_h(t) \right) \tag{2.14}$$

is the instantaneous distortion power, and

$$p_{ii}(t) = v_1(t) \sum_{h \in H} i_h(t) + i_1(t) \sum_{h \in H} v_h(t) \tag{2.15}$$

is the instantaneous distortion intrinsic power. If the set H is composed only by harmonic components, then $p_H(t)$ and $p_{ii}(t)$ can be called instantaneous harmonic power and instantaneous harmonic intrinsic power, respectively.

The active power P is the average rate of energy flow over a given period of time. Mathematically,

$$P = \frac{1}{kT}\int_{\tau}^{\tau+kT} p(t)dt \tag{2.16}$$

where τ is the moment the measurement started, k is a multiplier (preferably integer[1]) that defines the window of calculation, and T is the period of the sinusoidal fundamental voltage $v_1(t)$. The active power can be decomposed in terms of frequency components as

$$P = P_1 + P_H \tag{2.17}$$

in which

$$P_1 = V_1 I_1 \cos(\theta_1) \tag{2.18}$$

is the fundamental active power, and

$$P_H = \sum_{h\in H} V_h I_h \cos(\theta_h) \tag{2.19}$$

is the nonfundamental active power. It is worth mentioning that $p_{ii}(t)$ has nil average value and, for this reason, it does not contribute to the active power P.

The active power P can either represent the energy transferred to a load or dissipated in the transmission process. The load usually converts the electrical energy carried by P into thermal, mechanical, or another form of energy. Thus, the load owner is interested in how much active power the load needs to perform its job. On the other hand, utilities are also concerned about the transmission losses, which can be significantly affected by the load's current. Transmission losses higher than the typical values may endanger equipment integrity and indicate problems (such as faults or energy theft). For this reason, it is important to account for the effects of each load on the grid. The following example shows the necessity of establishing a figure of merit to quantify the load's usage of the transmission system caused by the phase displacement between current and voltage.

Example 1 *[Usage of the transmission system not caused by the active power]*

Consider the case where the transmission system is represented by a series resistor R_L, as shown in Figure 2.1. The transmission loss ΔP is given by

$$\Delta P = R_L I^2, \tag{2.20}$$

in which I is the current RMS given by (2.10). The transmission losses are mainly due to the Joule effect, converting electrical energy into thermal energy (heat). A very high value of ΔP can indicate over heating of the transmission equipment. In fact, the heating of such equipment is so related to the flow of current that it is common to find the thermal limit of transmission cables defined as the maximum current RMS they can safely carry.

[1] If the multiplier k is not integer, the window of calculation will not be a multiple of the period T. This will result in measurement errors.

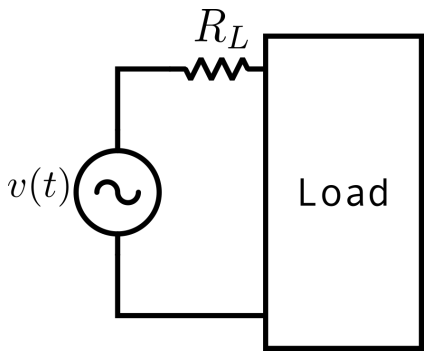

Figure 2.1: Single-phase system in which a generator supplies sinusoidal voltage to a load by means of a transmission line

One may think that monitoring the load's active power is enough to ensure proper values of current in the transmission system. However, loads can draw different currents and still have the same active power. For simplicity, consider only the fundamental active power, described in (2.18). If P_1 and V_1 are constant, then I_1 is inversely proportional to $\cos(\theta_1)$. As a result, a decrease of $\cos(\theta_1)$ causes an increase of I_1 and, consequently, an increase of ΔP. Although utilities can monitor the current of each load, it is challenging to establish limits for this quantity because it depends on the customer's "size", that is, the amount of consumed active power. Given that θ_1 has a well-defined range of $[-90°, 90°]$, it is possible to make general rules for θ_1 regardless of the customer's "size".

The fundamental current phase shift θ_1 is often related to the load's reactive elements (inductors and capacitors). Such elements draw currents that are orthogonal to the voltage applied to them. In other words, θ_1 is $-90°$ for inductors and $90°$ for capacitors. One can immediately check in (2.18) that the load does not consume fundamental active power if $\theta_1 = \pm 90°$. Nevertheless, the load still draws current from the generator, causing transmission losses. In this case, the customer would not pay for energy consumption because there is none. However, he should still be responsible for the transmission system's usage and losses. This simple example highlights the importance of establishing a figure of merit to quantify the usage of the transmission system caused by the phase displacement between current and voltage. The existing attempts employ the concepts of PF, apparent and reactive power. Definitions for such quantities are provided next.

2.2.1.1 Fundamental Power Factor

The electrical system is designed to operate constantly close to the nominal frequency, usually 50 Hz or 60 Hz. Components at other frequency values (such as harmonics, interharmonics, and subharmonics) are undesired and result from the nonlinearities of grid-connected equipment. As utilities seek to diminish the presence of these nonfundamental components, the bulk of energy flow occurs at the fundamental frequency. So, it is necessary to have a clear definition for the fundamental PF, apparent and reactive power. Also, reference [11] points out the fundamental reactive power as the fairest for billing purposes of a residential customer supplied by a low-voltage single-phase system.

Taking into account only the fundamental frequency components, the instantaneous fundamental power

shown in (2.13) can be decomposed into

$$p_1(t) = p_{1p}(t) + p_{1q}(t) \tag{2.21}$$

where

$$p_{1p}(t) = V_1 I_1 \cos(\theta_1)\,[1 - \cos(2\omega t)] \tag{2.22}$$

is the instantaneous fundamental active power, and

$$p_{1q}(t) = V_1 I_1 \sin(\theta_1)\sin(2\omega t) \tag{2.23}$$

is the instantaneous fundamental reactive power.

Figure 2.2 illustrates $p_1(t)$, $p_{1p}(t)$, and $p_{1q}(t)$, considering $\omega \approx 377$ rad/s, $V_1 = 1$ V, $I_1 = 1$ A, and $\theta_1 = 30°$. It is noteworthy that $p_1(t)$ is oscillatory and sometimes it becomes negative, meaning that the energy flows back from the load to the source. The contributions of each component ($p_{1p}(t)$ and $p_{1q}(t)$) to the inversion of energy flow and to the transmission of the active power P are investigated next.

It is noteworthy that $\cos(2\omega t)$ and $\sin(2\omega t)$ are symmetric about the t-axis, resulting in a null mean over a given period multiple of T. Also, they are in the range $[-1, 1]$. As a result, $p_{1p}(t)$ is always greater than zero, with mean and amplitude given by P_1. Since $p_{1p}(t)$ is the only component that contributes to P_1, it is called instantaneous fundamental active power. On the other hand, $p_{1q}(t)$ oscillates around zero with amplitude equal to the fundamental reactive power, that is

$$Q_1 = V_1 I_1 \sin(\theta_1). \tag{2.24}$$

Q_1 is greater than zero only if $\sin(\theta_1)$ is greater than zero, resulting in negative values of $p_1(t)$ for some t. So, at the fundamental frequency, the instantaneous inversion of energy flow occurs due to the phase displacement between voltage and current, which causes transmission losses as shown in Example 1.

The oscillatory component of $p_1(t)$ satisfies the following relation

$$V_1 I_1 \cos(2\omega t + \theta_1) = V_1 I_1 \left[\cos(\theta_1)\cos(2\omega t) - \sin(\theta_1)\sin(2\omega t)\right], \tag{2.25}$$

that can be further simplified into

$$S_1 \cos(2\omega t + \theta_1) = P_1 \cos(2\omega t) - Q_1 \sin(2\omega t) \tag{2.26}$$

in which

$$S_1 = V_1 I_1 \tag{2.27}$$

is the fundamental apparent power. Equation (2.26) can be graphically represented with the coordinate system that has the x-coordinate associated to $\cos(2\omega t)$ and the y-coordinate associated to $-\sin(2\omega t)$, as shown in Figure 2.3, often referred to as the power triangle. Notice that the angle between S_1 and P_1 is equal to θ_1. Additionally, this triangle is rectangle meaning that

$$S_1 = \sqrt{P_1^2 + Q_1^2}. \tag{2.28}$$

Back to the problem of establishing a figure of merit to quantify the usage of the transmission system, it is noteworthy that the matter can be discussed considering the concepts of S_1 and Q_1. The fundamental apparent

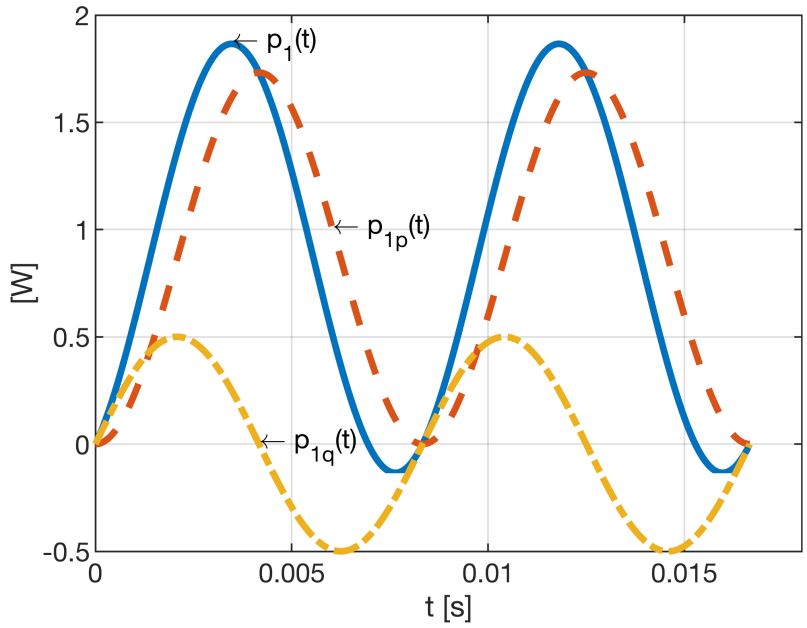

Figure 2.2: Instantaneous fundamental power and its active and reactive components.

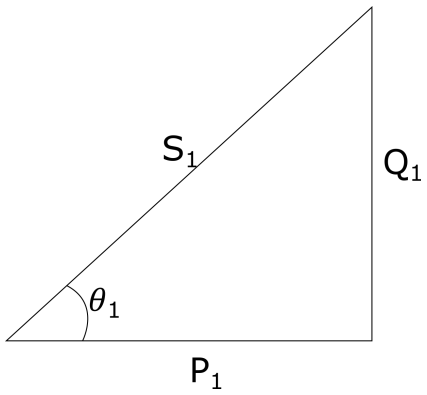

Figure 2.3: Power triangle for the fundamental components of single-phase systems

power S_1 is directly proportional to I_1 and the transmission losses. As a result, the degree of utilization of the system can be quantified by S_1, which can also be interpreted as the maximum active power that can be delivered to the load, considering V_1 and I_1 constant. Ideally, the transmission system should be used only to transfer active power, that is $S_1 = P_1$. However, in most practical situations, loads draw currents with some phase shift relative to the voltage. This results in the usage of the grid to transfer reactive power Q_1. In Example 1, the loads had the same P_1 but different S_1 because one had a higher Q_1. Although S_1 and Q_1 can be used to quantify how much of the transmission system is being used by the customer, these two quantities depend on the customer's "size". As a result, it is difficult to establish general rules for different customers.

Seeking to define a figure of merit that does not depend on the customer's "size", an alternative is to use the fundamental power factor (PF_1) defined as

$$PF_1 = \frac{P_1}{S_1}. \tag{2.29}$$

PF_1 can be understood as the ratio of the actual fundamental active power and the maximum fundamental active power possible, considering V_1 and I_1 constant. Applying (2.28) into (2.29), PF_1 can be rewritten as

$$PF_1 = \frac{P_1}{\sqrt{P_1^2 + Q_1^2}}. \tag{2.30}$$

Alternatively, it can be defined in terms of the phase shift between the current and voltage

$$PF_1 = \cos(\theta_1). \tag{2.31}$$

It is noteworthy that (2.29), (2.30) and (2.31) are equivalent to each other.

The issues regarding Budeanu's power definitions are extensively pointed out in [21] and [57]. In [57], the concept of reactive power is defined as the amplitude of the alternating flow of energy generalized from (2.23). Reference [57] showed that the instantaneous power can have an alternating flow of energy when Q_B is zero. So, the behavior of Q_B is not uniquely related to the alternating flow of energy. Reference [12] also points out that Q_B may be zero due to the cancellation between different frequency components. According to [21], there are several ways of compensating Q_B. Some of them can increase the current RMS values, but only one can reduce the current RMS value. This leads to a non-optimal condition that cannot be assessed by Q_B. In [57], it is also pointed out that there is no physical meaning for D_B. For instance, distorted power may be zero if a nonsinusoidal voltage supplies a resistor. Additionally, there are cases where the distorted power is zero and the load's current does not have the same waveform as the voltage supply. In other words, the current waveform is distorted in relation to the voltage waveform. Therefore, Budeanu's power definitions do not provide basis for performing compensation or quantifying the voltage and current distortions.

2.2.2 Three-Phase Systems

In three phase systems, there are three energized (or hot) conductors with voltages that contain fundamental components and may contain nonfundamental components of order h. In this work, we adopt the following notation. The first subscript indicates how frequency components are addressed. If the first subscript is 1, then only the fundamental frequency component is being accounted for. If it is equal to h, then only frequency

components of order h are being accounted for. The first subscript can also be equal to N or B indicating that frequency components are addressed with Fryze's or Buedanu's power theories. The second subscript, if it exists, represents each of the system phases. For example, Budeanu's reactive power of phase "b" is denoted by $Q_{B,b}$, where the the upper case subscript "B" indicates Budeanu's definition, whereas subscript "b" represents the phase "b". At last, the superscript indicates the aggregating method to deal with different values between phases.

The instantaneous voltages measured with respect to a neutral point (the ground, a neutral conductor or the virtual star point) are given by

$$v_a(t) = v_{1,a}(t) + \sum_{h \in H} v_{h,a}(t) \tag{2.32}$$

$$v_b(t) = v_{1,b}(t) + \sum_{h \in H} v_{h,b}(t) \tag{2.33}$$

$$v_c(t) = v_{1,c}(t) + \sum_{h \in H} v_{h,c}(t) \tag{2.34}$$

in which

$$v_{1,a}(t) = \sqrt{2} V_{1,a} \sin(\omega t) \tag{2.35}$$

$$v_{1,b}(t) = \sqrt{2} V_{1,b} \sin(\omega t - \gamma_{1,ab}) \tag{2.36}$$

$$v_{1,c}(t) = \sqrt{2} V_{1,c} \sin(\omega t + \gamma_{1,ca}) \tag{2.37}$$

are the instantaneous fundamental voltages of phases a, b, and c, respectively; and

$$v_{h,a}(t) = \sqrt{2} V_{h,a} \sin(\omega t + \beta_h) \tag{2.38}$$

$$v_{h,b}(t) = \sqrt{2} V_{h,b} \sin(\omega t + \beta_h - \gamma_{h,ab}) \tag{2.39}$$

$$v_{h,c}(t) = \sqrt{2} V_{h,c} \sin(\omega t + \beta_h + \gamma_{h,ca}) \tag{2.40}$$

are the instantaneous voltages of order h of phases a, b, and c, respectively. The upper case $V_{1,x}$ is the RMS value of the fundamental voltage of phase $x = a, b, c$. $\gamma_{1,ab}$ and $\gamma_{1,ca}$ are the phase shifts between the fundamental voltages of phases a-b and c-a. Similarly, $V_{h,x}$ is the RMS value of the voltage of order h of phase $x = a, b, c$. $\gamma_{h,ab}$ and $\gamma_{h,ca}$ are the phase shifts between the voltages of order h of phases a-b and c-a. At last, β_h is the phase shift of $v_{h,a}(t)$ with respect to $v_{1,a}(t)$.

In the absence of accessible neutral points, such as ground or fourth conductor, phase-to-phase voltage measurements can be employed. Being computed as

$$v_{ab}(t) = v_a(t) - v_b(t) \tag{2.41}$$

$$v_{bc}(t) = v_b(t) - v_c(t) \tag{2.42}$$

$$v_{ca}(t) = v_c(t) - v_a(t), \tag{2.43}$$

phase-to-phase voltages have the property of adding up to zero. So, their values can be determined only by two measurements. For example, if $v_{bc}(t)$ and $v_{ca}(t)$ are measured, then $v_{ab}(t)$ can be computed as

$$v_{ab}(t) = -\left[v_{bc}(t) + v_{ca}(t)\right]. \tag{2.44}$$

The instantaneous currents flowing through each phase are defined as

$$i_a(t) = i_{1,a}(t) + \sum_{h \in H} i_{h,a}(t) \tag{2.45}$$

$$i_b(t) = i_{1,b}(t) + \sum_{h \in H} i_{h,b}(t) \tag{2.46}$$

$$i_c(t) = i_{1,c}(t) + \sum_{h \in H} i_{h,c}(t) \tag{2.47}$$

where

$$i_{1,a}(t) = \sqrt{2} I_{1,a} \sin(\omega t + \theta_{1,a}) \tag{2.48}$$

$$i_{1,b}(t) = \sqrt{2} I_{1,b} \sin(\omega t - \gamma_{1,ab} + \theta_{1,b}) \tag{2.49}$$

$$i_{1,c}(t) = \sqrt{2} I_{1,c} \sin(\omega t + \gamma_{1,ca} + \theta_{1,c}) \tag{2.50}$$

are the instantaneous fundamental currents of phases a, b, and c, respectively; and

$$i_{h,a}(t) = \sqrt{2} I_{h,a} \sin(\omega t + \beta_h + \theta_{h,a}) \tag{2.51}$$

$$i_{h,b}(t) = \sqrt{2} I_{h,b} \sin(\omega t + \beta_h - \gamma_{h,ab} + \theta_{h,b}) \tag{2.52}$$

$$i_{h,c}(t) = \sqrt{2} I_{h,c} \sin(\omega t + \beta_h + \gamma_{h,ca} + \theta_{h,c}) \tag{2.53}$$

are the instantaneous current of order h of phases a, b, and c, respectively. $I_{1,x}$ is the RMS value of the fundamental current of phase $x = a, b, c$, and $\theta_{1,x}$ is the phase shift between $i_{1,x}(t)$ and $v_{1,x}(t)$. Likewise, $I_{h,x}$ is the RMS value of the current of order h of phase $x = a, b, c$, and $\theta_{h,x}$ is the phase shift of $i_{h,x}(t)$ with respect to $v_{h,x}(t)$.

The instantaneous power transmitted by each phase is given by

$$p_a(t) = v_a(t) i_a(t) \tag{2.54}$$

$$p_b(t) = v_b(t) i_b(t) \tag{2.55}$$

$$p_c(t) = v_c(t) i_c(t). \tag{2.56}$$

Each phase instantaneous power can be decomposed as shown in (2.12). The active power of each phase (P_x, $x = a, b, c$) is defined as the average of the instantaneous power of that phase, in the same way as in single-phase systems. P_x, $x = a, b, c$, can be decomposed as in (2.17). The three-phase (or total, or load) instantaneous power $p_{3\phi}(t)$ is given by the summation

$$p_{3\phi}(t) = \sum_{x=a,b,c} p_x(t). \tag{2.57}$$

If the system has only three-wires without ground-connection, then $p_{3\phi}(t)$ can be computed with phase-to-phase voltages as

$$p_{3\phi}(t) = v_{ab}(t) i_a(t) - v_{bc}(t) i_c(t). \tag{2.58}$$

The three-phase active power is defined as the average of $p_{3\phi}(t)$, that is,

$$P_{3\phi} = \frac{1}{kT} \int_{\tau}^{\tau + kT} p_{3\phi}(t) dt, \tag{2.59}$$

but can also be computed as the summation of each phase active power, *i.e.*

$$P_{3\phi} = \sum_{x=a,b,c} P_x. \tag{2.60}$$

If the voltage supply is perfectly sinusoidal, then $v_{h,x}(t)$ is nil for all values of h, x and t. As a result, $V_x = V_{1,x}$ for $x = a, b, c$ and $\gamma_{h,ab} = \gamma_{h,ca} = 0$. If the voltage supply is perfectly sinusoidal and balanced (symmetrical), then $V_a = V_b = V_c$, and $\gamma_{1,ab} = \gamma_{1,ca} = 120°$. If the load is also perfectly sinusoidal and balanced, then $I_x = I_{1,x}$ for $x = a, b, c$, and $I_a = I_b = I_c$, and $\theta_{1,a} = \theta_{1,b} = \theta_{1,c}$. In this specific case, the oscillatory components of the instantaneous power of each phase add up to zero, and $p_{3\phi}(t)$ is equal and constant to $P_{3\phi}$. Additionally, each phase has the same value of active power, composed only by the fundamental active power, that is $P_x = P_{1,x}$ with $x = a, b, c$. Similarly, the reactive and apparent power are composed only by fundamental components and each phase has the same value as the remaining phases. In this case, the definition employed (Fundamental, Fryze or Budeanu) does not matter.

If the voltage supply or the load is not perfectly balanced, then each phase will have different instantaneous active powers as well as different PFs, apparent, and reactive powers. In this case, how to compute the load PF? The following sections shows some load PF definitions.

2.2.2.1 The Fundamental Arithmetic Power Factor

One way of computing the load PF is to compute the load fundamental apparent power as the arithmetic sum of each phase fundamental apparent power, that is,

$$S_1^a = S_{1,a} + S_{1,b} + S_{1,c}. \tag{2.61}$$

The fundamental arithmetic power factor is given by

$$PF_1^a = \frac{P_{1,3\phi}}{S_1^a}. \tag{2.62}$$

2.2.2.2 The Fundamental Geometric Power factor

The fundamental geometric apparent power is defined as

$$S_1^g = \sqrt{P_{1,3\phi}^2 + Q_{1,3\phi}^2}, \tag{2.63}$$

where

$$Q_{1,3\phi} = \sum_{x=a,b,c} Q_{1,x} \tag{2.64}$$

is the three-phase fundamental reactive power.

The fundamental geometric power factor is defined as

$$PF_1^g = \frac{P_{1,3\phi}}{S_1^g}. \tag{2.65}$$

Figure 2.4 shows graphically the difference between the fundamental arithmetic apparent power (S_1^a) and the fundamental geometric apparent power ($S1^g$). S_1^g takes into account the direction of each apparent power,

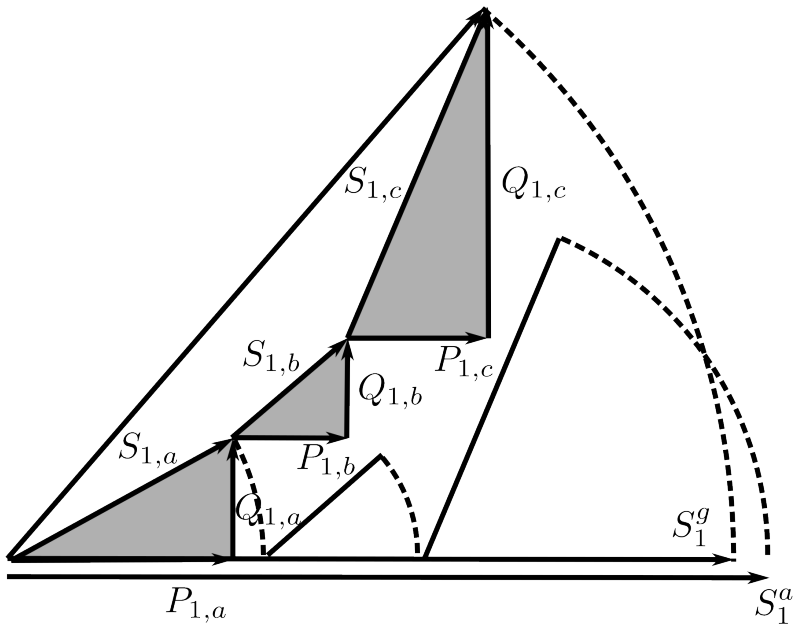

Figure 2.4: Power triangles for each phase of an unbalanced system, and the resulting fundamental arithmetic apparent power and the fundamental geometric apparent power. Based on [1].

adding them up geometrically. S_1^a, on the other hand, adds the modulus of each phase apparent power, not taking into account their direction. As a result, the relation $S_1^a \geq S_1^g$ is always true, or alternatively $PF_1^a \leq PF_1^g$.

The definitions presented in (2.62) and (2.65) allows computing the load PF. Although these definitions use fundamental components only, they can be extended with usage of different reactive and apparent power definitions. For example, they can be used with Budeanu's definitions, leading to the Budeanu's Arithmetic PF or to the Budeanu's geometric PF.

2.2.2.3 The Fundamental Positive Sequence Power Factor

According to Fortescue's theory of symmetrical components, the voltages and currents of any three-phase unbalanced system can be computed by the voltages and currents of three balanced three-phase systems denoted as positive, negative and zero sequence, respectively. Since these equivalent circuits are balanced, they can be represented only by one of the phases, usually phase "A". The voltages can be computed by the voltages in the sequence domain as

$$\begin{bmatrix} \mathbf{V_{1,a}} \\ \mathbf{V_{1,b}} \\ \mathbf{V_{1,c}} \end{bmatrix} = \underbrace{\begin{bmatrix} 1 & 1 & 1 \\ 1 & \boldsymbol{\alpha}^2 & \boldsymbol{\alpha} \\ 1 & \boldsymbol{\alpha} & \boldsymbol{\alpha}^2 \end{bmatrix}}_{F} \begin{bmatrix} \mathbf{V_1^z} \\ \mathbf{V_1^+} \\ \mathbf{V_1^-} \end{bmatrix} \tag{2.66}$$

where F is Fortescue's matrix, $\boldsymbol{\alpha} = 1\angle 120°$, and $\mathbf{V_1^z}, \mathbf{V_1^+}$, and $\mathbf{V_1^-}$ are the fundamental zero, positive and negative-sequence voltage components, respectively. The currents can be computed analogously.

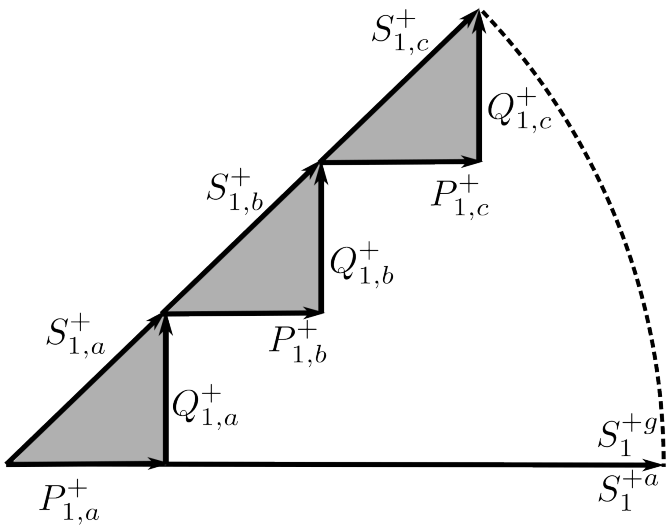

Figure 2.5: Power triangles for each phase of the positive sequence, and the resulting fundamental positive sequence arithmetical apparent power and the fundamental positive sequence geometrical apparent power.

Alternatively, the load PF can be adopted as the fundamental positive sequence PF given by

$$PF_1^+ = \frac{P_1^+}{S_1^+}, \tag{2.67}$$

in which the superscript + indicates positive sequence components, being P_1^+ the fundamental positive sequence active power and S_1^+ the fundamental positive sequence apparent power. The positive sequence system is completely balanced meaning that each phase has the same powers as the other phases, as shown in Figure 2.5. As a result, S_1^+ can be computed as $S_1^+ = S_1^{+a}$ or $S_1^+ = S_1^{+g}$ in which

$$S_1^{+a} \triangleq S_{1,a}^+ + S_{1,b}^+ + S_{1,c}^+ \tag{2.68}$$

is the fundamental positive sequence arithmetical apparent power, and

$$S_1^{+g} \triangleq \sqrt{\left(P_1^+\right)^2 + \left(Q_1^+\right)^2} \tag{2.69}$$

is the fundamental positive sequence geometrical apparent power.

Setting $S_1^+ = S_1^{+a}$ or $S_1^+ = S_1^{+g}$ in (2.67) leads respectively to the fundamental positive sequence arithmetical power factor

$$PF_1^{+a} = \frac{P_1^+}{S_1^{+a}} \tag{2.70}$$

and to the fundamental positive sequence geometrical power factor

$$PF_1^{+g} = \frac{P_1^+}{S_1^{+g}}. \tag{2.71}$$

The quantities S_1^{+a} and S_1^{+g} (consequently, PF_1^{+a} and PF_1^{+g}) are mathematically equivalent as can be observed from Figure 2.5. Nonetheless, S_1^{+a} and S_1^{+g} may have different values depending on the chosen measurement

method[2]. Since this subsection deals only with definitions, the fundamental positive sequence power factor will be simply denoted by PF_1^+.

2.2.2.4 The Effective Power Factor

It is also possible to employ the effective power factor (PF^e) as the load PF. The effective power factor is computed as

$$PF^e = \frac{P_{3\phi}}{S^e} \tag{2.72}$$

in which

$$S^e = 3V^e I^e \tag{2.73}$$

is the effective apparent power, and V^e and I^e are the effective voltage and current respectively. In terms of symmetrical sequence components, they are computed as

$$V^e = \sqrt{(V^+)^2 + (V^-)^2 + \frac{(V^z)^2}{1+\xi}} \tag{2.74}$$

$$I^e = \sqrt{(I^+)^2 + (I^-)^2 + (1+3\rho)\,(I^0)^2}, \tag{2.75}$$

where V^+, V^-, and V^z are the positive, negative, and zero sequence voltage RMS values, respectively. It is worth mentioning that all distortion components of order h should be considered for the computation of the RMS value. For instance,

$$V^+ = \sqrt{\left(V_1^+\right)^2 + \sum_{h\in H}\left(V_h^+\right)^2}. \tag{2.76}$$

V^- and V^z are computed analogously. Likewise, I^+, I^-, and I^0 refer to the currents sequence components RMS values. The variables ξ and ρ are used to consider the effects of zero sequence components in four-wire systems. If ξ and ρ are unknown, it is recommended to set them to one [1]. In three-wire systems, the effective voltage and current is computed with (2.74) and (2.75), considering that $V^z = I^0 = 0$.

2.3 Measurement Methods

This section collects methods for the measurement of the power factor definitions presented in Section 2.2. It is worth mentioning that the methods may differ on the algorithms used as well the quantities employed. For instance, the value of $PF_{1,a}$ can be obtained with the measurement of: $P_{1,a}$ and $S_{1,a}$ (using the measurements of $V_{1,a}$ and $I_{1,a}$); or $P_{1,a}$ and $Q_{1,a}$. The quality of the measurement depends on the implemented algorithms.

There is a wide range of algorithms inspired on different techniques. Existing solutions range from the usage of phasor measurement units (PMUs), which estimates voltage and current phasor for each harmonic, to solutions based on voltage and current instantaneous samples [126]. Some phasor estimation techniques

[2]The apparent power S_1^{+a} can be measured based on the RMS values of fundamental positive sequence voltage and current of each phase, whereas S_1^{+g} requires the measurement of fundamental active and reactive power. The methods for measuring the voltage and current RMS values are different from those used to measure the active and reactive power. As a result, the measurements of PF_1^{+a} and PF_1^{+g} may have different values.

include those based on the fast Fourier transform (FFT) [127] and on the wavelet transform [42,46]. According to [11], accuracy, simplicity and the ease of calculation are often taken into account when selecting which method to be implemented in the energy meter.

2.3.1 Fourier Transform

Usage of voltage and current harmonic decomposition gives high accuracy and flexibility to work with different PF definitions. For instance, it allows measuring power harmonic components defined by IEEE Standard 1459-2010 [1]. Other power quantities, such as those proposed by the currents physical components (CPC) [13] and by the conservative power theory (CPT) [20], can also be assessed. On the other hand, it increases computational complexity.

2.3.2 Active Power Measurement Method

It is known that the total three-phase active power is obtained by adding up the total active power of each phase. According to [1], the total active power, in balanced nonsinusoidal conditions, can be decomposed into fundamental active power (P_1) and total harmonic active power (P_H). In unbalanced sinusoidal situations, the active power can be decomposed into positive, negative, and zero sequence powers, denoted by P^+, P^-, and P^0, respectively. In the general case, where voltage unbalance and harmonic distortion can be present, these last two decompositions can be superimposed resulting in 6 components: P_1^+, P_1^-, P_1^0, P_H^+, P_H^-, and P_H^0.

The total and the positive sequence active powers are measured, respectively, by [1]

$$P_{3\phi} = \sum_{x=a,b,c} \frac{1}{kN} \sum_{s=\tau}^{\tau+kN} v_x(s) i_x(s) \tag{2.77}$$

$$P^+ = 3\frac{1}{kT} \sum_{s=\tau}^{\tau+kN} v_a^+(s) i_a^+(s), \tag{2.78}$$

where $v_x(s)$ and $i_x(s)$ are the voltage and current samples from phase $x = a, b, c$; $v_x^+(s)$ and $i_x^+(s)$ are the positive sequence voltage and current samples from phase $x = a, b, c$; τ is the first sample measured in the window of calculations; N is the number of samples per cycle; and k is the total number of cycles measured.

2.3.3 Reactive Power Measurement Methods

Since the main objective of this work is to compare PF definitions, we restrict the study of measurement techniques to two simple algorithms: the methods of voltage integration and of 90º displacement of voltage. These techniques can be easily and cheaply implemented in the development of a meter.

2.3.3.1 90º Displacement of Voltage

The 90° displacement of voltage, proposed by [126], allows an approximate computation of the reactive power of each phase of the system. For this purpose, a delayed voltage signal is employed in order to simulate

a 90° phase shift. Mathematically, the reactive power measured is

$$Q_{x,\text{displacement}} = \frac{1}{kT}\int_{\tau}^{\tau+kT} v_x\left(t-\frac{T}{4}\right)\cdot i_x(t)dt \tag{2.79}$$

If the phase x has sinusoidal voltage and current, then

$$Q_{x,\text{displacement}} = \frac{-2V_xI_x}{kT}\int_{\tau}^{\tau+kT} \cos(\omega t)\sin(\omega t+\theta_x)\,dt \tag{2.80}$$

$$Q_{x,\text{displacement}} = \frac{-2V_xI_x}{kT}\int_{\tau}^{\tau+kT} \left[\sin(\omega t)\cos(\omega t)\cos(\theta_x)+\sin(\theta_x)\cos^2(\omega t)\right]dt. \tag{2.81}$$

After some simplifications,

$$Q_{x,\text{displacement}} = V_xI_x\sin(\theta_x) \tag{2.82}$$

is exactly equal to the definition of reactive power in sinusoidal conditions.

If the phase x has nonsinusoidal voltage and current, then

$$Q_{x,\text{displacement}} = \frac{-2}{kT}\int_{\tau}^{\tau+kT} \left[v_{1,x}\left(t-\frac{T}{4}\right)+\sum_{h\in H} v_{h,x}\left(t-\frac{T}{4}\right)\right]\left[i_{1,x}(t)+\sum_{h\in H} i_{h,x}(t)\right]dt. \tag{2.83}$$

After some simplifications,

$$Q_{x,\text{displacement}} = Q_1 - P_2 - Q_3 + P_4 - Q_5\ldots \tag{2.84}$$

It is noteworthy that $Q_{x,\text{displacement}}$ is not any of the reactive power definitions discussed in Section 2.2. Nevertheless, in the study performed by [11] using common distortion levels, $Q_{x,\text{displacement}}$ was approximately equal to $Q_{1,x}$.

2.3.3.2 Voltage Integration

In the voltage integration method proposed by [120], the reactive power is estimated using a 90° phase shift in sinusoidal signals obtained from voltage integration as follows

$$Q_{x,\text{integration}} = \frac{\omega}{kT}\int_{\tau}^{\tau+kT} \left[\int v_x(t)dt\right] i_x(t)dt. \tag{2.85}$$

If the phase x has sinusoidal voltage and current, then

$$Q_{x,\text{integration}} = \frac{-2V_xI_x}{kT}\int_{\tau}^{\tau+kT} \cos(\omega t)\sin(\omega t+\theta_{1,x})\,dt. \tag{2.86}$$

$$Q_{x,\text{integration}} = \frac{-V_xI_x}{kT}\int_{\tau}^{\tau+kT} \left[\sin(2\omega t+\theta_1)-\sin(\theta_1)\right]dt. \tag{2.87}$$

After some simplifications,

$$Q_{x,\text{integration}} = V_xI_x\sin(\theta_x) \tag{2.88}$$

is exactly equal to the definition of reactive power in sinusoidal conditions.

If the phase x has nonsinusoidal voltage and current, then

$$Q_{x,\text{integration}} = \frac{1}{kT}\int_{\tau}^{\tau+kT}\left[\int v_{1,x}(t)dt + \sum_{h\in H}\int v_{h,x}dt\right]\left[i_{1,x}(t) + \sum_{h\in H} i_{h,x}(t)\right]dt. \tag{2.89}$$

After some simplifications,

$$Q_{x,\text{integration}} = Q_1 + \frac{Q_2}{2} + \frac{Q_3}{3} + \frac{Q_4}{4} + \ldots \tag{2.90}$$

It is noteworthy that $Q_{x,\text{integration}}$ is not any of the reactive power definitions discussed in Section 2.2. The harmonic components are reduced by a factor equivalent to its harmonic order. In the study performed by [11] using common distortion levels, $Q_{x,\text{integration}}$ was approximately equal to $Q_{1,x}$.

2.3.4 Positive Sequence Power Measurement Algorithms

It is known that performing FFT is computationally costly and that physical filters have limitations [128–130]. Therefore, we propose here the usage of v_a^+ and i_a^+ to measure P_1^+, Q_1^+, and PF_1^{+g}.

First, the phase "a" instantaneous positive sequence voltage is extracted with the proposed algorithm of [131] as follows,

$$v_a^+(t) = \frac{1}{3}\left[v_a(t) + v_b\left(t - \frac{2T}{3}\right) + v_c\left(t - \frac{T}{3}\right)\right]. \tag{2.91}$$

The instantaneous positive sequence current $i_a^+(t)$ is computed analogously. Then, it is assumed that P_1^+ is approximately equal to P^+, which is computed by (2.78). According to [11], $Q_{x,\text{integration}}$ and $Q_{x,\text{displacement}}$ are approximately equal to $Q_{1,x}$ under common distortion levels. So, Q_1^+ is estimated with the 90° displacement of voltage as

$$Q^+_{1,x,\text{displacement}} \approx \frac{3}{kT}\int_{\tau}^{\tau+kT} v_a^+\left(t - \frac{T}{4}\right)\cdot i_a^+(t)dt \tag{2.92}$$

or Q_1^+ is estimated with the voltage integration as

$$Q^+_{1,x,\text{integration}} \approx \frac{3\omega}{kT}\int_{\tau}^{\tau+kT}\left[\int v_a^+(t)dt\right] i_a^+(t)dt. \tag{2.93}$$

Having computed P_1^+ and Q_1^+, the value of PF_1^{+g} is obtained by

$$PF_1^{+g} = \frac{P_1^+}{\sqrt{(P_1^+)^2 + (Q_1^+)^2}}. \tag{2.94}$$

To obtain the value of PF_1^{+a} as

$$PF_1^{+a} = \frac{P_1^+}{S_{1,a} + S_{1,b} + S_{1,c}}, \tag{2.95}$$

it is necessary to calculate the fundamental RMS value of the voltage and current of each phase, which was achieved with the method proposed in [127].

CHAPTER 3

Methodology for Computational and Experimental Investigation of PF Fairness

In order to assess the fairness of each PF definition and measurement algorithm, we adopt the PF value measured with a given definition under balanced sinusoidal nominal voltages (at the point of connection of the load) as the reference for that PF definition. Each PF definition may have its own reference value, which may differ from others. It is expected that, if the load remains constant, a fair PF definition should retain its reference value even when the voltages are not balanced and sinusoidal anymore. With this viewpoint, the fairest PF definition to be applied in billing purposes is the one that changes only when the load changes. To evaluate the proposed definition of fairness, the methodology applied in the computational simulations is presented followed by the experimental tests. Lastly, the methodology to assess the accuracy of some measurement algorithms by means of a time-domain computational simulation is presented.

3.1 Computational Simulations of Power Factor Definitions from the Fairness Perspective

The computational simulations were performed with Matlab student license [132]. We simulated a set of unbalanced nonsinusoidal voltage conditions (UNVC) applied to the point of connection of a given load which is kept constant throughout the simulations. An electrical model is employed to compute the load's current and, consequently, the different PF definitions.

This work considers three different types of loads in the simulations. The first load is a constant impedance, following the literature trend [1, 12, 14, 31, 33, 37, 44, 45, 52, 95]. The second load is a TIM because, in the policies studied in Section 1.2, PF billing applies for medium and large customers, and the TIM represents approximately 65–70% of industries total energy consumption [133]. The third load is an unbalanced set of light-emitting diode (LED) lamps. In the following we present the specific details for each simulated load.

Table 3.1: Voltage Harmonics

Harmonic order	1	3	5	7
Magnitude [% of nominal]	100	2	3	1
Angle [degrees]	0	70	−90	−145

3.1.1 Constant Impedance Loads

Three-phase constant impedance loads can have distinct types of connections.In this work, we use delta-connected loads with the following values $Z_{ab} = Z_{bc} = Z_{ca} = 1\angle\cos^{-1}(0.95)$ pu, $Z_{ab} = Z_{bc} = Z_{ca} = 54\ \Omega$, and $Z_{ab} = 56\ \Omega$ and $Z_{bc} = Z_{ca} \to \infty$ (open circuit between phases "b"-"c" and "c"-"a"). This load is said to be constant if both the impedance magnitude and angle are constant.

The unbalanced voltage conditions used in the simulations and experimental tests are applied directly at the point of connection of the load. They consist of nil zero-sequence ($V^z = 0$), nominal positive-sequence ($V^+ = 1$ pu $= 220$ V) and several negative-sequence magnitudes (V^-) and angles (θ_1^-). All combinations of $V^- \in [0, 0.03]$ pu in steps of 0.0005 pu (61 values) and $\theta_1^- \in [0°, 345°]$ in steps of 15° (24 values) are considered. The angle θ^+ is zero in all cases, because it is the angular reference. The magnitude of V^- was chosen so that the maximum voltage unbalance factor (VUF), given by

$$\text{VUF} = \frac{V^-}{V^+}, \tag{3.1}$$

is equal to 3%, which is slightly higher than the VUF usual limits in existing regulations, but common in real distribution systems according to [83].

After defining the set of unbalanced conditions, the voltage harmonics described in Table 3.1 are superimposed proportionally to each of the system unbalanced voltages. According to [11], the third, fifth and seventh harmonics components (with their magnitude and angle values presented in Table 3.1) are typical for voltage distortions in power systems. Proceeding in this way, a total of 1 464 unbalanced nonsinusoidal voltage conditions (UNVC) are simulated.

3.1.2 Three-Phase Induction Motor

The simulated TIM is delta-connected, 220 V (line-to-line), 7.5 kW, 60 Hz and has six poles. It is modeled accordingly to [84,134] with the electrical parameters shown in Table 3.2. Figure 3.1 shows the electrical model of the motor, in which

$$s_h = \frac{hn_s - n_m}{hn_s}, \tag{3.2}$$

is the motor slip at frequency order h[1],

$$n_s = \frac{120f}{\text{poles}}, \tag{3.3}$$

is the motor synchronous speed, n_m is the rotor speed, in rotations per minute (r.p.m), and f is the system frequency in Hz. It is worth mentioning that s_h approaches 1 as h increases. For example, if a motor operates

[1]For concision purposes, we refer to the motor slip at the fundamental frequency if the order h is not specified.

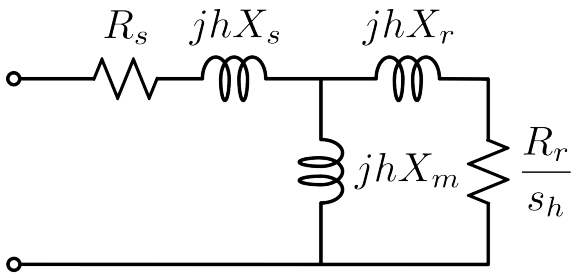

(a) Positive sequence.

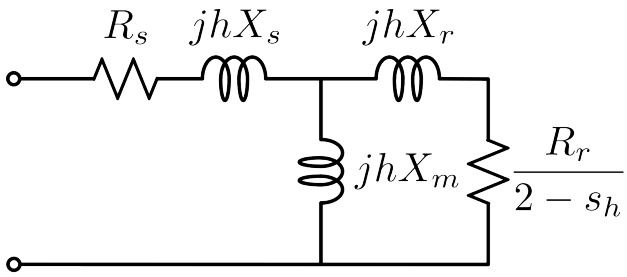

(b) Negative sequence.

Figure 3.1: Three-phase induction motor electrical model, having X_s, X_r and X_m measured at the fundamental frequency.

Table 3.2: TIM Equivalent Circuit Parameters at 60 Hz

Parameter	R_S	R_r	X_S	X_r	X_m
Value (Ω)	0.294	0.144	0.503	0.209	13.25

with $n_m = 1780$ rpm and $n_s = 1800$ rpm, then $s_1 = 0.01$ and $s_7 = 0.86$. This means that at higher harmonic orders, the active power transmitted to the shaft of the motor (which is proportional to the variable resistances R_r/s_h and $R_r/(2 - s_h)$) is lower than at the fundamental. Also, the closer s_h is to 1, the closer the positive and negative sequence models are to each other.

It should be highlighted that the motor operates a mechanical load with constant speed, meaning that s_1 is set to 1.5% for all conditions. Since the desired mechanical output is constant and the motor parameters are not modified throughout the simulations, the load can be considered constant from the customer's perspective. In fact, when the motor speed is constant, the electrical model simplifies to a special type of constant impedance load with admittance matrix given by

$$Y_h^{z+-} = \begin{bmatrix} 0 & 0 & 0 \\ 0 & \mathbf{Y_h^+} & 0 \\ 0 & 0 & \mathbf{Y_h^-} \end{bmatrix}, \tag{3.4}$$

where $\mathbf{Y_h^+}$ and $\mathbf{Y_h^-}$ are the equivalent positive and negative-sequence admittances, respectively. At last, the motor reactive power is partially compensated by balanced delta-connected capacitors so that its PF_{ref} is equal to 0.95.

The UNVC consists of positive, negative and zero sequence voltages with different magnitudes and angles. After defining the unbalanced conditions, a set of harmonics is applied proportionally to each phase. All combinations of $V^+ \in [0.9, 1.1]$ pu in steps of 0.05 pu and of V^- and $V^0 \in [0, 0.03]$ pu in steps of 0.005 pu are considered. These magnitudes were chosen so that the positive sequence is never greater or less than 10% of the nominal voltage and so that the maximum VUF (3.1) is below 3.5%, which is slightly higher than the VUF usual limits in existing regulations [83, 112]. In fact, a voltage unbalance between 1% and 3% is present in 32% of the distributions systems in the United States, according to [83]. In terms of standards, the European Standard EN 51060, for example, establishes that the VUF should be lower than 2% in 95% of 10 minutes periods, according to [83]. The angles θ^0 and θ^- used in the database range from 0 to 330° in steps of 30°.

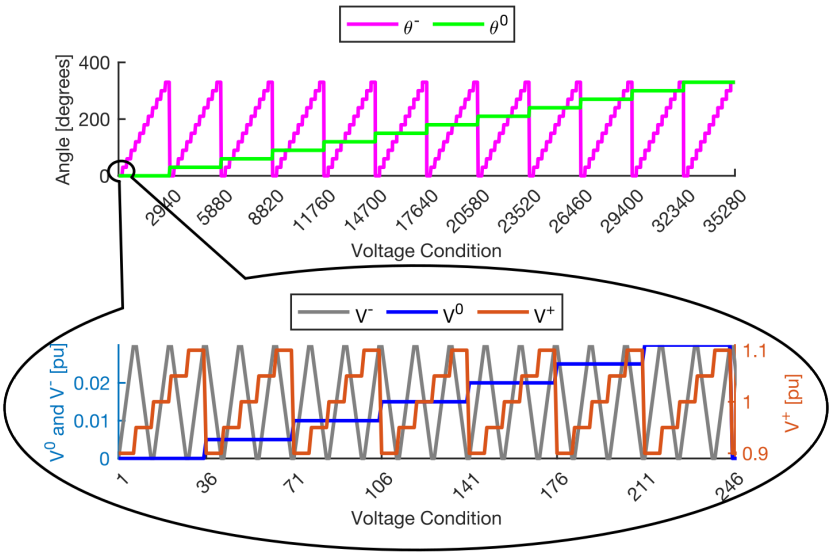

Figure 3.2: Set of unbalanced voltage conditions employed in the computational simulations of the TIM.

The angle θ^+ is zero in all cases, because it is the angular reference.

Figure 3.2 illustrates the set of unbalanced voltage conditions selected for the simulations. It is noteworthy that the first 245 conditions, shown in the bottom graph of Figure 3.2, refer to the variation of V^+, V^- and V^0, while keeping $\theta^- = \theta^0 = 0$. Then, the value of θ^- is changed and the 245 combinations of V^+, V^- and V^0 are repeated for this new value of θ^-. The last variable to change is θ^0. Combining all possible values of V^+ (5 different values), V^- (7), V^0 (7), θ^- (12), θ^0 (12), results in $5 \times 7 \times 7 \times 12 \times 12 = 35280$ different voltage conditions. After defining the set of unbalanced conditions, the voltage harmonics described in [11] are superimposed proportionally to each of the system unbalanced voltages. According to [11], the third, fifth and seventh harmonics components (with their magnitude and angle values presented in Table 3.1) are typical for voltage distortions in power systems. Proceeding in this way, a total of 35280 UNVC are simulated.

3.1.3 Unbalanced Non-linear load

The unbalanced non-linear load selected for analysis was a set of light-emitting diode (LED) lamps as shown in Figure 3.3 (a). The lamps are connected between a phase and the ground (grounded-wye). In each phase, all lamps are connected in parallel, so that they are submitted to the same voltages and the total current is simply the addition of each lamp's current. The load consists of 500 lamps at phase "a", 250 at phase "b" and 1 000 at phase "c". Each lamp was simulated using the electrical model provided in [135] and illustrated in Figure 3.3 (b). The parameters for the LED model are shown in Table 3.3. The same set of UNVC applied to the motor is applied to the unbalanced non-linear load.

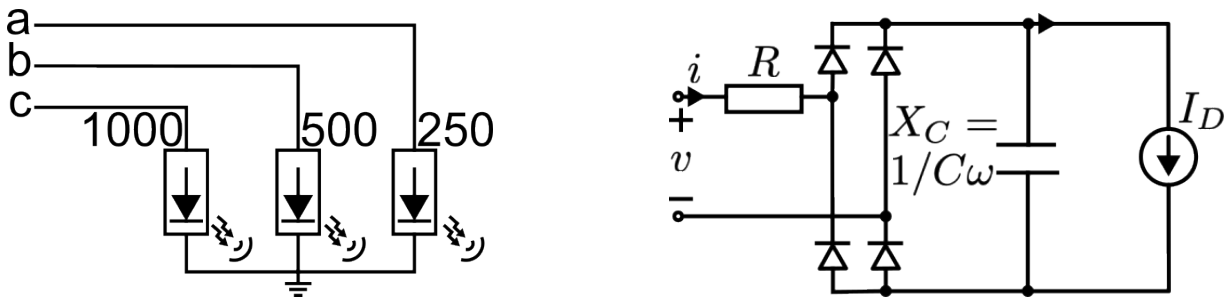

(a) (b)

Figure 3.3: (a)Unbalanced non-linear load consisting of LED lamps connected in grounded-wye configuration. (b) Electrical model for each LED lamp.

Table 3.3: Parameters for each LED lamp simulated.

Parameter	Value
R	22.26 Ω
C	3.04 μF
I_D	35 mA

3.2 Computational Simulations of Measurement Algorithms

Existing power meters can be categorized into analog (electromechanical) and digital (electronic) meters. Analog meters were prevalent in the very early applications but are prone to issues with loose electromechanical parts, dust accumulation and metal oxidation. With advancements in integrated circuits (ICs) and microcontrollers, digital meters have become more reliable and cost-effective compared to traditional analog meters [136]. The ongoing trend indicates that, as technology matures and becomes more affordable, digital meters will likely replace analog meters as the primary choice in facilities worldwide.

Figure 3.4 shows a very simplified diagram of a digital meter. The first stage of the meter is composed by current transformers (CT) and potential transformers (PT). Then, the analog signals are filtered and digitalized. Lastly, the digital signals serve as input for the metering algorithms implemented in a computing processing unit (CPU, encompassing various implementations such as microcontrollers) and the results are displayed by a human-machine (HM) interface.

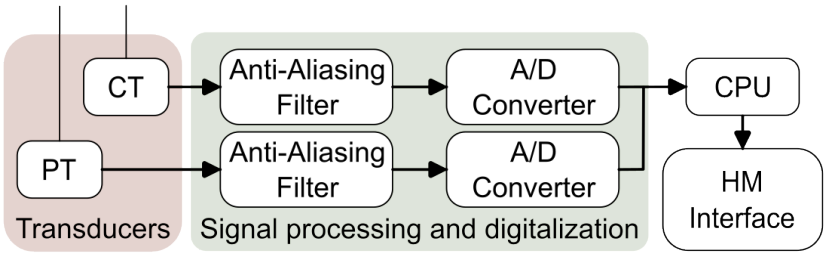

Figure 3.4: Simplified diagram of a digital meter.

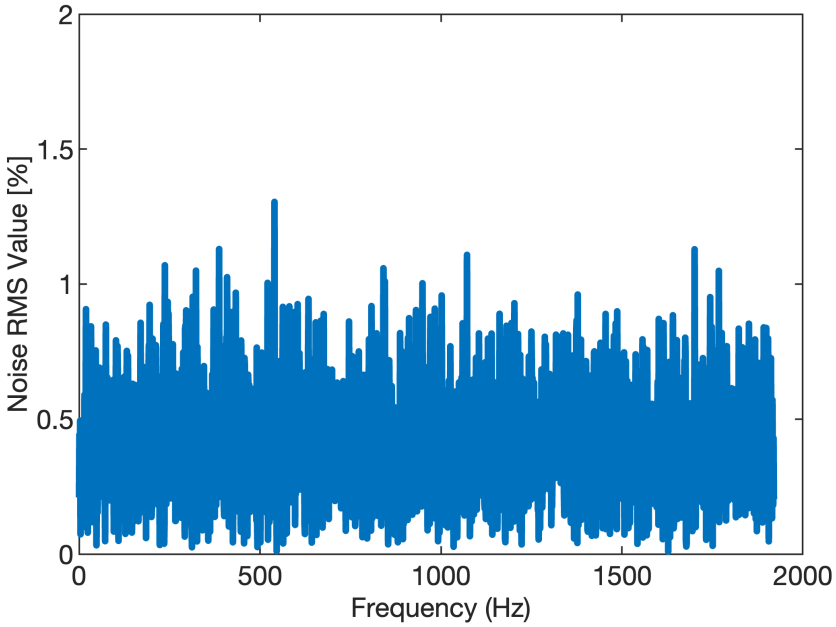

Figure 3.5: Voltage noise spectrum.

There are different algorithms for power metering that can be implemented in a CPU as shown in Section 2.3. Some of them, like those based on Fourier or Wavelet transforms, provide more accurate results at the cost of higher computational power, thus requiring more expensive CPUs. On the other hand, the 90° displacement of voltage and the voltage integration algorithms can be implemented with very low computational power, thus with cheaper CPUs, but at the cost of higher metering errors.

We have developed a digital simulation to evaluate the metering algorithms implemented in a CPU. For this purpose, the same loads and set of UNVC described in Section 3.1 are employed. The voltage and current waveforms are considered already filtered, sampled at a rate of 64 samples per cycle and digitalized. This means that we are not simulating an analog signal being filtered, sampled and digitalized. In fact, our evaluation considers the current and voltage signals that will serve as inputs to the CPU. A window of calculations of 1s is employed for each condition of the set of UNVC. In the case of instantaneous positive sequence components, values in the first cycle are not taken into account since the estimation process is only possible after two thirds of a cycle.

After the processes of filtering, sampling and digitalization, the current and voltage signals should be almost noiseless. However, depending on the quality of the meter's parts, the digitalized signal may still be contaminated with noise. In order to evaluate the effects of noise in the input signal of the metering algorithms, we simulate two sets of signals (with and without noise). We adopt an additive white gaussian noise (AWGN) with standard deviation of 0.2 pu, that is equivalent to a signal-to-noise ratio (SNR) of approximately 14 dB. For each UNVC a different AWGN signal is generated with the same sampling rate as the voltage and current signals. It is noteworthy that 64 samples per cycle in a 60 Hz system results in a sampling rate of $3,840$ Hz. Since the noise is white, the noise spectrum is almost flat for all frequencies evaluated from 0 to 1920 Hz, considering the Nyquist criteria. Figure 3.5 shows the noise spectrum RMS value in the voltage signal for one of the conditions. It is noteworthy that for each individual frequency the noise magnitude is lower than (1.5%), however the SNR is not as low due to the spread over all evaluated frequencies.

The following approximations are considered to compute PF_1^g and PF_1^{+g}. The harmonic active power is considered negligible with respect to the total fundamental active power [37, 137]. So, P_1 is measured applying (2.77). Similarly, P_1^+ is measured with (2.78). According to [11], the reactive power computed by the 90° displacement of voltage (2.79) and the voltage integration (2.85) methods is approximately equal to the fundamental reactive power considering common distortion levels.

To measure PF_1^{+a}, it is necessary to compute P_1^+ and S_1^{+a}. It is noteworthy that S_1^{+a} can be obtained using voltage and current RMS measurements or using active and reactive power measurements. Since we are already using P_1^+ and Q_1^+ to obtain PF_1^{+g}, we are going to use measurements of V_1^+ and I_1^+ to obtain PF_1^{+a}. For this purpose, the FFT-based method proposed in [127] is applied to $v^+(t)$ and $i^+(t)$ to extract the RMS value at the fundamental frequency. Then, S_1^{+a} is computed as

$$S_1^{+a} = 3V_1^+ I_1^+. \tag{3.5}$$

At last, the error (ΔPF) is computed as the difference between the PF measurement ($PF_{\text{meas.}}$) and the $PF_{\text{ref.}}$. In particular, the error for PF_1^g is

$$\Delta PF_1^g = PF_{1,\text{meas.}}^g - PF_{\text{ref.}}, \tag{3.6}$$

for PF_1^{+g} is

$$\Delta PF_1^{+g} = PF_{1,\text{meas.}}^{+g} - PF_{\text{ref.}}, \tag{3.7}$$

and for PF_1^{+a} is

$$\Delta PF_1^{+a} = PF_{1,\text{meas.}}^{+a} - PF_{\text{ref.}}, \tag{3.8}$$

where $PF_{1,\text{meas.}}^g$, $PF_{1,\text{meas.}}^{+a}$, and $PF_{1,\text{meas.}}^{+g}$ are computed with (2.65), (2.70), and (2.71), respectively.

3.3 Experimental Tests of Power Factor Definitions from the Fairness Perspective

The experimental tests were performed for both the constant impedance loads and the induction motor. Currently, it was not possible to evaluate the unbalanced non-linear load experimentally.

The basic setup consists of a computer, a controlled voltage source (California Instruments CSW 11110), a power quality analyzer (Elspec G4500 Blackbox) and the load being evaluated. A control algorithm was developed in the computer which allows to establish several unbalanced nonsinusoidal voltage conditions and the duration that each condition should be applied to the load. The algorithm automatically changes conditions after the specified time and it also reads the power quality measurements every three seconds. The computer controls the CSW 1110 by a serial cable RS232 protocol and controls the power quality analyzer by a serial cable using RS485 Modbus protocol.

Considering that each load requires adaptations to the basic setup described above and that a different set of UNVC was employed to each load, we provide the specific details regarding the experimental tests with the constant impedance load and the induction motor in the following sections.

(a) (b) (c)

Figure 3.6: Equipment used in the experimental setup. (a) Computer and controlled voltage source California Instruments CSW 11110. (b) Power quality meter Eslpec G4500 Blackbox. (c) Three-phase variable resistor.

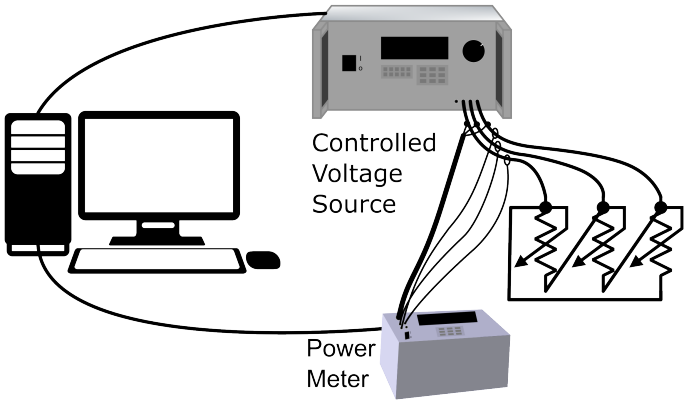

Figure 3.7: Experimental setup diagram for the constant impedance load.

3.3.1 Constant Impedance Load

For the constant impedance load, in addition to the basic setup described, it is also employed a three-phase variable resistor (from Micateck). Figure 3.6 show the equipment used for this load. Figure 3.8 shows a diagram of the experimental setup. The CSW 1110 applies the unbalanced and nonsinusoidal voltages defined to supply the three-phase variable resistor. The power quality analyzer is used to measure the voltage and the current phasors of each condition, which are then used by the computer to calculate the different PF definitions.

It is noteworthy that the same loads and set of UNVC employed in the simulations of the constant impedance load (see section 3.1.1) is also employed in the experimental tests.

3.3.2 Three-Phase Induction Motor

The experimental setup consists of a controlled voltage source (California Instruments CSW 11110), a power quality analyzer (Elspec G4500 Blackbox), a speed sensor, a 4 kW DC generator, a variable resistor (from Micateck) and a 1,5 kW three-phase squirrel cage induction motor (4 poles, 60 Hz, 220 V and delta-connected).

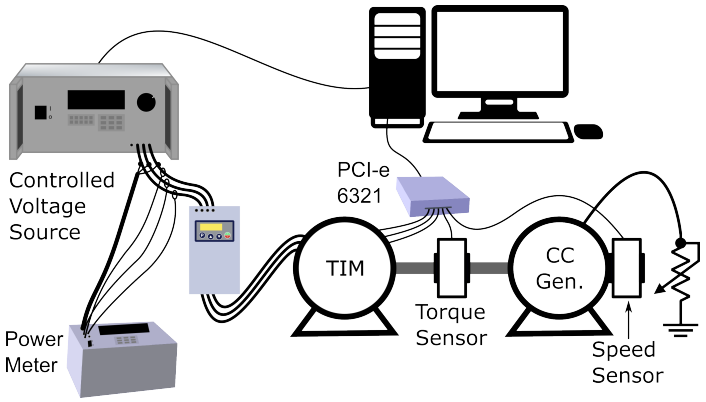

Figure 3.8: Connections of the equipment used in the experimental setup for the three-phase induction motor.

Figure 3.9: Motor and CC generator with coupled shafts employed in the experimental tests

The CSW 1110 supplies the motor with unbalanced and nonsinusoidal voltages. The motor drives the DC generator, which feeds the variable resistor. The DC generator and the variable resistor, working together, emulate a mechanical load in the motor shaft. The variable resistor is adjusted so that the motor operates with nominal power. A speed sensor is used to check if the motor speed was constant throughout the experiment. The power quality analyzer measures voltage and current phasors every 3 seconds. These measurements are then employed in the computer to obtain the PF value of each definition. The connections between the equipment are shown in Figure 3.8. Figure 3.9 shows the motor and the CC generator with their shafts coupled by a torque sensor.

The experimental tests were elaborated in order to assess the validity of the conclusions drawn from the simulations study. For this purpose, the evaluation of the PF definitions was performed with a TIM (different from the one used in the simulations) operating close to nominal power and with different supply conditions (another collection of VUF values, harmonic spectra, and distortion levels). In the construction of the set of unbalanced voltages, 9 values of V^+ are taken into consideration, starting from 0.86 up to 1.06 in steps of

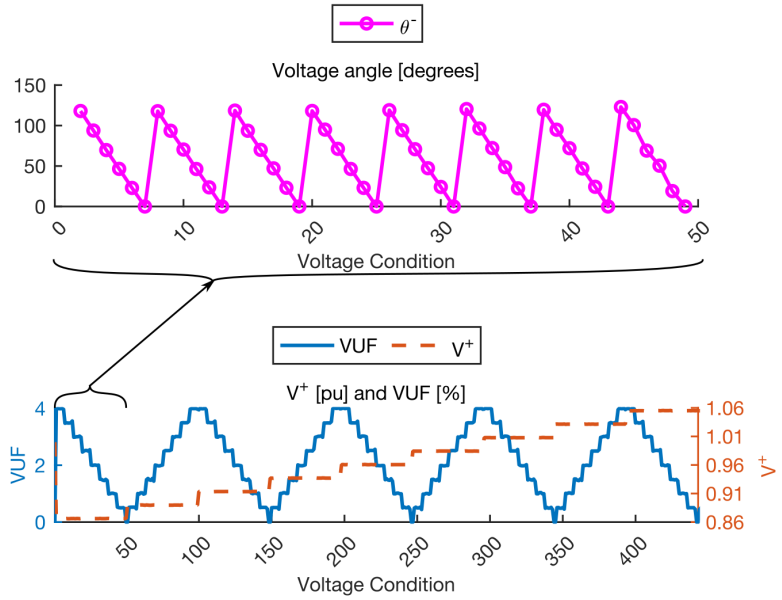

Figure 3.10: Set of unbalanced voltage conditions employed in the experimental tests.

0.025 pu. For each value of V^+, the following scenarios are evaluated: 8 with VUF $\in [0.5, 4]\%$ in steps of 0.5%, and 6 with $\theta^- \in [0°, 120°]$ in steps of 24°; resulting in $9 \times 8 \times 6 = 432$ unbalanced conditions. Additionally, the 10 balanced scenarios with nil VUF and $V^+ \in [0.86, 1.06]$ in steps of 0.025 pu and with $V^+ = 1$ pu are considered, leading to a set of 442 conditions, which are shown in Figure 3.10. First, different values of θ^- are combined with a given value of V^+ and VUF. Then, the value of VUF changes and the variation of θ^- is repeated. At last, after evaluating different values of VUF and θ^- for a given value of V^+, we change the value V^+ and repeat the process.

For the harmonics, it is considered the pairs of harmonics: (third, fifth), (third, seventh), and (fifth, seventh). Individual distortion levels of 2%, 5% and 8% are considered for each pair of harmonics. In total, 9 harmonic conditions are considered. The final set of supply scenarios is obtained by the combination of the 442 voltage unbalance values with the 9 harmonic distortion values. Applying combinatory analysis, the total set of 442×9 =3978 conditions is applied to the motor for 30 seconds each.

After running the experiment, we noticed that the motor speed (consequently, the motor slip) was not constant during the simulation. Figure 3.11 shows the motor slip as a function of the VUF. It can be observed that the motor slip varied from 2% up to 3.2% throughout the test. Additionally, it seems that the VUF did not significantly affect the motor slip. Given that we want to consider the motor as a constant load from the customer's perspective, we want to evaluate conditions in which the motor slip is approximately constant. For this purpose, we selected the intermediate value of 2.5% slip with ±0.1% tolerance. 901 conditions met the criteria and were selected to perform the analysis.

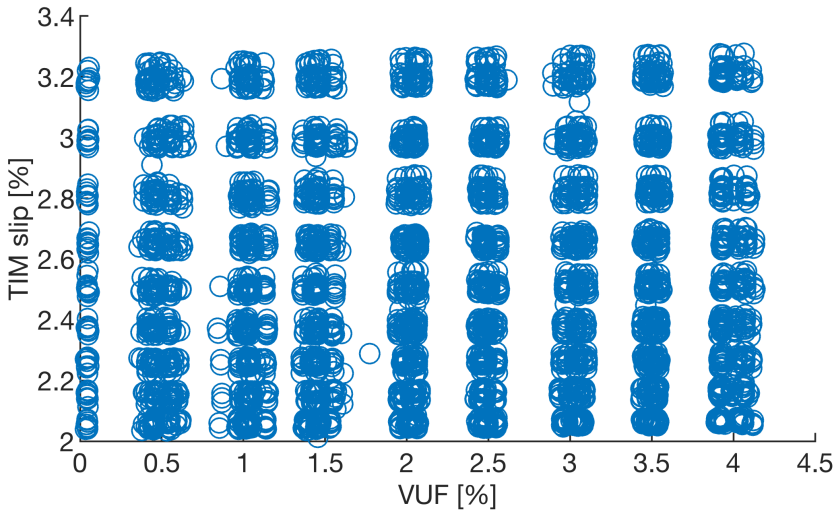

Figure 3.11: TIM slip as a function of the VUF with experimental data (THD of 2%, 5%, and 8%).

CHAPTER 4

Computational Evaluation of Power Factor Definitions and Measurement Methods

4.1 Computational Evaluation of Power Factor Definitions from the Fairness Perspective

This chapter presents the findings of the computational simulations considering the fairness perspective. The results for each load is presented in a separate section. Lastly, the chapter's conclusions are summarized.

4.1.1 Balanced Constant Impedance Loads

4.1.1.1 Per-phase Power Factor Definition

After running the computational simulations of 1 464 voltage conditions applied to both balanced constant impedance loads, the voltage and current phasors were obtained for each condition. Figure 4.1 shows the results for the $PF_{1,a}$ as a function of the VUF for the load having $Z_{ab} = Z_{bc} = Z_{ca} = 1\angle\cos^{-1}(0.95)$ pu. It can be observed that $PF_{1,a}$ is not affected by the voltage unbalance and it was equal to the reference PF. The same result was obtained for phases "b" and "c".

4.1.1.2 Three-phase Power Factor definitions

The three-phase PF definitions were computed and are shown in Figure 4.2 as a function of the VUF for the load having $Z_{ab} = Z_{bc} = Z_{ca} = 1\angle\cos^{-1}(0.95)$ pu. It is noteworthy that $PF_1^g = PF_1^e = PF_1^a = PF_1^+ = PF_{\text{ref}} = 0.95$ for all simulated values of VUF. Analogous results were obtained for the load having $Z_{ab} = Z_{bc} = Z_{ca} = 54\ \Omega$, with the difference that the reference value of each definition was equal to 1.

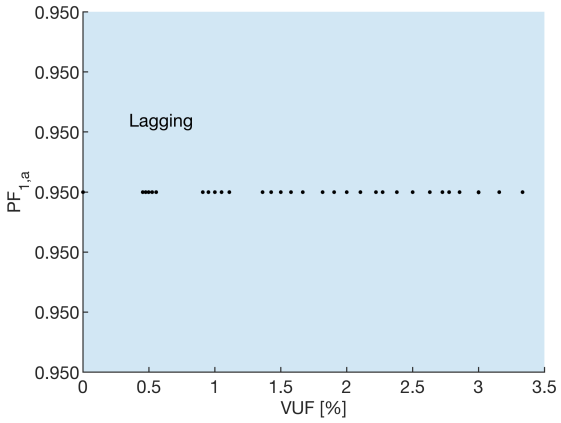

Figure 4.1: $PF_{1,a}$ of the delta-connected balanced constant impedance load, having $Z_{ab} = Z_{bc} = Z_{ca} = 1\angle\cos^{-1}(0.95)$ pu, as a function of VUF with simulated data (THD of 3.74%).

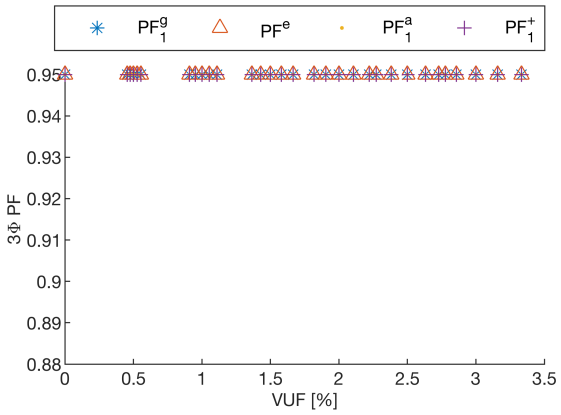

Figure 4.2: Different 3ϕ PF definitions computed for the balanced constant impedance load, having $Z_{ab} = Z_{bc} = Z_{ca} = 1\angle\cos^{-1}(0.95)$ pu, as a function of the VUF with simulated data (THD of 3.74%).

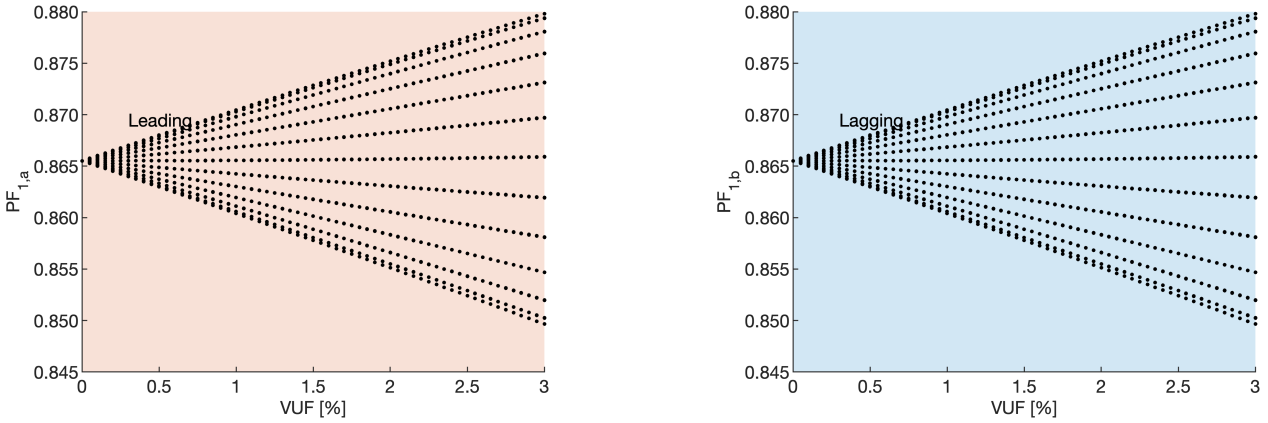

(a) (b)

Figure 4.3: Per Phase PF of the unbalanced resistive load as a function of VUF with simulated data. (a) $PF_{1,a}$. (b) $PF_{1,b}$.

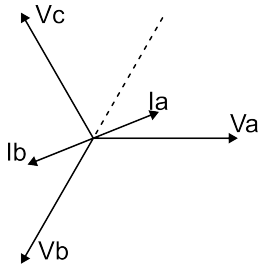

Figure 4.4: Phasor diagram for the voltages and currents of the unbalanced resistive load.

4.1.2 Unbalanced Constant Impedance Loads

For the unbalanced constant impedance load, in balanced sinusoidal conditions some PF definitions have distinct values [13, 14, 95, 97]. So, it is expected that they may also provide different values in unbalanced nonsinusoidal conditions. For this reason, the results for each PF definition are presented next. At last, a comparative analysis is performed to summarize the findings of the simulation.

4.1.2.1 Fundamental Per-Phase Power Factor

Figure 4.3 shows the fundamental PF for phases "a" and "b" as a function of the VUF with the simulated data. It is not possible to compute $PF_{1,c}$ because the current at phase "c" is zero. Analyzing Figure 4.3, it can be observed that in this case both $PF_{1,a}$ and $PF_{1,b}$ have a unique value of 0.866 when the VUF is equal to zero. When the VUF is greater than zero, there are several different values of $PF_{1,a}$ and $PF_{1,b}$ for a given VUF and $PF_{1,a}$ is always leading, whereas $PF_{1,b}$ is lagging[1]. As the VUF increases, the range of values of $PF_{1,a}$ and $PF_{1,b}$ also increases.

[1]It is worth recalling that there are several voltage conditions which lead to the same VUF. In the particular case of this work, for each VUF there are 24 different values for the angle of the negative-sequence voltage, resulting in 24 different voltage conditions. Also, there are some overlapping points in Figure 4.3.

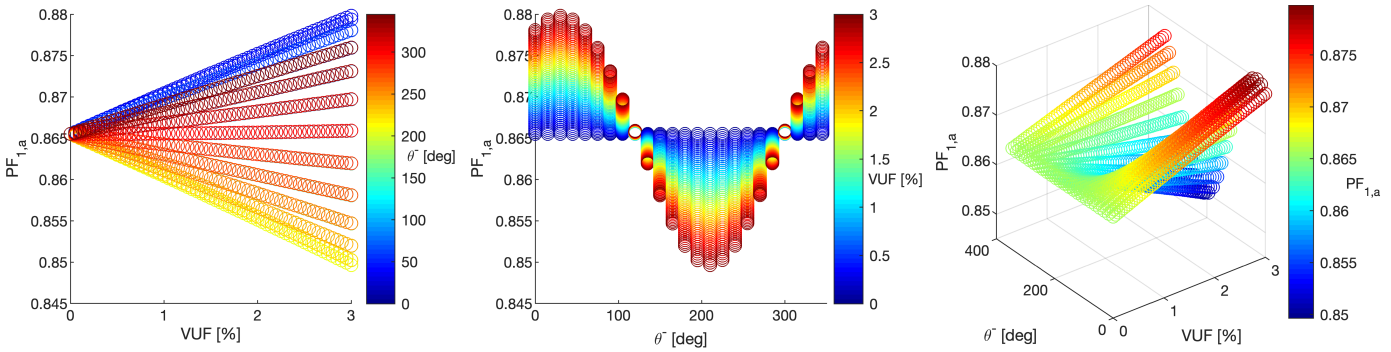

(a) (b) (c)

Figure 4.5: Per Phase PF of the unbalanced resistive load with simulated data. (a) 2D scatter plot of $PF_{1,a}$ as a function of VUF with the θ_1^- as the colorbar. (b) 2D scatter plot of $PF_{1,a}$ as a function of θ_1^- with the VUF as the colorbar. (c) 3D scatter plot of $PF_{1,a}$ as a function of the VUF and θ_1^- $PF_{1,a}$ as the colorbar.

The fact that $PF_{1,b}$ is lagging and $PF_{1,a}$ is leading can be partially explained by the special asymmetry of the load, which causes phase "a" current to be the negative of phase "b" current and phase "c" current to be equal to zero. As shown in Figure 4.4, if the phase shift between the fundamental voltage and current at phase "a" is lower than the complementary of the phase shift between the fundamental voltages at phases "a" and "b", it is expected that the fundamental PF at each phase will have opposite "signs" (one leading and the other lagging). It is noteworthy that, although the currents of phases "a" and "b" have equal absolute value, the fundamental PF at each phase may have different values. In general, as the current comes near to the voltage in phase "a" (increasing $PF_{1,a}$), the opposite happens with the voltage and current at phase "b", that is, they move away from each other, thus decreasing $PF_{1,b}$.

Figure 4.5 shows the scatter plot of $PF_{1,a}$ as a function of both the VUF and the negative-sequence voltage angle (θ_1^-). It can be observed that $PF_{1,a}$ is affected by both the VUF and θ_1^-. When the VUF is equal to zero, $PF_{1,a}$ had only one value equal to its reference (0.866). When the VUF increases, $PF_{1,a}$ may have different values for the same VUF depending on the value of θ_1^-. In Figure 4.5 (b), for a given value of the VUF (equivalently for a given color in the graph), it can be observed an approximately sinusoidal dependence of $PF_{1,a}$ with respect to θ_1^-, in which the VUF appears to increase the amplitude of the sine. The result of considering different values for the VUF is a stack of these sine-shaped curves. The curve shows that for the VUF greater than zero, there are two values of θ_1^- (120° and 300°) which lead to $PF_{1,a}$ values equal to the reference. Conversely, for certain values of θ_1^- (approximately between $[0°, 120°]$ and $[300°, 360°]$), an increase in the VUF results in an elevation of $PF_{1,a}$. Likewise, certain θ_1^- values (approximately within $[120°, 300°]$) result in a decline of $PF_{1,a}$ as the VUF increases.

4.1.2.2 Three-phase Power Factor definitions

Figure 4.6 shows the scatter plot for each three-phase PF definition computed for the unbalanced resistive load as a function of the VUF with simulated data. Due to the load asymmetry, the PF definitions have different reference values measured under balanced sinusoidal nominal voltage conditions. Considering that there are different PF references, it is necessary to evaluate each PF definition separately with respect to its

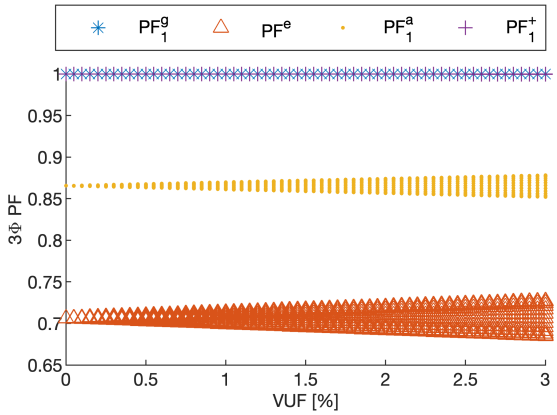

Figure 4.6: 3ϕ PF definitions computed for the unbalanced load as a function of the VUF with simulated data.

reference. When the VUF is equal to zero, PF_1^g and PF_1^+ are equal to their reference PF value of 1. Similarly, PF_1^a is equal to its reference of 0.866, which is the same value obtained for the reference of $PF_{1,a}$. These definitions (PF_1^g, PF_1^+, and PF_1^a) consider only the fundamental component. For this reason, their value under balanced nonsinusoidal nominal voltage is equal to their reference. Although PF^e considers all voltage harmonics, its value when the voltage is balanced is approximately equal to its reference (0.707). When the VUF is greater than zero, PF_1^g and PF_1^+ have the same value as their reference, that is 1, for all voltage conditions, being therefore unaffected by the VUF. On the other hand, there are several voltage conditions that lead to different values of PF_1^a and PF^e. As a matter of fact, the values of PF_1^a are very similar to those obtained for $PF_{1,x}, x \in [a, b]$. The variations of PF_1^a and PF^e around their reference values (0.866 and 0.707, respectively) are approximately symmetrical and increase with the VUF. The highest and lowest values obtained for PF_1^a are 0.879 and 0.853, and for PF^e are 0.728 and 0.686. Comparing PF^e with PF_1^a, it can be observed that the variation (in terms of absolute values) of PF^e is higher than the observed for PF_1^a, that is 0.042 against 0.026. Also, in the obtained results $PF^e \leq PF_1^a \leq PF_1^g = PF_1^+$ independently of the VUF.

Considering that PF^e and PF_1^a had multiple values for the same VUF, a detailed analysis of these two definitions is provided next.

Figure 6.1 and 4.8 show the scatter plot of PF^e and PF_1^a, respectively, as a function of the VUF (or equivalently V^-, since V^+ was equal to 1) and the negative-sequence voltage angle (θ_1^-). It can be observed that the results are analogous to those obtained with $PF_{1,a}$ in Figure 4.5. In both cases, the graphs show a sinusoidal dependence with respect to θ_1^-, being the VUF the sine amplitude.

When the VUF is equal to zero, PF^e and PF_1^a have only one value approximately equal to their reference values of 0.707 and 0.866, respectively. When the VUF is greater than zero, there are two values of θ_1^- (approximately 150° and 330°) which lead to PF^e and PF_1^a being equal to their references. Also, there are some values of θ_1^- (between $[0°, 150°]$ and $[330°, 360°]$, approximately) in which an increase of the VUF leads to higher PF^e and PF_1^a. Likewise, there are some values of θ_1^- (between 150° and 330°) in which an increase of the VUF results in a decrease of PF^e and PF_1^a.

The results obtained also allow comparing unbalanced and balanced loads. It was shown in subsection 6.3.1 that for balanced constant impedance loads the PF definitions investigated provided the same constant value independently of the VUF. On the other hand, for the unbalanced load, $PF_{1,x}, x = a, b, c$, PF^e, and PF_1^a

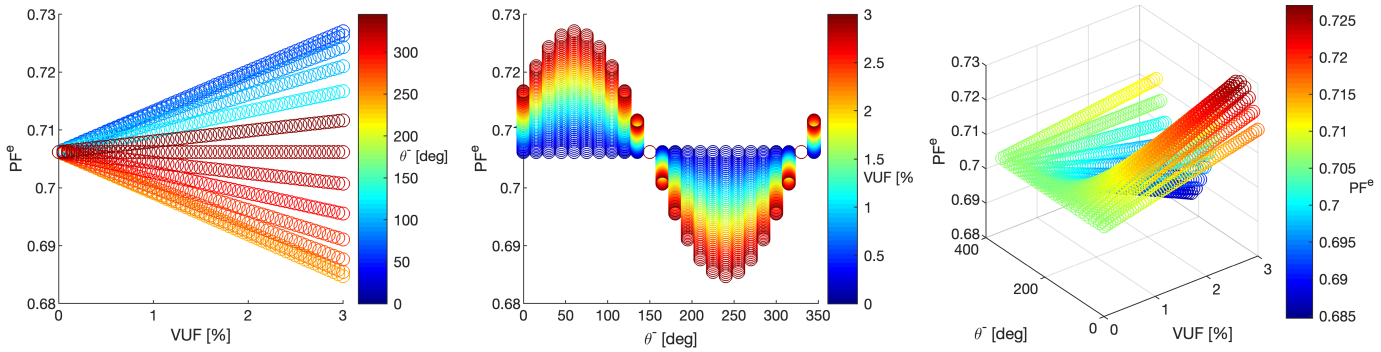

Figure 4.7: PF^e of the unbalanced resistive load with simulated data. (a) 2D scatter plot of PF^e as a function of VUF with the θ_1^- as the colorbar. (b) 2D scatter plot of PF^e as a function of θ_1^- with the VUF as the colorbar. (c) 3D scatter plot of PF^e as a function of the VUF and θ_1^- with PF^e as the colorbar.

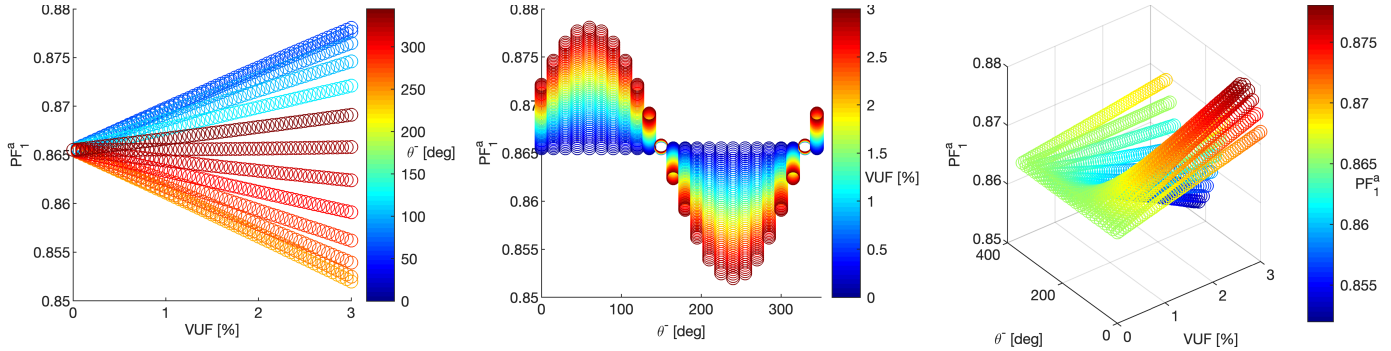

Figure 4.8: PF_1^a of the unbalanced resistive load with simulated data. (a) 2D scatter plot of PF_1^a as a function of VUF with the θ_1^- as the colorbar. (b) 2D scatter plot of PF_1^a as a function of θ_1^- with the VUF as the colorbar. (c) 3D scatter plot of PF_1^a as a function of the VUF and θ_1^- with PF_1^a as the colorbar.

were sensitive to the voltage unbalance because each of them had multiple values for a given VUF greater than zero. In particular, there were several values of PF^e when the VUF was greater than zero. The spreading of PF^e was symmetrical around the value measured at zero VUF and it increased with the VUF. In the case of the unbalanced load, it can be concluded that the proposed equivalence by the effective PF is not always true when the VUF is greater than zero, because the PF^e of the balance load is unaffected by the VUF while the PF^e of the unbalanced load is affected by the VUF. As a matter of fact, the two loads had the same PF^e only when θ^- was equal to 150° or 330°.

Table 6.2 summarizes the values obtained in the simulations for each PF definition. The results obtained allow comparing a specific PF definition when applied to unbalanced and balanced loads by comparing the values along the same row of Table 6.2. Selecting a column and comparing the values across rows allows comparing the application of different PF definitions for the same load and voltage condition.

Comparing the PF definitions for the same load, it can be observed that all the investigated definitions yield the same result for the balanced load independently of the voltages applied. For the unbalanced load under

Table 4.1: Summary of the simulation results.

	Balanced Load		Unbalanced Load	
	Balanced Voltages	Unbalanced Voltages	Balanced Voltages	Unbalanced Voltages
$PF_{1,a}$	1	1	0.866	$[0.850, 0.880]$
PF_1^a	1	1	0.866	$[0.853, 0.879]$
PF_1^g	1	1	1	1
PF_1^+	1	1	1	1
PF^e	1	1	0.707	$[0.686, 0.728]$

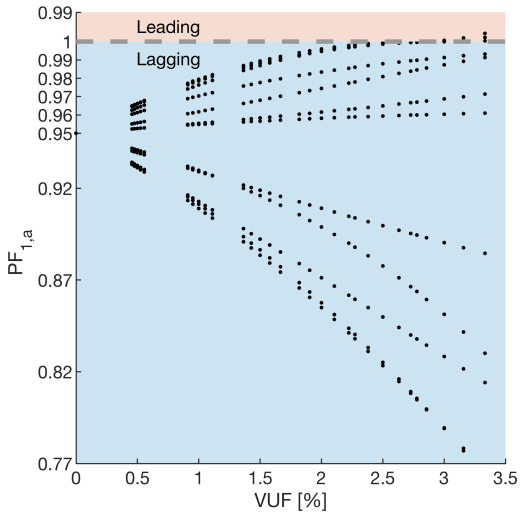

Figure 4.9: $PF_{1,a}$ of the TIM as a function of VUF with simulated data (THD of 3.74%).

balanced voltage conditions, the fundamental per-phase PF have the same value as the fundamental arithmetic PF. The fundamental geometric and positive-sequence PFs have the same value of 1 (equal to the balanced load). In this case, the following inequality holds $PF_1^g = PF_1^+ \geq PF_{1,a} = PF_1^a \geq PF^e$. For the unbalanced load under unbalanced voltage conditions, the fundamental per-phase PF, the fundamental arithmetic PF and the effective PF are significantly affected by the voltage unbalance and they do not have a unique value. The highest variation was observed for PF^e (0.042), followed by $PF_{1,a}$ (0.03) and PF_1^a (0.026).

4.1.3 Three-Phase Induction Motors

4.1.3.1 Per-phase Power Factor Definitions

Figure 4.9 shows a scatter plot of $PF_{1,a}$ as a function of the VUF for all 35280 conditions of the database. Many of these conditions result in the same pair of VUF and PF values, leading to the superimposition of points in the graph. From Figure 4.9, it can be observed that $PF_{1,a}$ can have different values for the same

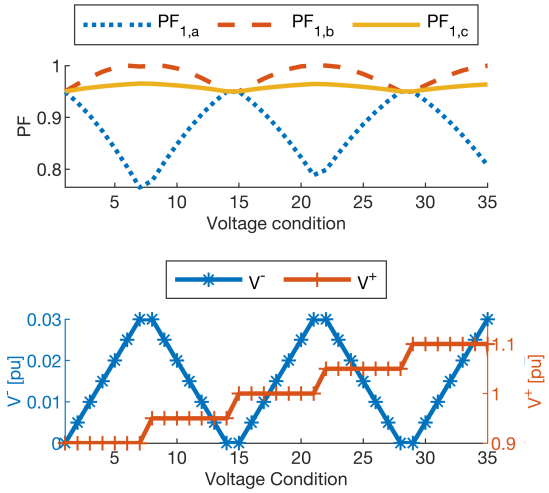

Figure 4.10: TIM $PF_{1,x}, x = a, b, c$ values for the first 35 unbalanced nonsinusoidal voltage conditions simulated ($\theta^- = \theta^0 = V^0 = 0$, and THD of 3.74%).

Table 4.2: TIM Fundamental Power Factor per phase for two conditions.

Condition	$PF_{1,a}$	PF_{1B}	PF_{1C}
$V_1 = 1\angle 0$ $V_2 = 0.01\angle 0$	0.91	0.97	0.96
$V_1 = 1\angle 0$ $V_2 = 0.01\angle 30°$	0.96	0.97	0.91

VUF. For instance, a 1.5% VUF results in $PF_{1,a}$ values ranging from 0.88 lagging up to 0.99 lagging. For a VUF of 3%, there are conditions that lead to $PF_{1,a}$ values in between 0.8 lagging and 0.999 leading. Therefore, it can be concluded that the interval of possible values for $PF_{1,a}$ increases with the VUF. Additionally, leading PF is unacceptable in some regulations as shown in Section 1.2.

The results for phases "b" and "c" are analogous to those presented for phase "a" in Figure 4.9. From Figure 4.10, which shows $PF_{1,x}, x = a, b, c$ for the first 35 UNVC, it can be observed that each phase have a different PF value for each condition. In these first 35 conditions ($\theta^- = \theta^0 = V^0 = 0$), $PF_{1,a} \leq PF_{1,c} \leq PF_{1,b}$. However, for a different value of θ^- the relation between the values of $PF_{1,a}$, $PF_{1,c}$, and $PF_{1,b}$ may change, as shown in Table 4.2, which presentes two different conditions with 1% VUF. In the first, $\theta^- = \theta^0 = V^0 = 0°$ and $PF_{1,a} \leq PF_{1,c} \leq PF_{1,b}$. In the second, $\theta^0 = V^0 = 0$ and $\theta^- = 30°$ and $PF_{1,c} \leq PF_{1,a} \leq PF_{1,b}$.

In order to assess the VUF associated with conditions that causes charges in at least one of the phases, the minimum value of the fundamental PF between phases ($PF_{1\text{min}}$) is computed for each condition, and is shown in Figure 4.11.

Similarly to $PF_{1,a}$ shown in Figure 4.9, there are conditions with the same VUF that leads to different values of $PF_{1\text{min}}$ as shown in Figure 4.11. The range of possible values also increases with the VUF. From Figure 4.11, it can be observed that for a VUF of 1% there are some conditions conducting to $PF_{1\text{min}} < 0.92$, which means that $PF_{1,x}$, $x = a, b, c$ is lower than 0.92 in at least one of the phases. For VUF equal or greater

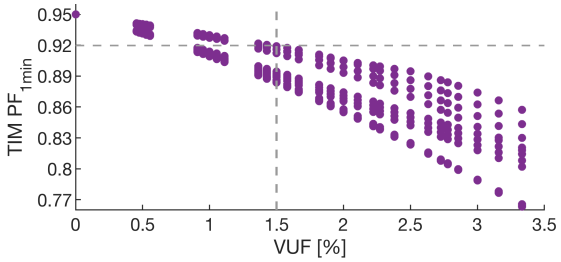

Figure 4.11: $PF_{1\text{min}}$ of the TIM as a function of VUF with simulated data (THD of 3.74%).

than 1.5%, all simulated conditions yielded $PF_{1\text{min}} < 0.92$, meaning that at least one phase $PF_{1,x}$, $x = a, b, c$ is lower than the commonly acceptable value of 0.92. In both situations, the VUF is still within the usually acceptable limit of 2% [83], and the utility has no obligation to improve the supply quality. Nonetheless, the existing unbalance in the grid may result in PF charges if a per phase charging is applied or if $PF_{1\text{min}}$ is utilized as the three-phase definition.

Summarizing, there are several conditions with the same VUF yielding different $PF_{1,x}$ values. Some conditions can even result in leading PF, which is unacceptable in some regulations as shown in Section 1.2. Moreover, when the VUF is equal or greater than 1.5%, at least one of $PF_{1,x}$, $x = a, b, c$ is less than 0.92. What stands out is that the customer's load was held constant with PF_{ref} equal to 0.95. Therefore, these approaches are not suitable for billing purposes of TIMs.

4.1.3.2 Three-phase Power Factor Definitions

Figure 4.12 shows the scatter plot for each definition computed for the TIM against the respective VUF associated with the supply condition. First, it should be noted that for balanced conditions, PF_1^a, PF_1^g, PF^e and PF_1^+ are equal to the reference value of 0.95. For unbalanced conditions, it can be observed that PF_1^a and PF^e are lower than PF_{ref}. For unbalance close to 2.5%, their values are lower than 0.92 and the customer may be penalized. Also, PF_1^a can have different values for the same VUF. Similarly to the per phase $PF_{1,a}$ presented in Section 4.1.3.1, the range of possible values for PF_1^a increase with the VUF. So, neither PF_1^a nor PF^e are suitable for billing purposes given their sensitivity to the VU. On the other hand, both PF_1^g and PF_1^+ are approximately constant and equal to PF_{ref}. Therefore, PF_1^g and PF_1^+ are recommended for revenue purposes.

We also performed a simulation with the TIM considering fixed values of VUF equal to 1.5% and 2%. The harmonics are kept with the same angle and proportion to each other. The THD varies from 3.74% up to 8%. Figure 4.13 (a) shows the results obtained for the investigated PF definitions as a function of the THD considering VUF of 1.5%. It can be noticed that PF_1^g, PF_1^a, and PF_1^+ are not significantly affected by the variation of the THD because these definitions are based on the fundamental components of voltage and current. On the other hand, the increase of the THD reduced the value of the PF^e. This makes sense because the THD increases the RMS value of the voltage and current, consequently increasing the effective apparent power. As a result, the PF^e decreases with respect to the THD increase. At last, it is worthy mentioning that the definitions do not have the same values because of the VUF equal to 1.5%. Similar results are observed with VUF equal to 2%, as shown in Figure 4.13.

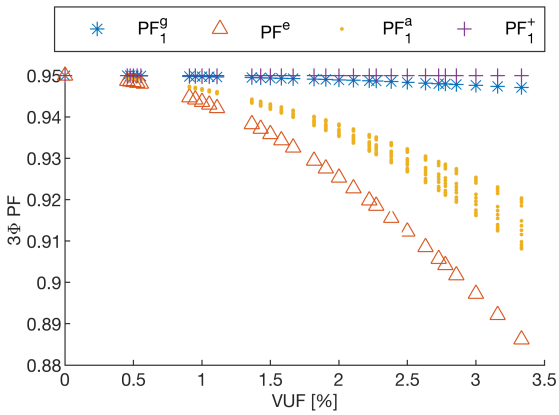

Figure 4.12: Different 3ϕ PF definitions computed for the TIM as a function of the VUF with simulated data (THD of 3.74%).

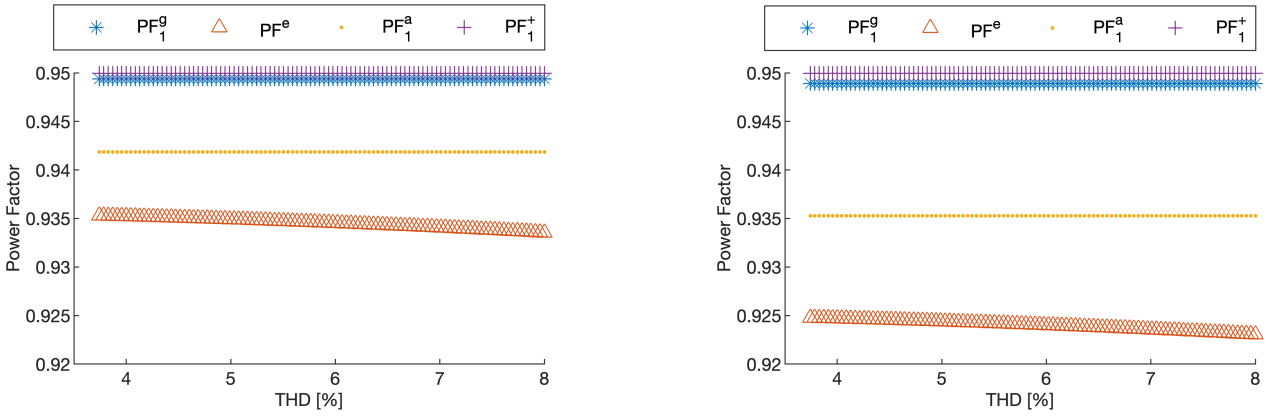

(a) VUF of 1.5%

(b) VUF of 2%

Figure 4.13: Different 3ϕ PF definitions computed for the TIM as a function of the THD with simulated data.

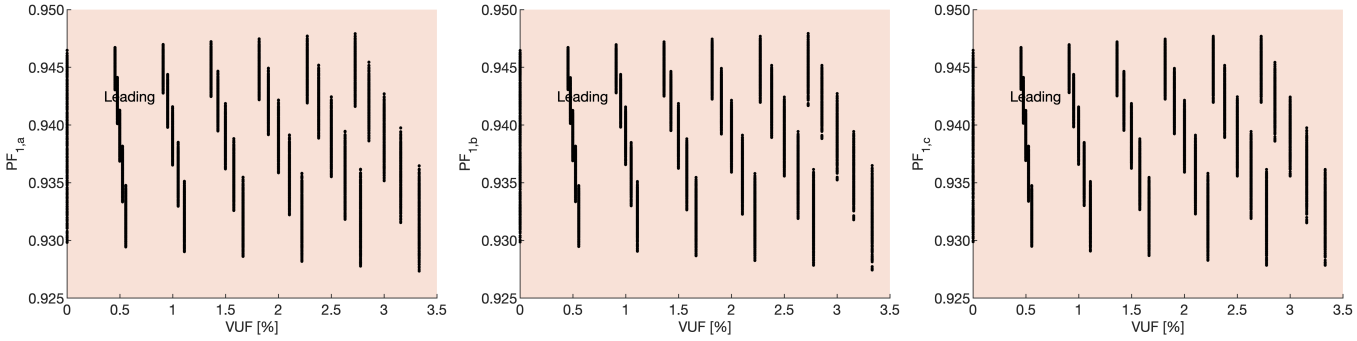

(a) $PF_{1,a}$ (b) $PF_{1,b}$ (c) $PF_{1,c}$

Figure 4.14: Per Phase PF of the LED load as a function of VUF with simulated data (THD of 3.74%).

Summarizing, PF_1^a and PF_1^e were shown to be significantly affected by the VUF. With VUF of 2%, their values were already below 0.92 and the customer may be penalized. Also, PF_1^a can have different values for the same VUF. The range of possible values of PF_1^a is shown to increase with the VUF. With respect to different THD values, PF^e is the most affected definition. Hence, PF_1^a and PF_1^e are not suitable for billing purposes of TIMs. On the other hand, PF_1^g and PF_1^+ were constantly close to the PF_{ref} independently of the VUF and THD. Therefore, PF_1^g and PF_1^{+g} are recommended for billing purposes of TIMs.

4.1.4 Light Emitting Diodes (LEDs)

4.1.4.1 Fundamental Per-Phase Power Factor

Figure 4.14 shows the fundamental PF for phases "a", "b", and "c" as a function of the VUF with the simulated data having THD of 3.74%. It can be observed in Figure 4.14 that all phases had the same PF behavior. So, the analyzes of $PF_{1,a}$ applies to the other phases. $PF_{1,a}$ is always leading and there are several different values of $PF_{1,a}$ when the VUF is equal to zero. As the VUF increases, the range of values of $PF_{1,a}$ also slightly increases.

One may ask why $PF_{1,a}$ have multiple values even when the VUF is zero. This can be explained due to the reference point of voltage measurement. If a common point is selected as a reference for all voltage measurements, this point acts as a common mode voltage component, which can be computed based on the zero sequence voltage. As the reader may recall, the voltage dataset employed in this simulations (the same employed for the TIM) contains 7 different values of V^z, starting from 0 to 0.03 pu in steps of 0.005 pu. Also, the dataset contains 12 different values for the zero sequence angle, θ^z, starting from 0 to 330° in steps of 30°. Since the zero sequence voltage component affects all phases in the same way, any changes in this component is equivalent to changing the reference point of measurement. As a result, all PF definitions that are affected by the choice of the reference point of measurement will be affected by the value of V^z and θ^z. It is noteworthy that this behavior was not observed for the TIM, even though the same set of UNVC was employed.

In order to visualize the effects of V^z, Figure 4.15 shows $PF_{1,a}$ of the set of LED lamps as a function of V^z with the VUF equal to zero. It can be observed that for V^z equal to zero and the VUF equal to zero, there are different values for $PF_{1,a}$ according to the positive-sequence voltage magnitude V^+. For each value of V^+,

the range of value of $PF_{1,a}$ increases with V^z. It is noteworthy that this spread of the values of $PF_{1,a}$ occurs symmetrically around the value measured with V^z equal to zero. Also the spread of $PF_{1,a}$ does not appear to be affected by V^+.

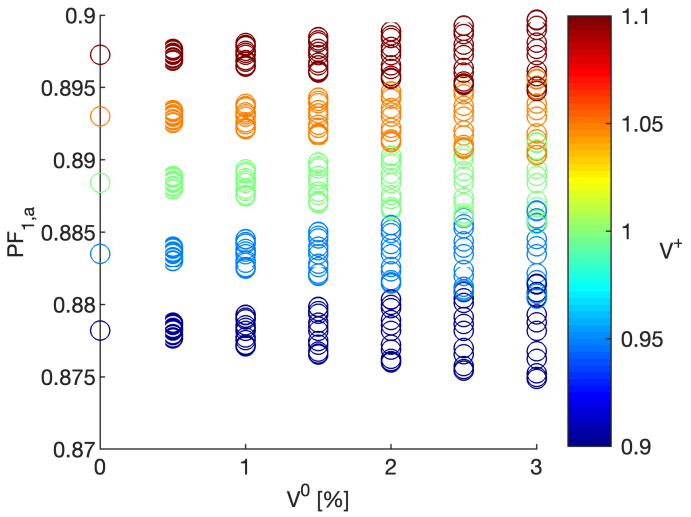

Figure 4.15: $PF_{1,a}$ of the LED load as a function of V0 with VUF equal to zero.

4.1.4.2 Three-phase Power Factor Definitions

Figure 4.16 shows the scatter plot for each definition computed for the unbalanced non-linear load (set of LED lamps) as a function of the VUF. It should be noted that even for balanced conditions, PF_1^a, PF_1^g, PF^e and PF_1^+ have multiple values. Remember the dataset contains 5 different values of V^+ and 7 different values of V^z. In order to exclude these two variables, we filter the dataset to those conditions with $V^+ = 1$ pu and $V^z = 0$.

Figure 4.17 shows the scatter plot for each definition computed for the unbalanced non-linear load (set of LED lamps) as a function of the VUF considering the subset with $V^+ = 1$ pu and $V^z = 0$. In this case when the VUF is zero, all definitions had only one value which was equal to their reference values. As the VUF increases, the range of possible values for each definition also increased. In terms of absolute values, the highest variation was observed for PF^e (0.0114), followed by PF_1^+ (0.0106), then PF_1^g and PF_1^a (both with 0.0021). It is noteworthy that in the case of the LED lamps, the variations with respect to the VUF are lower 1.2×10^{-2}.

Considering the full dataset (with all different values of V^+ and V^z), the highest variation was observed for PF_1^+ (0.0407), followed by PF^e (0.0255), then PF_1^g and PF_1^a (both with 0.0233). So, it can be concluded that, for this specific load, the impacts of V^+ and V^z on the PF values were higher than the VUF.

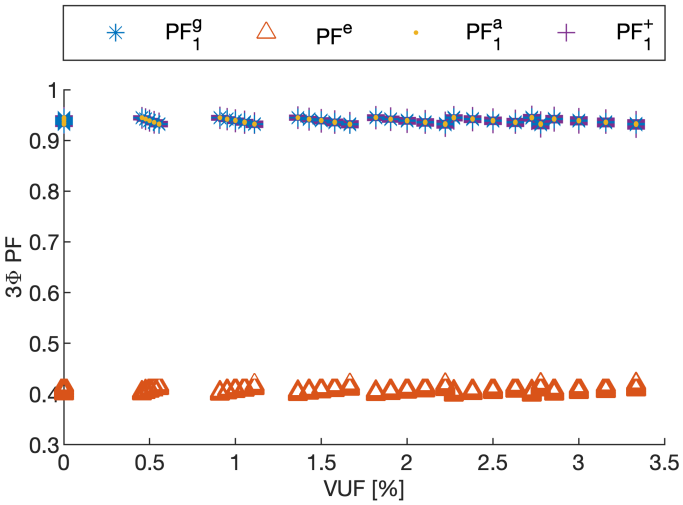

Figure 4.16: Different 3ϕ PF definitions computed for the set of LED lamps as a function of the VUF with simulated data (THD of 3.74%).

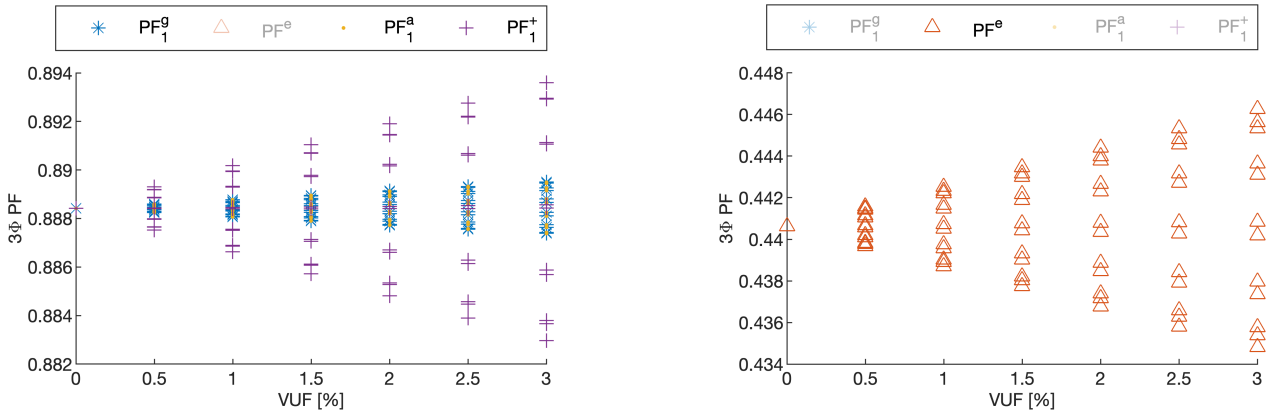

(a) (b)

Figure 4.17: Different 3ϕ PF definitions computed for the set of LED lamps as a function of the VUF with the subset of simulated data having $V^+ = 1$ pu and $V^z = 0$ (THD of 3.74%).

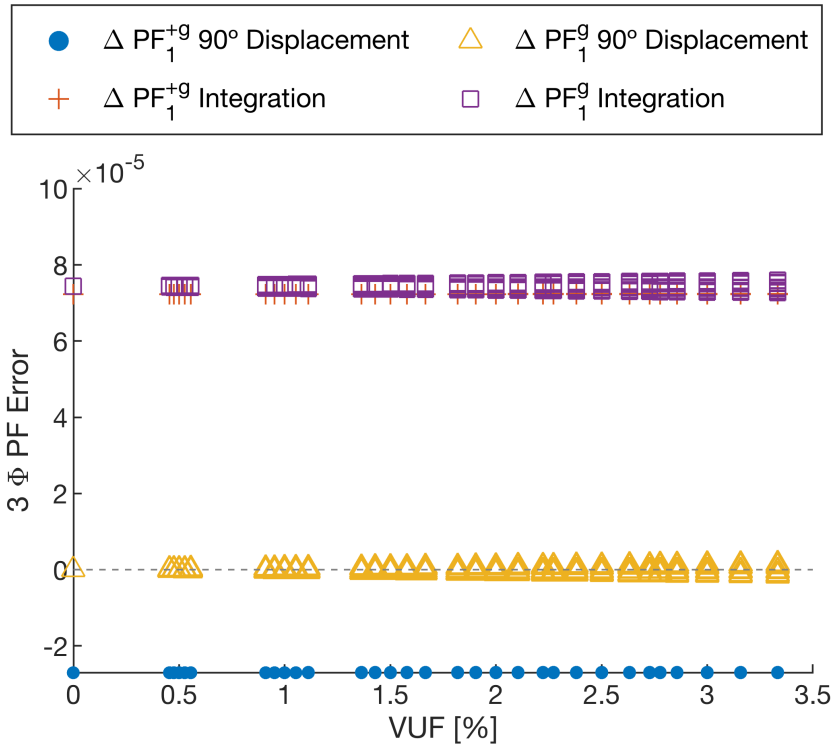

Figure 4.18: ΔPF_1^{+g} and ΔPF_1^{g} with 90° voltage displacement and voltage integration measurement methods for the constant impedance load with simulated data (THD of 3.74%).

4.2 Computational Evaluation of Measurement Algorithms' Effects on the Fairest Power Factor Definitions

This chapter evaluates the accuracy of the measurement methods discussed in Section 2.3.3 considering the methodology presented in Section 3.2. The accuracy here is assessed by the difference between the measured and the reference values of that PF definition for that load.

4.2.1 Accuracy of Measurement Algorithms Without Noise

The values of ΔPF_1^{+a} obtained without noise for the constant impedance load ($Z_{ab} = Z_{bc} = Z_{ca} = 1\angle\cos^{-1}(0.95)$ pu and the TIM were approximately constant (lower than 0.0003 in module) with regard to the VUF. Therefore, the computation of PF_1^{+a} with the FFT-based method proposed in [127] is shown to be accurate.

Fig. 4.18 shows ΔPF_1^{g} and ΔPF_1^{+g} for the constant impedance load obtained by the 90° displacement of voltage and by the voltage integration techniques as function of VUF. From Fig. 4.18, it is possible to verify small errors (of order 10^{-5}) for both measurement methods.

Fig. 4.19 shows ΔPF_1^{g} and ΔPF_1^{+g} for the TIM obtained by the 90° displacement of voltage and by the voltage integration techniques as function of VUF. From Fig. 4.19, it is possible to verify small errors (of order 10^{-3}) for both measurement methods. Errors of order 10^{-3} are negligible within the existing regulations

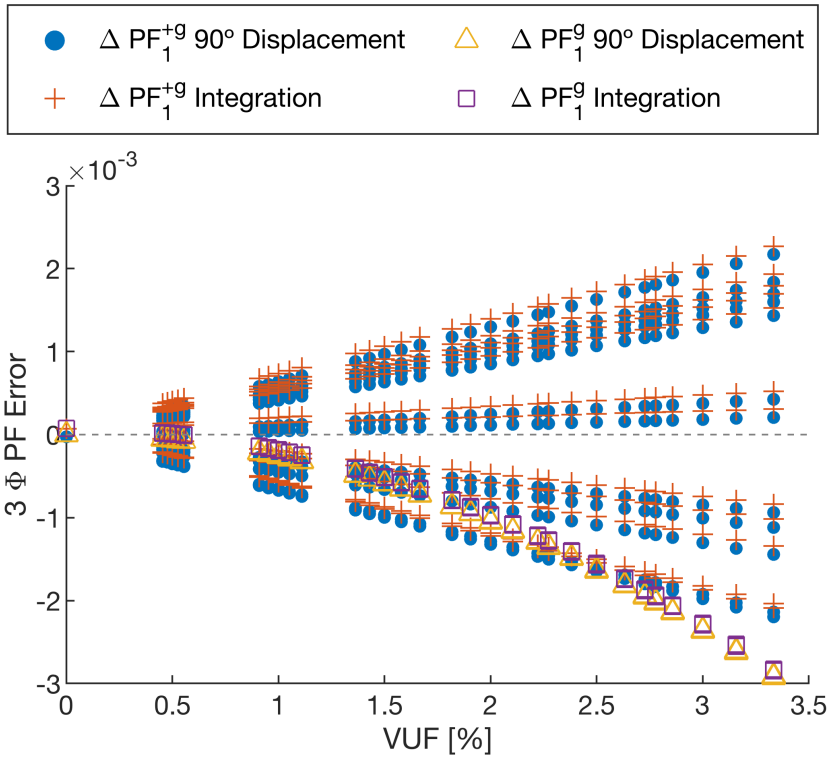

Figure 4.19: ΔPF_1^{+g} and ΔPF_1^{g} measured with the 90° voltage displacement and voltage integration methods for the TIM considering noiseless voltage and current signals of simulated data (THD of 3.74%).

discussed in Section 1.2.

It can also be observed that for VUF equal to zero, both techniques had deviations close to zero. On the other hand, for a 3% VUF, the methods applied to obtain PF_1^{+g} presented errors from -2×10^{-3} up to $+2 \times 10^{-3}$, depending on the VU condition. As a mater of fact, PF_1^{+g} reading presented different errors for the same VUF (greater than zero) depending on the condition. This phenomenon is noted to be intensified proportionally to the increase of VUF. This behaviour was not verified for PF_1^{g}. On the other hand, PF_1^{g} readings deviate negatively from its reference value, resulting in ΔPF_1^{g} up to -3×10^{-3} for VUF equal to 3.4%. For VUF greater than 2.5%, ΔPF_1^{g} readings are higher in module than ΔPF_1^{+g}.

4.2.2 Accuracy of Measurement Algorithms With Noise

In this section, it is evaluated how the measurement methods perform with noisy voltage and current signals. For this purpose, an additive white Gaussian noise with standard deviation of 0.2 pu was superimposed in the signals used in Section 4.2.1. For concision purposes, the results are presented only for the TIM.

The values of the TIM ΔPF_1^{+a} obtained with noise were approximately constant (lower, in module, than 0.0003) with regard to the VUF. Therefore, the computation of PF_1^{+a} with the FFT-based method proposed in [127] is shown to be robust to the presence of noise in the voltage and current signals.

Fig. 4.20 shows, as a function of the VUF, the measurement errors of the TIM PF_1^{+g} and PF_1^{g} employing the 90° displacement of voltage and the voltage integration methods. It can be seen that the values of ΔPF_1^{g}

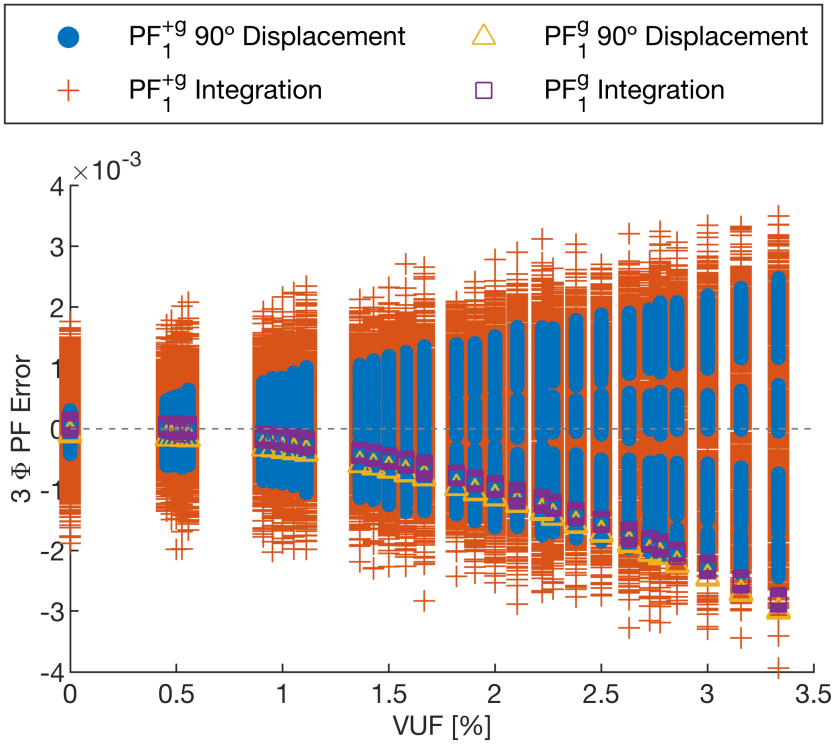

Figure 4.20: ΔPF_1^{+g} and ΔPF_1^{g} measured with the 90° voltage displacement and voltage integration methods for the TIM considering noisy voltage and current signals of simulated data (THD of 3.74%).

measured with both methods is approximately equal to those obtained in Fig. 4.19. On the other hand, the results of PF_1^{+g} evaluations with the 90° displacement of voltage or the voltage integration methods are sensitive to noise. Nonetheless, the maximum and minimum values of ΔPF_1^{+g} are similar to those obtained under noiseless conditions (of order 10^{-3}). Therefore, both PF_1^{g} and PF_1^{+g} can be accurately measured by the 90° displacement of voltage and the voltage integration methods considering voltage and current signals with noise up to 0.2 pu.

4.3 Chapter Remarks

In this chapter, we investigated different PF definitions and measurement methods by means of computational simulations. The application of different PF definitions to balanced and unbalanced constant impedance loads, to an induction motor and to an unbalanced non-linear load composed by light-emitting diode (LED) lamps revealed that each PF definition had a different behavior for each load.

For the balanced constant impedance load, all definitions provided constant values equal to their references even when the voltages were unbalanced and nonsinusoidal. For the unbalanced constant impedance load, only the fundamental geometric and the fundamental positive sequence PFs were constant and equal to their reference values. The fundamental per-phase, the fundamental arithmetic and the effective PFs under unbalanced voltages can be lower or higher than their reference values. In this sense, their application may lead to billing scenarios unfair to the utility (if the customer would be charged under balanced voltages, but his PF gets higher due to the voltage unbalance) or the customer (if he would not be charged under balanced

voltages).

For the induction motor, only the fundamental geometric and the fundamental positive sequence PFs were constant and equal to their reference values. In this case, the fundamental arithmetic and the effective PFs under unbalanced voltages were lower than their reference values. The fundamental per-phase PF, on the other hand, could be higher or lower than its reference value, potentially leading to billing scenarios unfair to the utility or the customer.

For the unbalanced non-linear load composed by LED lamps, it was observed that the fundamental per-phase PF is affected by both the zero and positive-sequence magnitudes. As a result voltage levels higher or lower than the nominal may increase or reduce (respectively) the fundamental per-phase PF with respect to its reference value. Lastly, the sensitivity to the zero-sequence component implies that this PF definition is affected by the choice of the measurement point. All three-phase definitions were shown to be affected by V^z, V^+, and V^-. However, for nominal voltages ($V^+ = 1$ pu) and zero common mode voltages ($V^z = 0$), their variation with respect to the VUF was lower than 1.14×10^{-2}. On the other hand, when all possible values of V^z, V^+, and V^- from the dataset were present, the variations of each PF definitions were lower than 4.1×10^{-2}. It can be concluded that none of these definitions were able to maintain the load's PF equal to its reference value when the voltages are not balanced, sinusoidal and nominal anymore.

Lastly, this chapter has also assessed the accuracy of the measurement algorithms for the fairest PF definitions obtained in the simulations. It is noteworthy that the simulation did not consider all the parts of a digital meter but only the measurement algorithms implemented in a CPU. An experimental test could potentially increase the noise in the input signals of the algorithms, but this has also been evaluated computationally by changing the SNR. It was shown the sample-based active power method and the reactive power methods of the 90° displacement of voltage and the voltage integration were tested to measure PF_1^g and PF_1^{+g}. In the case of PF_1^{+g}, estimation of instantaneous positive sequence components was performed with a time-delay method. The measurement of PF_1^{+a} was performed with the modified cosine method [127]. Simulations results showed that PF_1^g, PF_1^{+g}, and PF_1^{+a} have the property of being accurately measurable even considering an approximately 14 db of SNR in the voltage and current signals. Additionally, PF_1^g and PF_1^{+g} can be accurately measured by simple methods such as the 90° displacement and voltage integration methods. In other words, the measured values of PF_1^g, and PF_1^{+g} have little sensibility on the measurement algorithm, and they are not significantly affected even if the utility delivers unbalanced nonsinusoidal voltages

CHAPTER 5

Experimental Evaluation of Power Factor Definitions from the Fairness Perspective

5.1 Unbalanced Constant Impedance Loads

5.1.1 Per-phase Power Factor Definition

This section presents the results of the experimental tests with the unbalanced constant impedance load. Figure 5.1 shows the fundamental PF for phases "a" and "b" as a function of the VUF with the experimental data. It is not possible to compute $PF_{1,c}$ because the current at phase "c" is zero. Analyzing Figure 4.3, it can be observed that the overall behavior is very similar to that obtained in the simulations (Figure 4.3), but with some distinct values. For example, $PF_{1,a}$ and $PF_{1,b}$ are equal to 0.85 and 0.88, respectively, when the VUF is close to zero.

Figure 5.2 shows the experimental results in the form of a scatter plot of $PF_{1,a}$ as a function of both the negative-sequence voltage magnitude (V^-) and angle (θ^-). It can be observed that the simulations and experimental results are very similar, having the same overall shape. The values in Figure 5.2 are different from those of the simulation because the experimental load had to be smaller (drawing less active power) due to practical limitations. Nonetheless, the conclusion derived from the curve shape are ratified with the experimental tests.

The experimental results corroborate the conclusions drawn from the simulation outcomes. Although the numerical values for each voltage condition did not precisely align with those obtained in the simulations, it was evident that the overall trends exhibited by each definition closely mirrored those observed in the simulations. Notably, under balanced voltage conditions with a VUF equal to zero, the per-phase fundamental PF exhibited the most distinct variation from the simulation results. In this case, the difference is lower than 0.015.

The application of the per-phase fundamental PF or the fundamental arithmetic PF or the effective PF for billing purposes may lead to unexpected PF values and to possible unequal treatment between customers.

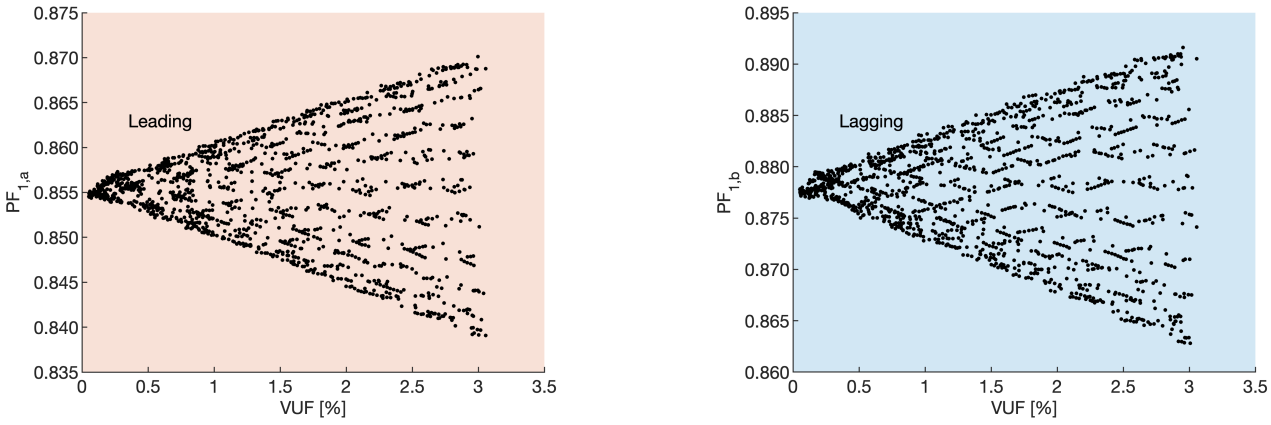

(a) (b)

Figure 5.1: Per Phase PF of the unbalanced resistive load as a function of VUF with experimental data.(a) $PF_{1,a}$. (b) $PF_{1,b}$.

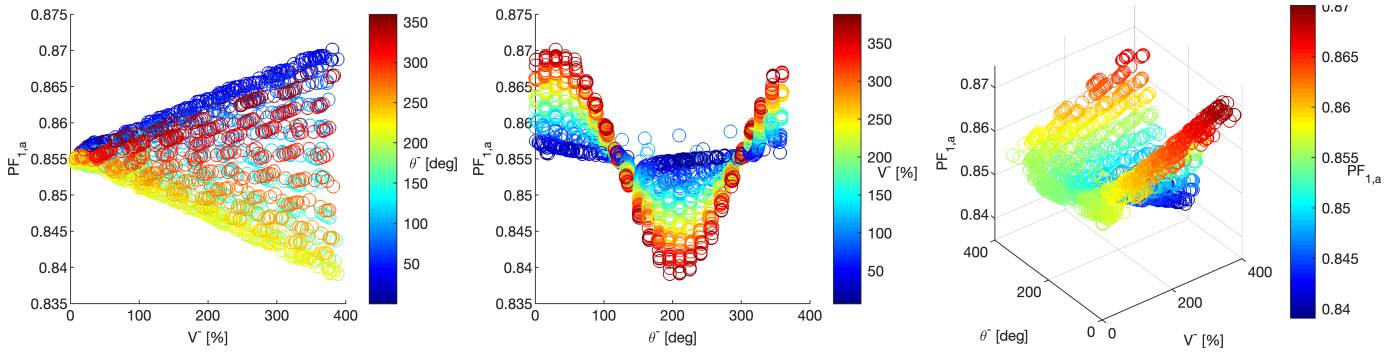

(a) (b) (c)

Figure 5.2: Per Phase PF of the unbalanced resistive load with experimental data (a) 2D scatter plot of $PF_{1,a}$ as a function of VUF with the θ^- as the colorbar. (b) 2D scatter plot of $PF_{1,a}$ as a function of θ^- with the VUF as the colorbar. (c) 3D scatter plot of $PF_{1,a}$ in the z-axis, θ^- in the x-axis, and the VUF in the y-axis with $PF_{1,a}$ as the colorbar.

For example, consider two customers with identical loads submitted to the same VUF. The application of any of these definitions may lead to the PF of one of the customers being lower than the other. The reason for different readings in this hypothetical situation is the angle of the negative-sequence component of the voltages supplied to both customers.

On the other hand, the application of the per-phase fundamental PF or the three-phase fundamental arithmetic or effective PFs may potentially lead to unfair billing scenarios for the utility. Remember, the variations of these PFs can be positive or negative with respect to their reference value. This can lead to a situation where the customer's PF under balanced sinusoidal voltages would be lower than the established limits, resulting in charges. However, the voltages supplied are not balanced due to other factors (such as the influence of other customers). As a result, the actual PF of that customer gets higher than the utility limits. This conducts to the customer that should be charged not being charged as a consequence of other factors unrelated to him. This case, therefore, represents an unfair billing scenario from the utility perspective.

Another hypothetical situation that may happen when employing the fundamental per-phase PF is that, depending on the local charging policy, the customer may be charged twice. The first time for a lagging low PF value in one the phases. The second for a leading low PF value in another phase. In addition to a low PF value in both phases, the customer may also be charged due to the fact that one of the phases has a leading PF, which according to [9] is not allowed by some utilities (e.g. Hydro-Quebec in Canada or Synergy in Australia). This situation, where one of the phases is lagging and the other is leading, can be observed with the simulation results shown in Table 5.1. Such double charge should be thoroughly discussed since the fundamental per-phase PF in this case is not behaving like in balanced sinusoidal voltage conditions, in which according to [11] most PF billing policies were designed.

Table 5.1: Values of the fundamental PF for phases "a" and "b" for the same voltage condition.

Condition	$PF_{1,a}$	$PF_{1,b}$
$\mathbf{V_1^-} = 0.03\underline{/30°}$	0.88 leading	0.87 lagging

At last, only the usage of PF_1^g and PF_1^+ is shown to always provide the same value for the unbalanced load even under unbalanced and nonsinusoidal voltage conditions. So, these two definitions are the only reliable ones to employ for billing purposes of resistive constant impedance loads.

5.1.2 Three-phase PF definitions

Figure 5.3 shows the scatter plot for each three-phase PF definition computed for the unbalanced resistive load as a function of the VUF with experimental data. It can be observed that the simulations and experimental results are very similar, having the same overall shape but different values. When the VUF is equal to zero, PF_1^g and PF_1^+ are equal to their reference PF value of 1, and PF_1^a and PF^e are equal to their reference values of 0.866 and 0.706, respectively. When the VUF is greater than zero, PF_1^g and PF_1^+ still have the same reference value of 1 for all voltage conditions, being therefore unaffected by the VUF. On the other hand, there are several voltage conditions that lead to different PF_1^a and PF^e values. The highest and lowest values obtained for PF_1^a were 0.878 and 0.852, respectively, and for PF^e were 0.727 and 0.685, respectively. The variations of PF_1^a and PF^e around theirs reference values are approximately symmetrical and increased

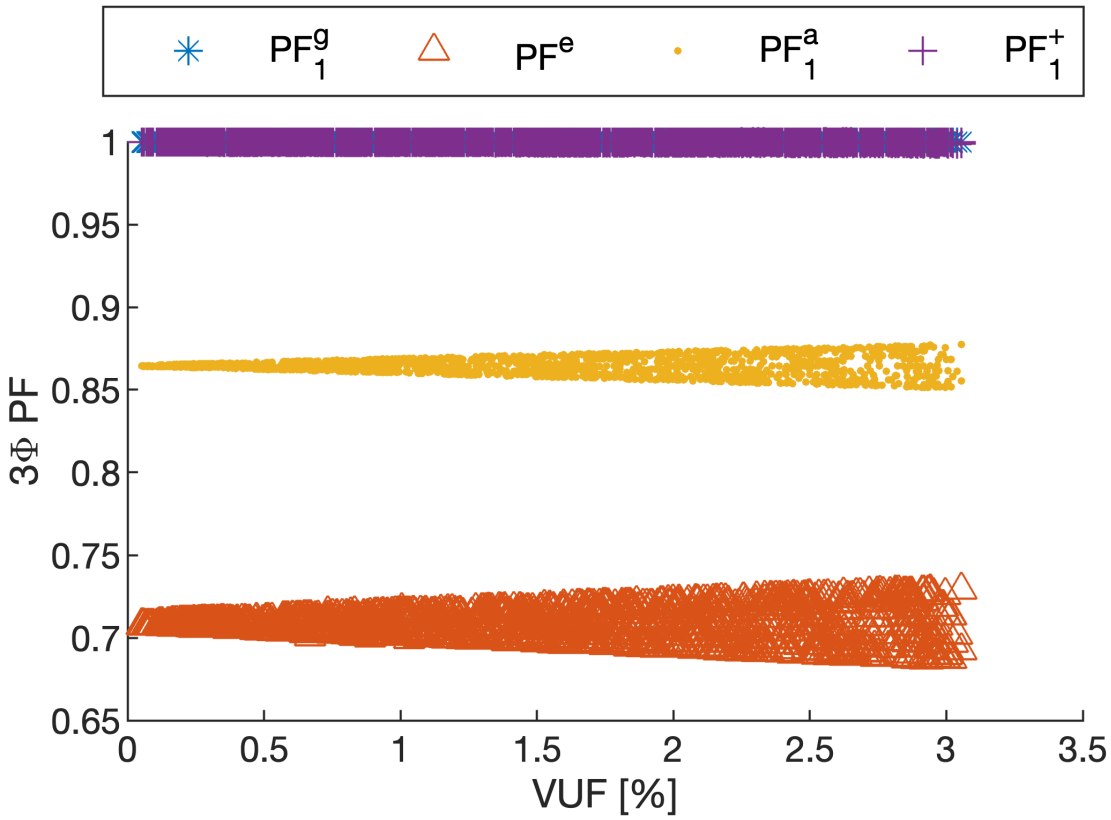

Figure 5.3: 3ϕ PF definitions computed for the unbalanced resistive load as a function of the VUF with experimental data.

with the VUF. Comparing PF^e with PF^a_1, it can be observed that the variation (in terms of absolute values) of PF^e was higher than the observed for PF^a_1, that is 0.021 against 0.012. Like simulations results, in the experimental results $PF_e \leq PF^a_1 \leq PF^g_1 = PF^+_1$ independently of the VUF.

Figure 5.4 shows the scatter plot of PF^e as a function of both the negative-sequence voltage magnitude (V^-) and angle (θ^-). Analogous results have been found for PF^a_1 (which is not shown here for concision purposes) and for $PF_{1,a}$ as shown in Figure 5.2. It can be observed a sinusoidal dependance with respect to θ^-, being V^- the sine amplitude. When V^- is equal to zero, PF^e and PF^a_1 had only one value approximately equal to their reference values of 0.71 and 0.866, respectively. When V^- is greater than zero, there are two values of θ^- (approximately 150° and 330°) which lead to PF^e and PF^a_1 values equal to their reference values. Also, there are some values of θ^- (between $[0°, 150°]$ and $[330°, 360°]$, approximately) which cause PF^e and PF^a_1 to increase with the increase of V^-. Likewise, there are some values of θ^- (between 150° and 330°) which cause PF^e and PF^a_1 to decrease with the increase of V^-.

In the experimental results, $PF_{1,a}$ and $PF_{1,b}$ were equal to 0.85 and 0.88 when the VUF was close to zero, respectively, but the former was leading while the latter was lagging. In the simulations, both phases had the same fundamental PF value when the VUF was close to zero. In both simulations and experimental tests, for a given value of the VUF greater than zero, there were different values for $PF_{1,x}, x = a, b$ and this range of values increased symmetrically around the reference value with the VUF increase.

It was shown that, similar to the simulations, each three-phase PF definition had a different behavior in

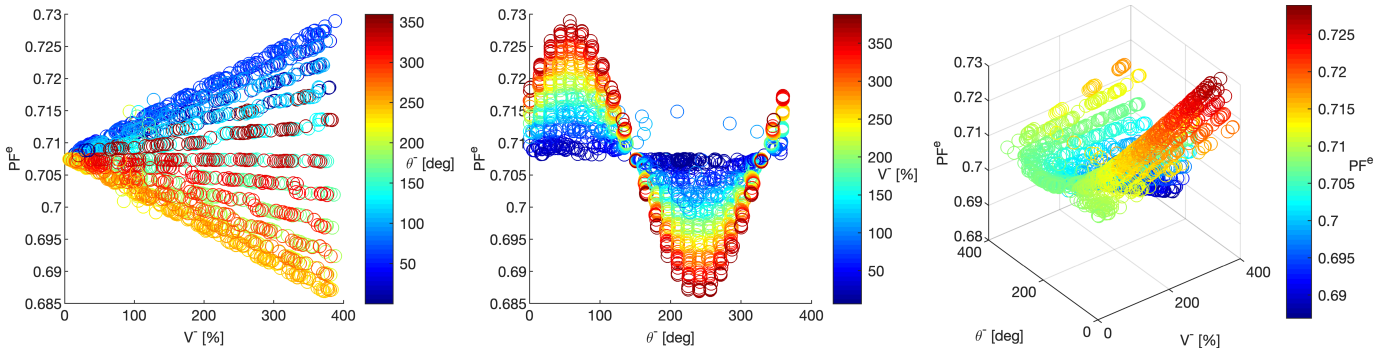

Figure 5.4: PF^e of the unbalanced resistive load with experimental data. (a) 2D scatter plot of PF^e as a function of VUF with the θ^- as the colorbar. (b) 2D scatter plot of PF^e as a function of θ^- with the VUF as the colorbar. (c) 3D scatter plot of PF^e in the z-axis, θ^- in the x-axis, and the VUF in the y-axis with PF^e as the colorbar.

the experimental results. PF_1^g, PF^e, and PF_1^a had different reference PF values, so they had to be analyzed separately with respect to their own PF reference value. PF_1^g and PF_1^+ had the same reference value of 1 and were unaffected by the VUF. On the other hand, PF_1^a and PF_1^e were affected by V^- and θ^-. For a given VUF greater than zero, there were different values of PF^e and PF_1^a around their reference value (0.71 and 0.86, respectively, in the experimental results and 0.706, 0.865, respectively, in the simulations). In both simulations and experimental tests, the range of possible values of PF^e and of PF_1^a symmetrically increased with the VUF.

5.2 Three-Phase Induction Motors

In this section, the sensitivity to the voltage unbalance of different PF definitions is evaluated experimentally with a motor operating under unbalanced and distorted voltages. The methodology employed to obtain the results is described in section 3.3.

5.2.1 Per Phase PF Definitions

Figure 5.5 shows a scatter plot of $PF_{1,a}$ as a function of the VUF for the 901 experimental conditions. Many of these conditions result in the same pair of VUF and PF, leading to the superimposition of points in the graph. From Figure 5.5, it can be observed that $PF_{1,a}$ can have different values for the same VUF. For instance, a 1.5% VUF results in $PF_{1,a}$ ranging from 0.96 up to 0.99. For a VUF of 3%, there are conditions that lead to $PF_{1,a}$ in between 0.93 and 1. Therefore, it can be concluded that the interval of possible values for $PF_{1,a}$ increases with the VUF.

The results for phases "b" and "c" are analogous to those presented for phase "a". However, it was observed that each phase had a different PF value for each VU condition. Table 5.2 shows $PF_{1,x}, x = a, b, c$ for a given voltage condition with 1% VUF. It can be observed in this case that all phases have a distinct $PF_{1,x}, x = a, b, c$ value. More specifically, $PF_{1,b} \leq PF_{1,a} \leq PF_{1,c}$. In order to assess the VUF associated with conditions

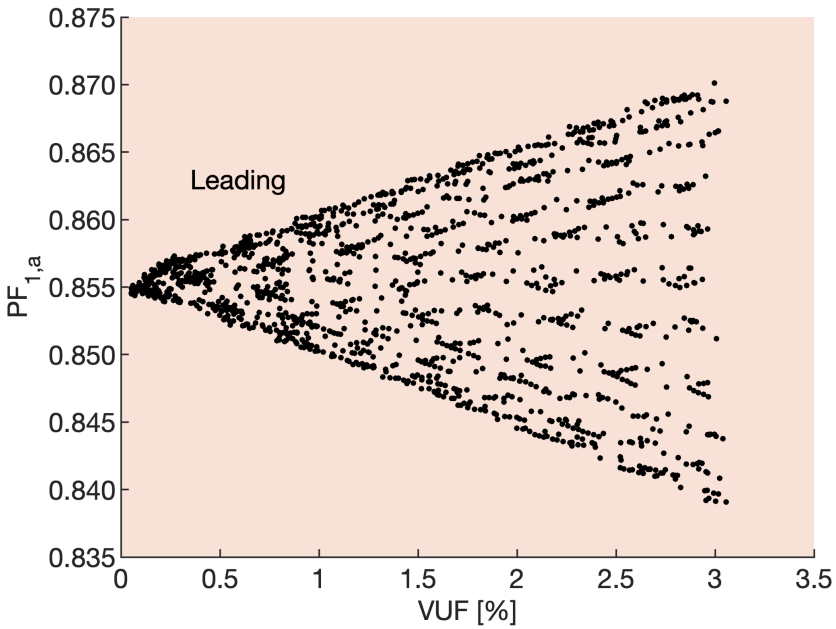

Figure 5.5: $PF_{1,a}$ of the TIM as a function of VUF with experimental data (THD values of 2%, 5%, and 8%).

Table 5.2: TIM Fundamental Power Factor per phase for two experimental conditions.

Condition	$PF_{1,a}$	$PF_{1,c}$	$PF_{1,c}$
$V_1 = 1\angle 0$ $V_2 = 0.01\angle 52°$	0.98	0.97	0.99

that causes charges in at least one of the phases, the minimum value of the fundamental PF between phases ($PF_{1\text{min}}$) is computed for each condition, and it is shown in Figure 4.11.

Similarly to $PF_{1,a}$ shown in Figure 4.9, there are conditions with the same VUF that leads to different values of $PF_{1\text{min}}$ as shown in Figure 4.11. The range of possible values also increases with the VUF. From Figure 4.11, it can be observed that for a VUF of 3.5% there are some conditions conducting to values of $PF_{1,x}$, $x = a, b, c$ lower than 0.92 in at least one of the phases. Therefore, the experimental result ratify that the per phase PF is not suitable for billing purposes of TIMs.

5.2.2 Three-Phase Power Factor Definitions

In Fig. 5.7, it can be seen that the TIM three-phase PFs have a more scattered pattern when compared to the correspondent PFs in Fig. 4.12. This scattering shows that the points obtained experimentally do not superimpose as perfectly as in Fig. 4.12, meaning that more supply conditions lead to results with the same VUF but different PF values. In Fig. 5.7, it can be seen that PF^e and PF_1^a definitions presented the greatest scattering bands for any fixed VUF. In other words, PF^e and PF_1^a are the most vulnerable to the VUF and the THD. Although all PF definitions present some sensitivity to the presence of unbalance and distortion, one can see that the general behavior of the PFs to the VUF is similar in Figures 5.7 and 4.12. When the VUF increases, it can be observed that the scattering band of PF^e and PF_1^a shifts down, the PF_1^g band shifts down slightly, and the position of the band of PF_1^+ is the most stable presenting the least

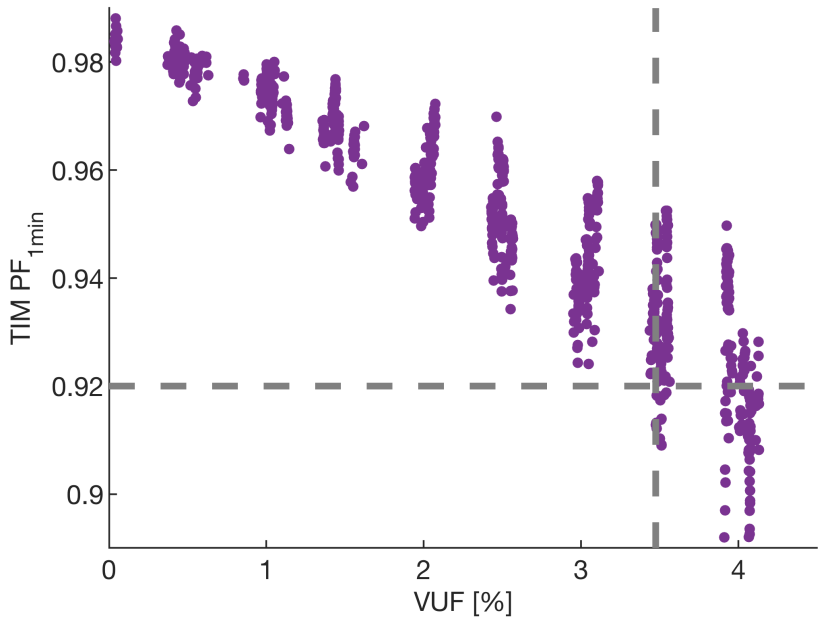

Figure 5.6: $PF_{1\text{min}}$ of the TIM as a function of VUF with experimental data (THD values of 2%, 5%, and 8%).

variation with respect to VUF changes. In particular, considering the worst case, it can be seen that, for any VUF, the lower values of PFs are such that $PF_1^+ \geq PF_1^g \geq PF_1^a \geq PF^e$. Based on these results, it can be concluded that the experimental investigation and the simulation study are in accordance, indicating that the most recommendable PF definitions for revenue purposes are PF_1^+ and PF_1^g.

5.3 Chapter Remarks

This Chapter presented the results of the experimental evaluation of power factor definitions from the fairness perspective, considering the unbalanced constant impedance load and the induction motor. With both loads, the experimental results corroborated the conclusions drawn from the simulation outcomes.

For the unbalanced constant impedance load, the same conditions of the simulations were employed. Although the numerical values for each voltage condition did not precisely align with those obtained in the simulations, it was evident that the overall trends exhibited by each power factor (PF) definition closely mirrored those observed in the simulations. Notably, under balanced voltage conditions with a VUF equal to zero, the per-phase fundamental PF exhibited the most distinct variation from the simulation results, though with a difference of less than 0.015.

For the motor, we considered a different motor with a different set of voltage conditions. As expected, the results for each VUF did not match the simulation results, neither their reference values. Nonetheless, the overall behavior with respect to the VUF confirmed the validity of the conclusions drawn from the simulations.

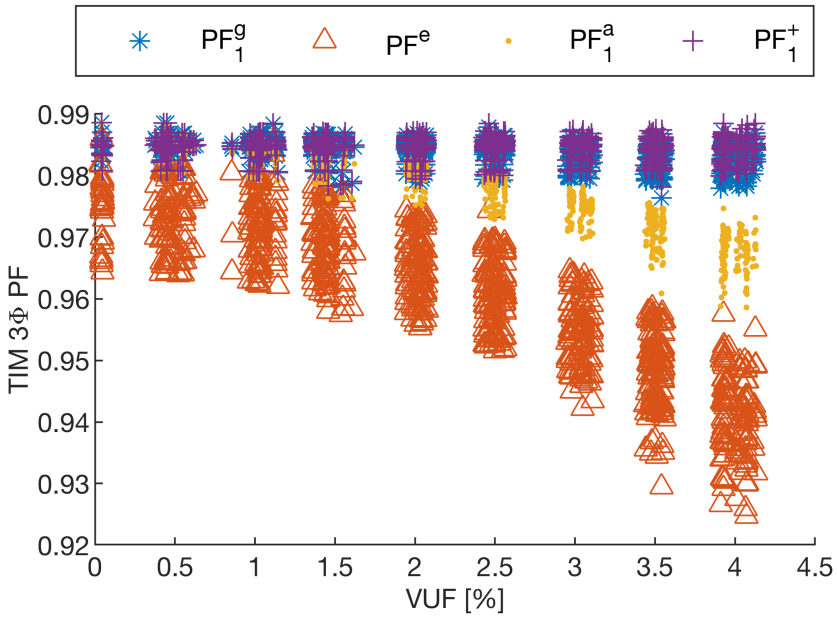

Figure 5.7: Different 3ϕ PF definitions computed for the TIM as a function of the VUF with experimental data (THD values of 2%, 5%, and 8%).

CHAPTER 6

Analytical Investigation of Power Factor Definitions for Constant Impedance Loads

6.1 Analytical Investigation of Power Factor Definitions for Constant Impedance Loads

Analytical expressions for each PF definition will be derived as functions of the load's parameters using voltage and current phasors. Since phasors are defined for a specific frequency, it is important to specify the frequency for which they are computed. In this section, all phasors are referenced at the fundamental frequency unless stated otherwise for the sake of conciseness. Additionally, we adopt the angle of the positive-sequence voltage at the fundamental frequency as the angular reference to simplify complex equations. We will first derive expressions for each PF definition while considering unbalanced loads. Subsequently, we will analyze the special case of balanced loads, where the load's parameters are evenly distributed between phases.

A load modeled as as constant impedance has a linear V-I curve with the slope defined by the impedance magnitude. In single-phase systems, the load impedance is a complex number defined in the frequency domain by the ratio of the voltage and current phasors. The inverse of the impedance is the admittance (y) which is very useful to rewrite the current in terms of the voltage.

In three-phase systems, a constant impedance load can be modeled by impedances connected between phases (in case of delta-connected loads) or between a phase and a common point (in the wye connection), and the common point may be connected to a fourth conductor or to the ground. Such loads can be represented in terms of admittance matrices which provide a transformation from the voltages to line currents. Further details on admittance matrices can be found in [138]. In the following, a short description of such matrices is given for delta-connected loads for the sake of conciseness. A more detailed investigation considering other connections and types of loads should be addressed in future works.

The line currents for a delta-connected load are given by

$$\underbrace{\begin{bmatrix}\mathbf{I_{h,a}}\\ \mathbf{I_{h,b}}\\ \mathbf{I_{h,c}}\end{bmatrix}}_{I_{h,abc}} = \underbrace{\begin{bmatrix}(\mathbf{y_{h,ab}}+\mathbf{y_{h,ca}}) & -\mathbf{y_{h,ab}} & -\mathbf{y_{h,ca}}\\ -\mathbf{y_{h,ab}} & (\mathbf{y_{h,bc}}+\mathbf{y_{h,ab}}) & -\mathbf{y_{h,bc}}\\ -\mathbf{y_{h,ca}} & -\mathbf{y_{h,bc}} & (\mathbf{y_{h,ca}}+\mathbf{y_{h,ab}})\end{bmatrix}}_{Y_{h,abc}} \underbrace{\begin{bmatrix}\mathbf{V_{h,a}}\\ \mathbf{V_{h,b}}\\ \mathbf{V_{h,c}}\end{bmatrix}}_{V_{h,abc}}. \tag{6.1}$$

where $\mathbf{y_{h,ab}}$, $\mathbf{y_{h,bc}}$, and $\mathbf{y_{h,ca}}$ are the admittances between phases "a"-"b", "b"-"c", and "c"-"a", respectively. It is noteworthy that in (6.1), the voltages are measured with respect to the ground voltage (that is a point with nil zero-sequence component).

Applying the Fortescue transformation (2.66) to the voltages and currents,

$$I_h^{z+-} = \underbrace{F^{-1}Y_{h,abc}F}_{Y^{z+-}} V_h^{z+-} \tag{6.2}$$

where $I_h^{z+-} = [\mathbf{I_h^z}, \mathbf{I_h^+}, \mathbf{I_h^-}]^T$ and $V_h^{z+-} = [\mathbf{V_h^z}, \mathbf{V_h^+}, \mathbf{V_h^-}]^T$, and Y^{z+-} is the admittance matrix in the sequence domain. For delta-connected loads, it can be shown that

$$Y_h^{z+-} = \begin{bmatrix}0 & 0 & 0\\ 0 & \mathbf{Y_h^s} & \mathbf{Y_h^{+-}}\\ 0 & \mathbf{Y_h^{-+}} & \mathbf{Y_h^s}\end{bmatrix}, \tag{6.3}$$

in which

$$\mathbf{Y_h^s} = \mathbf{y_{h,ab}} + \mathbf{y_{h,bc}} + \mathbf{y_{h,ca}} = |\mathbf{Y_h^s}|\underline{/\varphi_h^s} \tag{6.4}$$

$$\mathbf{Y_h^{-+}} = -(\mathbf{y_{h,ab}}\boldsymbol{\alpha}^2 + \mathbf{y_{h,bc}} + \mathbf{y_{h,ca}}\boldsymbol{\alpha}) = |\mathbf{Y_h^{-+}}|\underline{/\varphi_h^{-+}} \tag{6.5}$$

are the equivalent admittance and the unbalanced admittance proposed by [95], respectively, and

$$\mathbf{Y_h^{+-}} = -(\mathbf{y_{h,ab}}\boldsymbol{\alpha} + \mathbf{y_{h,bc}} + \mathbf{y_{h,ca}}\boldsymbol{\alpha}^2) = |\mathbf{Y_h^{+-}}|\underline{/\varphi_h^{+-}} \tag{6.6}$$

is the negative-to-positive transadmittance.

It is noteworthy that the equation for Y_{z+-} shows that delta-connected loads are not affected by zero-sequence voltages (first column of Y_{z+-} is composed of zeros) and they do not contribute with zero-sequence currents (first row of Y_{z+-} is composed of zeros).

If the voltage negative-sequence component is zero, then the load's current can be completely described in terms of $\mathbf{Y_h^s}$ and $\mathbf{Y_h^{-+}}$. The expressions for $\mathbf{Y_h^s}$ and $\mathbf{Y_h^{-+}}$ were found using a different approach in [95]. In the present approach, however, it is clearly shown that $\mathbf{Y_h^{-+}}$ does not fully reflect the load unbalance because it only accounts for the effects of the positive-sequence voltage on the negative-sequence current. In practical situations, the voltage has a negative-sequence component which also affects the positive-sequence current. This is accounted for by the term $\mathbf{Y_h^{+-}}$ In reference [95], this term was not obtained because only balanced voltages were considered, that is the voltage negative-sequence was zero. The existence of this additional impedance $\mathbf{Y_h^{+-}}$ makes sense in terms of mathematics because the load has three independent admittances (variables), therefore it cannot be fully represented in terms of only two fictitious admittances $\mathbf{Y_h^s}$ and $\mathbf{Y_h^{-+}}$. A third fictitious admittance $\mathbf{Y_h^{+-}}$ is necessary to fully represent the load.

With the admittance matrix in the sequence domain, it is possible to rewrite the active power and the different definitions for apparent power in terms of the voltages and admittances in the sequence domain. For that purpose, first we need to rewrite the currents and voltages of each phase. The phase voltages can be rewritten in terms of the sequence components, considering that $V^z = 0$, as

$$\begin{cases} \mathbf{V_{h,a}} = \mathbf{V_h^+} + \mathbf{V_h^-} \\ \mathbf{V_{h,b}} = \boldsymbol{\alpha}^2\mathbf{V_h^+} + \boldsymbol{\alpha}\mathbf{V_h^-} \\ \mathbf{V_{h,c}} = \boldsymbol{\alpha}\mathbf{V_h^+} + \boldsymbol{\alpha}^2\mathbf{V_h^-} \end{cases}, \tag{6.7}$$

and the currents likewise

$$\begin{cases} \mathbf{I_{h,a}} = \mathbf{I_h^+} + \mathbf{I_h^-} \\ \mathbf{I_{h,b}} = \boldsymbol{\alpha}^2\mathbf{I_h^+} + \boldsymbol{\alpha}\mathbf{I_h^-} \\ \mathbf{I_{h,c}} = \boldsymbol{\alpha}\mathbf{I_h^+} + \boldsymbol{\alpha}^2\mathbf{I_h^-} \end{cases}. \tag{6.8}$$

Considering the admittance matrix in the sequence domain, the phase currents can be rewritten in terms of the admittances and the voltages in the sequences as

$$\begin{cases} \mathbf{I_{h,a}} = (\mathbf{Y_h^s V_h^+} + \mathbf{Y_h^{+-} V_h^-}) + (\mathbf{Y_h^{-+} V_h^+} + \mathbf{Y_h^s V_h^-}) \\ \mathbf{I_{h,b}} = \boldsymbol{\alpha}^2(\mathbf{Y_h^s V_h^+} + \mathbf{Y_h^{+-} V_h^-}) + \boldsymbol{\alpha}(\mathbf{Y_h^{-+} V_h^+} + \mathbf{Y_h^s V_h^-}) \\ \mathbf{I_{h,c}} = \boldsymbol{\alpha}(\mathbf{V_h^+} + \mathbf{Y_h^{+-} V_h^-}) + \boldsymbol{\alpha}^2(\mathbf{Y_h^{-+} V_h^+} + \mathbf{Y_h^s V_h^-}) \end{cases}. \tag{6.9}$$

Grouping the common terms, the current of phase "a" is given by

$$\mathbf{I_{h,a}} = \mathbf{y_{h,a}^+ V_h^+} + \mathbf{y_{h,a}^- V_h^-} \tag{6.10}$$

where

$$\mathbf{y_{h,a}^+} = \mathbf{Y_h^s} + \mathbf{Y_h^{-+}} = \mathbf{y_{h,ab}}\boldsymbol{\beta} + \mathbf{y_{h,ca}}\boldsymbol{\beta}^* = g_h^+ + \mathbf{j}b_h^+ = |\mathbf{y_{h,a}^+}|\underline{/\varphi_{h,a}^+}, \tag{6.11}$$

$$\mathbf{y_{h,a}^-} = \mathbf{Y_h^s} + \mathbf{Y_h^{+-}} = \mathbf{y_{h,ab}}\boldsymbol{\beta}^* + \mathbf{y_{h,ca}}\boldsymbol{\beta} = g_h^- + \mathbf{j}b_h^- = |\mathbf{y_{h,a}^-}|\underline{/\varphi_{h,a}^-}, \tag{6.12}$$

and $\boldsymbol{\beta} = 1 - \boldsymbol{\alpha}^2 = \sqrt{3}\underline{/30°}$. It should be noticed that $\mathbf{y_{h,a}^+}$ is equal to $\mathbf{y_{h,a}^-}$ if and only if $\mathbf{y_{h,ab}}$ is equal to $\mathbf{y_{h,ca}}$.

The complex power of phase "a" in the sequence domain is simply the product of the voltage phasor and the current conjugated phasor, leading to

$$\mathbf{S_{h,a}} = (\mathbf{V_h^+} + \mathbf{V_h^-})(\mathbf{y_{h,a}^+ V_h^+} + \mathbf{y_{h,a}^- V_h^-})^*. \tag{6.13}$$

Similar expressions can be obtained for phases "b" and "c",

$$\begin{cases} \mathbf{S_{h,b}} = & (\boldsymbol{\alpha}\mathbf{V_h^+} + \mathbf{V_h^-})(\boldsymbol{\alpha}\mathbf{y_{h,b}^+ V_h^+} + \mathbf{y_{h,b}^- V_h^-})^* \\ \mathbf{S_{h,c}} = & (\mathbf{V_h^+} + \boldsymbol{\alpha}\mathbf{V_h^-})(\mathbf{y_{h,c}^+ V_h^+} + \boldsymbol{\alpha}\mathbf{y_{h,c}^- V_h^-})^* \end{cases}$$

where

$$\begin{cases} \mathbf{y_{h,b}^+} & = \mathbf{Y_h^s} + \boldsymbol{\alpha}^2\mathbf{Y_h^{-+}} = \mathbf{y_{h,bc}}\boldsymbol{\beta} + \mathbf{y_{h,ab}}\boldsymbol{\beta}^* \\ \mathbf{y_{h,b}^-} & = \mathbf{Y_h^s} + \boldsymbol{\alpha}\mathbf{Y_h^{+-}} = \mathbf{y_{h,bc}}\boldsymbol{\beta}^* + \mathbf{y_{h,ab}}\boldsymbol{\beta} \\ \mathbf{y_{h,c}^+} & = \mathbf{Y_h^s} + \boldsymbol{\alpha}\mathbf{Y_h^{-+}} = \mathbf{y_{h,ca}}\boldsymbol{\beta} + \mathbf{y_{h,bc}}\boldsymbol{\beta}^* \\ \mathbf{y_{h,c}^-} & = \mathbf{Y_h^s} + \boldsymbol{\alpha}^2\mathbf{Y_h^{+-}} = \mathbf{y_{h,ca}}\boldsymbol{\beta}^* + \mathbf{y_{h,bc}}\boldsymbol{\beta}. \end{cases}$$

It is noteworthy that $\mathbf{S_{h,a}}$ is a function of $\mathbf{y^+_{h,a}}$ and $\mathbf{y^-_{h,a}}$. As a result $\mathbf{S_{h,a}}$ depends only on $\mathbf{y_{h,ab}}$ and $\mathbf{y_{h,ca}}$, but not on $\mathbf{y_{h,bc}}$. This is expected since in delta-connected loads the current of phase "a" is not affected by the load's admittance between phases "b" and "c". In the case of $\mathbf{S_{h,b}}$, the expressions for $\mathbf{y^+_{h,b}}$ and $\mathbf{y^-_{h,b}}$ depend only on $\mathbf{y_{h,ab}}$ and $\mathbf{y_{h,bc}}$. Likewise, for $\mathbf{S_{h,c}}$ a dependance on $\mathbf{y_{h,bc}}$ and $\mathbf{y_{h,ca}}$ is observed.

The sum of the complex powers $\mathbf{S_{h,a}}$, $\mathbf{S_{h,b}}$, and $\mathbf{S_{h,c}}$ (using the angle of the positive-sequence voltage as the angular reference) is given by

$$\begin{aligned}\sum_{x\in[a,b,c]} \mathbf{S_{h,x}} &= (\mathbf{V^+_h}+\mathbf{V^-_h})(\mathbf{y^+_{h,a}}\mathbf{V^+_h}+\mathbf{y^-_{h,a}}\mathbf{V^-_h})^*+\\ &\quad(\boldsymbol{\alpha}\mathbf{V^+_h}+\mathbf{V^-_h})(\boldsymbol{\alpha}\mathbf{y^+_{h,b}}\mathbf{V^+_h}+\mathbf{y^-_{h,b}}\mathbf{V^-_h})^*+\\ &\quad(\mathbf{V^+_h}+\boldsymbol{\alpha}\mathbf{V^-_h})(\mathbf{y^+_{h,c}}\mathbf{V^+_h}+\boldsymbol{\alpha}\mathbf{y^-_{h,c}}\mathbf{V^-_h})^* \qquad (6.14)\\ \sum_{x\in[a,b,c]} \mathbf{S_{h,x}} &= \mathbf{y^+_{h,a}}^*|\mathbf{V^+_h}|^2+\mathbf{y^-_{h,a}}^*(V_h^-)^2+\mathbf{y^+_{h,a}}^*\mathbf{V^{+*}_h}\mathbf{V^-_h}+\mathbf{y^-_{h,a}}^*\mathbf{V^+_h}\mathbf{V^{-*}_h}+\\ &\quad\mathbf{y^+_{h,b}}^*|\mathbf{V^+_h}|^2+\mathbf{y^-_{h,b}}^*(V_h^-)^2+\boldsymbol{\alpha}^2\mathbf{y^+_{h,b}}^*\mathbf{V^{+*}_h}\mathbf{V^-_h}+\boldsymbol{\alpha}\mathbf{y^-_{h,b}}^*\mathbf{V^+_h}\mathbf{V^{-*}_h}+\\ &\quad\mathbf{y^+_{h,c}}^*|\mathbf{V^+_h}|^2+\mathbf{y^-_{h,c}}^*(V_h^-)^2+\boldsymbol{\alpha}\mathbf{y^+_{h,c}}^*\mathbf{V^{+*}_h}\mathbf{V^-_h}+\boldsymbol{\alpha}^2\mathbf{y^-_{h,c}}^*\mathbf{V^+_h}\mathbf{V^{-*}_h} \qquad (6.15)\end{aligned}$$

Grouping the terms by the voltages, leads to

$$\begin{aligned}\sum_{x\in[a,b,c]} \mathbf{S_{h,x}} &= (\mathbf{y^+_{h,a}}+\mathbf{y^+_{h,b}}+\mathbf{y^+_{h,c}})^*|\mathbf{V^+_h}|^2+(\mathbf{y^-_{h,a}}+\mathbf{y^-_{h,b}}+\mathbf{y^-_{h,c}})^*|\mathbf{V^-_h}|^2+\\ &\quad(\mathbf{y^+_{h,a}}+\boldsymbol{\alpha}\mathbf{y^+_{h,b}}+\boldsymbol{\alpha}^2\mathbf{y^+_{h,c}})^*\mathbf{V^{+*}_h}\mathbf{V^-_h}+\\ &\quad(\mathbf{y^-_{h,a}}+\boldsymbol{\alpha}^2\mathbf{y^-_{h,b}}+\boldsymbol{\alpha}\mathbf{y^-_{h,c}})^*\mathbf{V^+_h}\mathbf{V^{-*}_h} \qquad (6.16)\\ \sum_{x\in[a,b,c]} \mathbf{S_{h,x}} &= \left[(\mathbf{Y^s_h}+\mathbf{Y^{-+}_h})+(\mathbf{Y^s_h}+\boldsymbol{\alpha}^2\mathbf{Y^{-+}_h})+(\mathbf{Y^s_h}+\boldsymbol{\alpha}\mathbf{Y^{-+}_h})\right]^*|\mathbf{V^+_h}|^2+\\ &\quad\left[(\mathbf{Y^s_h}+\mathbf{Y^{+-}_h})+(\mathbf{Y^s_h}+\boldsymbol{\alpha}\mathbf{Y^{+-}_h})+(\mathbf{Y^s_h}+\boldsymbol{\alpha}^2\mathbf{Y^{+-}_h})\right]^*|\mathbf{V^-_h}|^2+\\ &\quad\left[(\mathbf{Y^s_h}+\mathbf{Y^{-+}_h})+\boldsymbol{\alpha}(\mathbf{Y^s_h}+\boldsymbol{\alpha}^2\mathbf{Y^{-+}_h})+\boldsymbol{\alpha}^2(\mathbf{Y^s_h}+\boldsymbol{\alpha}\mathbf{Y^{-+}_h})\right]^*\mathbf{V^{+*}_h}\mathbf{V^-_h}+\\ &\quad\left[(\mathbf{Y^s_h}+\mathbf{Y^{+-}_h})+\boldsymbol{\alpha}^2(\mathbf{Y^s_h}+\boldsymbol{\alpha}\mathbf{Y^{+-}_h})+\boldsymbol{\alpha}(\mathbf{Y^s_h}+\boldsymbol{\alpha}^2\mathbf{Y^{+-}_h})\right]^*\mathbf{V^+_h}\mathbf{V^{-*}_h}. \qquad (6.17)\end{aligned}$$

Considering the identity $1+\boldsymbol{\alpha}+\boldsymbol{\alpha}^2=0$, the sum of the complex powers simplifies to

$$\sum_{x\in[a,b,c]} \mathbf{S_{h,x}} = 3\left\{\left[|\mathbf{V^+_h}|^2+|\mathbf{V^-_h}|^2\right]\mathbf{Y^{s*}_h}+\mathbf{Y^{-+*}_h}\mathbf{V^{+*}_h}\mathbf{V^-_h}+\mathbf{Y^{+-*}_h}\mathbf{V^+_h}\mathbf{V^{-*}_h}\right\}. \qquad (6.18)$$

Extracting the real part of (6.18),

$$P_h = \Re\left(\sum_{x\in[a,b,c]} \mathbf{S_{h,x}}\right) \tag{6.19}$$

$$P_h = 3\Re\left\{\left[|\mathbf{V_h^+}|^2 + |\mathbf{V_h^-}|^2\right]\mathbf{Y_h^{s}}^* + \mathbf{Y_h^{-+}}^*\mathbf{V_h^+}^*\mathbf{V_h^-} + \mathbf{Y_h^{+-}}^*\mathbf{V_h^+}\mathbf{V_h^-}^*\right\} \tag{6.20}$$

$$P_h = 3\left\{\left[|\mathbf{V_h^+}|^2 + |\mathbf{V_h^-}|^2\right]\Re(\mathbf{Y_h^{s}}^*) + \Re(\mathbf{Y_h^{-+}}^*\mathbf{V_h^+}^*\mathbf{V_h^-}) + \Re(\mathbf{Y_h^{+-}}^*\mathbf{V_h^+}\mathbf{V_h^-}^*)\right\} \tag{6.21}$$

$$P_h = 3\left\{\left[|\mathbf{V_h^+}|^2 + |\mathbf{V_h^-}|^2\right]G_h^s + \Re(|\mathbf{Y_h^{-+}}|e^{-\mathbf{j}\varphi_h^{-+}}|\mathbf{V_h^+}|e^{-\mathbf{j}\theta_h^+}|\mathbf{V_h^-}|e^{\mathbf{j}\theta_h^-}) + \Re(|\mathbf{Y_h^{+-}}|e^{-\mathbf{j}\varphi_h^{+-}}|\mathbf{V_h^+}|e^{\mathbf{j}\theta_h^+}|\mathbf{V_h^-}|e^{-\mathbf{j}\theta_h^-})\right\} \tag{6.22}$$

$$P_h = 3\left\{\left[|\mathbf{V_h^+}|^2 + |\mathbf{V_h^-}|^2\right]G_h^s + \Re(|\mathbf{Y_h^{-+}}||\mathbf{V_h^+}||\mathbf{V_h^-}|e^{\mathbf{j}\theta_h^- - \mathbf{j}\varphi_h^{-+} - \mathbf{j}\theta_h^+}) + \Re(|\mathbf{Y_h^{+-}}||\mathbf{V_h^+}||\mathbf{V_h^-}|e^{-\mathbf{j}\theta_h^- + \mathbf{j}\theta_h^+ - \mathbf{j}\varphi_h^{+-}})\right\} \tag{6.23}$$

$$P_h = 3\left\{\left[|\mathbf{V_h^+}|^2 + |\mathbf{V_h^-}|^2\right]G_h^s + |\mathbf{V_h^+V_h^-}|\left[|\mathbf{Y_h^{-+}}|\cos(\theta_h^- - \theta_h^+ - \varphi_h^{-+}) + |\mathbf{Y_h^{+-}}|\cos(\theta_h^- - \theta_h^+ + \varphi_h^{+-})\right]\right\}. \tag{6.24}$$

Changing the order of the terms inside the squared brackets

$$P_h = 3\left\{\left[|\mathbf{V_h^+}|^2 + |\mathbf{V_h^-}|^2\right]G_h^s + |\mathbf{V_h^+V_h^-}|\left[|\mathbf{Y_h^{+-}}|\cos(\theta_h^- - \theta_h^+ + \varphi_h^{+-}) + |\mathbf{Y_h^{-+}}|\cos(\theta_h^- - \theta_h^+ - \varphi_h^{-+})\right]\right\}. \tag{6.25}$$

Considering the trigonometric identity (I.1), shown in appendix I, with $x = \theta_h^- - \theta_h^+$, $\mathbf{a} = \mathbf{Y_h^{+-}}$ and $\mathbf{b} = \mathbf{Y_h^{-+}}^*$, then $\mathbf{c} = \mathbf{Y_h^P} = |\mathbf{Y_h^P}|\underline{/\varphi_h^P}$ and

$$P_h = 3\left\{\left[|\mathbf{V_h^+}|^2 + |\mathbf{V_h^-}|^2\right]G_h^s + |\mathbf{V_h^+V_h^-}||\mathbf{Y_h^P}|\cos(\theta_h^- - \theta_h^+ + \varphi_h^P)\right\}. \tag{6.26}$$

It is worth noting that $\mathbf{Y_h^P}$ can be rewritten only in terms of the load's conductances as

$$\mathbf{Y_h^P} = \mathbf{Y_h^{+-}} + \mathbf{Y_h^{-+}}^* = -2(G_{h,ab}\boldsymbol{\alpha} + G_{h,bc} + G_{h,ca}\boldsymbol{\alpha}^2). \tag{6.27}$$

Adding up the individual harmonic active powers, its is found that the total active power is given by

$$P = \sum_{h\in H} 3|\mathbf{V_h^+}|^2\left[G_h^s(1+\mathrm{VUF}^2) + |\mathbf{Y_h^P}|\cos(\theta_h^- - \theta_h^+ + \varphi_h^P)\mathrm{VUF}\right], \tag{6.28}$$

where G_h^s is the equivalent conductance given by the real part of $\mathbf{Y_h^s}$ and $\mathbf{Y_h^P} = \mathbf{Y_h^{+-}} + (\mathbf{Y_h^{-+}})^* = |\mathbf{Y_h^P}|\underline{/\varphi_h^P}$.

Extracting the imaginary part of (6.18),

$$Q_h = \Im\left(\sum_{x\in[a,b,c]} \mathbf{S_{h,x}}\right) \tag{6.29}$$

$$Q_h = 3\Im\left\{\left[|\mathbf{V_h^+}|^2 + |\mathbf{V_h^-}|^2\right]\mathbf{Y_h^{s}}^* + \mathbf{Y_h^{-+}}^*\mathbf{V_h^+}^*\mathbf{V_h^-} + \mathbf{Y_h^{+-}}^*\mathbf{V_h^+}\mathbf{V_h^-}^*\right\} \tag{6.30}$$

$$Q_h = 3\left\{\left[|\mathbf{V_h^+}|^2 + |\mathbf{V_h^-}|^2\right]\Im(\mathbf{Y_h^{s}}^*) + \Im(\mathbf{Y_h^{-+}}^*\mathbf{V_h^+}^*\mathbf{V_h^-}) + \Im(\mathbf{Y_h^{+-}}^*\mathbf{V_h^+}\mathbf{V_h^-}^*)\right\} \tag{6.31}$$

$$Q_h = 3\left\{\left[|\mathbf{V_h^+}|^2 + |\mathbf{V_h^-}|^2\right](-B_h^s) + \Im(|\mathbf{Y_h^{-+}}|e^{-\mathbf{j}\varphi_h^{-+}}|\mathbf{V_h^+}|e^{-\mathbf{j}\theta_h^+}|\mathbf{V_h^-}|e^{\mathbf{j}\theta_h^-}) + \Im(|\mathbf{Y_h^{+-}}|e^{-\mathbf{j}\varphi_h^{+-}}|\mathbf{V_h^+}|e^{\mathbf{j}\theta_h^+}|\mathbf{V_h^-}|e^{-\mathbf{j}\theta_h^-})\right\} \tag{6.32}$$

$$Q_h = 3\left\{\left[|\mathbf{V_h^+}|^2 + |\mathbf{V_h^-}|^2\right](-B_h^s) + \Im(|\mathbf{Y_h^{-+}}||\mathbf{V_h^+}||\mathbf{V_h^-}|e^{\mathbf{j}\theta_h^- - \mathbf{j}\varphi_h^{-+} - \mathbf{j}\theta_h^+}) + \Im(|\mathbf{Y_h^{+-}}||\mathbf{V_h^+}||\mathbf{V_h^-}|e^{-\mathbf{j}\theta_h^- + \mathbf{j}\theta_h^+ - \mathbf{j}\varphi_h^{+-}})\right\} \tag{6.33}$$

$$Q_h = 3\left\{\left[|\mathbf{V_h^+}|^2 + |\mathbf{V_h^-}|^2\right](-B_h^s) + |\mathbf{V_h^+V_h^-}|\left[|\mathbf{Y_h^{-+}}|\sin(\theta_h^- - \theta_h^+ - \varphi_h^{-+}) - |\mathbf{Y_h^{+-}}|\sin(\theta_h^- - \theta_h^+ + \varphi_h^{+-})\right]\right\}. \tag{6.34}$$

Changing the order of the terms inside the squared brackets

$$Q_h = 3\Big\{ \left[|\mathbf{V_h^+}|^2 + |\mathbf{V_h^-}|^2\right](-B_h^s) - |\mathbf{V_h^+V_h^-}|\left[|\mathbf{Y_h^{+-}}|\sin(\theta_h^- - \theta_h^+ + \varphi_h^{+-}) - |\mathbf{Y_h^{-+}}|\sin(\theta_h^- - \theta_h^+ - \varphi_h^{-+})\right]\Big\}. \tag{6.35}$$

Considering the trigonometric identity (I.2), shown in appendix I, with $x = \theta_h^- - \theta_h^+$, $\mathbf{a} = \mathbf{Y_h^{+-}}$ and $\mathbf{b} = -\mathbf{Y_h^{-+*}}$, then $\mathbf{c} = \mathbf{Y_h^Q} = |\mathbf{Y_h^Q}|\underline{/\varphi_h^Q}$ and

$$Q_h = -3\Big\{ \left[|\mathbf{V_h^+}|^2 + |\mathbf{V_h^-}|^2\right] B_h^s + |\mathbf{V_h^+V_h^-}||\mathbf{Y_h^Q}|\sin(\theta_h^- - \theta_h^+ + \varphi_h^Q)\Big\}. \tag{6.36}$$

It is worth noting that $\mathbf{Y_h^Q}$ can be rewritten only in terms of the load's susceptances as

$$\mathbf{Y_h^Q} = \mathbf{Y_h^{+-}} - \mathbf{Y_h^{-+*}} = -2(B_{h,ab}\boldsymbol{\alpha} + B_{h,bc} + B_{h,ca}\boldsymbol{\alpha}^2). \tag{6.37}$$

Considering the fundamental positive-sequence voltage as the angular reference, leads to $\theta_1^+ = 0$, $\mathbf{V_1^+} = V_1^+$ and the fundamental active power is

$$P_1 = 3|\mathbf{V_1^+}|^2\left[G_1^s(1 + \mathrm{VUF}^2) + |\mathbf{Y_1^P}|\cos(\theta_1^- + \varphi_1^P)\mathrm{VUF}\right] \tag{6.38}$$

Likewise, the fundamental reactive power is given by

$$Q_1 = -3|\mathbf{V_1^+}|^2\left[B_1^s(1 + \mathrm{VUF}^2) + |\mathbf{Y_1^Q}|\sin(\theta_1^- + \varphi_1^Q)\mathrm{VUF}\right]. \tag{6.39}$$

With the expressions for the active and complex powers of each phase, we investigate the PF definitions next.

6.1.1 Fundamental Per-Phase Power Factor

In the following, we proceed to rewrite $PF_{1,a}$ in terms of the VUF and the load admittances. First, the active and apparent power are obtained in terms of the VUF and the load admittances. Then, these powers are used to compute $PF_{1,a}$. Although only $PF_{1,a}$ is obtained and discussed for the sake of concision, analogous equations and conclusions can be obtained for phases "b" and "c".

After some algebraic manipulations, the fundamental active power of phase "a" can be rewritten as

$$P_{1,a} = |\mathbf{V_1^+}|^2\left[g_1^+ + |\mathbf{y_{1,a}^P}|\cos(\theta_1^- + \varphi_{1,a}^P)\mathrm{VUF} + g_1^-\mathrm{VUF}^2\right] \tag{6.40}$$

where $\mathbf{y_{1,a}^P} = (\mathbf{y_{1,a}^+})^* + \mathbf{y_{1,a}^-}$. Considering the positive-sequence voltage as the angular reference, the cosine law can be applied to the complex power in (6.13) to obtain the fundamental apparent power of phase "a" as in (6.41). Dividing the active power (6.40) by the apparent power (6.41), the fundamental PF of phase "a" is found as (6.42). It can be observed that (6.42) is a non-linear function of the VUF and the load's admittances. So, first, we are going to examine the non-linear PF expression considering the scenarios in which the load and/or the voltages are balanced. Then, we are linearizing (6.42) in order to discuss the expected behavior when both the load and the voltages are unbalanced.

$$S_{1,a} = |V^+|^2\sqrt{1 + 2\cos(\theta_1^-)\text{VUF} + \text{VUF}^2}\sqrt{|\mathbf{y^+_{1,a}}|^2 + 2|\mathbf{y^+_{1,a}}||\mathbf{y^-_{1,a}}|\cos(\theta_1^- + \varphi^-_{1,a} - \varphi^+_{1,a})\text{VUF} + |\mathbf{y^-_{1,a}}|^2\text{VUF}^2} \tag{6.41}$$

$$PF_{1,a} = \frac{g^+ + |\mathbf{y^P_{1,a}}|\cos(\theta_1^- + \varphi^P_{1,a})\text{VUF} + g^-\text{VUF}^2}{\sqrt{1 + 2\cos(\theta_1^-)\text{VUF} + \text{VUF}^2}\sqrt{|\mathbf{y^+_{1,a}}|^2 + 2|\mathbf{y^+_{1,a}}||\mathbf{y^-_{1,a}}|\cos(\theta_1^- + \varphi^-_{1,a} - \varphi^+_{1,a})\text{VUF} + |\mathbf{y^-_{1,a}}|^2\text{VUF}^2}} \tag{6.42}$$

When the voltages are balanced, *i.e.* the VUF is equal to zero, the fundamental power factor of phase "a" simplifies to

$$PF_{1,a} = \frac{g^+}{|\mathbf{y^+_{1,a}}|}, \text{ if VUF} = 0. \tag{6.43}$$

It is worth mentioning that (6.43) depends exclusively on the load's admittances $\mathbf{y_{1,ab}}$ and $\mathbf{y_{1,ca}}$. So it is not affected by any voltage parameters and it is valid for both balanced and unbalanced loads.

If the voltages are unbalanced but the load is balanced, then $V^- \neq 0$ and $\mathbf{y_{h,ab}} = \mathbf{y_{h,ca}} = \mathbf{y_{h,bc}} = y$, thus $\mathbf{y^+_{h,a}} = \mathbf{y^-_{h,a}} = \mathbf{Y^s_h}$. Under these constraints, the complex power of (6.13) simplifies to

$$\mathbf{S_{1,a}} = |\mathbf{V^+_1} + \mathbf{V^-_1}|^2(\mathbf{Y^s_1})^* \tag{6.44}$$

and the fundamental power factor of phase "a" is

$$PF_{1,a} = \frac{g^+}{|\mathbf{y^+_{1,a}}|} = \frac{G^s_1}{|\mathbf{Y^s_1}|}. \tag{6.45}$$

It can be observed that (6.45) is once again not affected by any voltage parameters, but only by the load's admittance angle.

At last, equation (6.42) can be linearized considering that in real distribution grids utilities seek to maintain the VUF within certain established limits. According to [83], a VUF up to 3% is common in real distribution systems, tough it may be higher than the VUF limits in some regulations. So, the non-linear formula for $PF_{1,a}$ can be linearized using the first two coefficients of its Taylor series, resulting in

$$PF_{1,a} \approx \frac{g^+}{|\mathbf{y^+_{1,a}}|} + \left|\frac{\mathbf{y^u_a}}{\mathbf{y^+_{1,a}}}\right|\cos(\theta_1^- + \varphi^u_{1,a})\text{VUF} \tag{6.46}$$

where $\mathbf{y^u_a} = \mathbf{y^P_{1,a}} - g^+(1 + \mathbf{y^-_{1,a}}/\mathbf{y^+_{1,a}})$. It can be observed that this linearized equation shows that $PF_{1,a}$ has a sinusoidal dependence with respect to the negative-sequence angle and having the VUF multiplying the sine amplitude, thus explaining the results observed in the simulations and experimental tests.

6.1.2 Fundamental Arithmetic Power Factor

The fundamental arithmetic PF can be computed in terms of the load's fundamental active power and arithmetic apparent power. The fundamental active power of delta-connected loads can be expressed in terms

of sequence components as in (6.38). The fundamental arithmetic apparent power can be obtained from the arithmetic sum of each phase fundamental apparent power. For phase "a", the fundamental apparent power is given by (6.41). The fundamental apparent powers of phases "b" and "c" are given by (6.47) and (6.48), respectively.

$$S_{1,b} = |\mathbf{V_1^+}|^2\sqrt{1+2\cos(\theta_1^- - 120°)\text{VUF}+\text{VUF}^2} \\ \sqrt{|\mathbf{y_{1,b}^+}|^2+2|\mathbf{y_{1,b}^+}||\mathbf{y_{1,b}^-}|\cos(\theta_1^- + \varphi_{1,b}^- - \varphi_{1,b}^+ - 120°)\text{VUF}+|\mathbf{y_{1,b}^-}|^2\text{VUF}^2} \tag{6.47}$$

$$S_{1,c} = |\mathbf{V_1^+}|^2\sqrt{1+2\cos(\theta_1^- + 120°)\text{VUF}+\text{VUF}^2} \\ \sqrt{|\mathbf{y_{1,c}^+}|^2+2|\mathbf{y_{1,c}^+}||\mathbf{y_{1,c}^-}|\cos(\theta_1^- + \varphi_{1,c}^- - \varphi_{1,c}^+ + 120°)\text{VUF}+|\mathbf{y_{1,c}^-}|^2\text{VUF}^2} \tag{6.48}$$

Having the fundamental apparent power for each phase, the fundamental arithmetic PF is found as

$$PF_1^a = \frac{3|\mathbf{V_1^+}|^2\left[G_1^s(1+\text{VUF}^2)+|\mathbf{Y_1^P}|\cos(\theta_1^- + \varphi_1^P)\text{VUF}\right]}{S_a+S_b+S_c}. \tag{6.49}$$

It can be observed that PF_1^a is a non-linear function of the VUF and the load's admittances.

When the source is balanced, the VUF is equal to zero and the fundamental arithmetic apparent power simplifies to

$$S_1^a = \sum_{x\in[a,b,c]}|\mathbf{S_x}| = |\mathbf{V_1^+}|^2A^a, \text{ if VUF} = 0 \tag{6.50}$$

where $A^a = |\mathbf{y_{1,a}^+}| + |\mathbf{y_{1,b}^+}| + |\mathbf{y_{1,c}^+}|$. In this case, the fundamental active power, given by

$$P_1 = 3G_1^s|\mathbf{V_1^+}|^2, \text{ if VUF} = 0, \tag{6.51}$$

depends only on the equivalent conductance G_1^s and on the fundamental positive-sequence voltage V_1^+. These simplifications lead to

$$PF_1^a = \frac{3G_1^s}{A^a}, \text{ if VUF} = 0, \tag{6.52}$$

which depends solely on the load's admittance and not on the voltages. It is noteworthy that (6.52) is valid for both balanced and unbalanced loads as long as the voltages are balanced.

When the source is unbalanced and the load is balanced, then $V^- \neq 0$, $\mathbf{y_{h,ab}} = \mathbf{y_{h,bc}} = \mathbf{y_{h,ca}}$, $\mathbf{Y_h^{+-}} = \mathbf{Y_h^{-+}} = 0$, and $\mathbf{y_{h,a}^+} = \mathbf{y_{h,a}^-} = \mathbf{y_{h,b}^+} = \mathbf{y_{h,b}^-} = \mathbf{y_{h,c}^+} = \mathbf{y_{h,c}^-} = \mathbf{Y_h^s}$. Under these constraints, (6.38) simplifies to

$$P_1 = 3G_1^s\left[|\mathbf{V_1^+}|^2+|\mathbf{V_1^-}|^2\right], \text{ if } \mathbf{y_{h,ab}} = \mathbf{y_{h,bc}} = \mathbf{y_{h,ca}}, \tag{6.53}$$

the fundamental arithmetic apparent power simplifies to

$$S_1^a = 3\left[|\mathbf{V_1^+}|^2+|\mathbf{V_1^-}|^2\right]|\mathbf{Y_1^s}|, \text{ if } \mathbf{y_{h,ab}} = \mathbf{y_{h,bc}} = \mathbf{y_{h,ca}} \tag{6.54}$$

and the fundamental arithmetic PF simplifies to

$$PF_1^a = \frac{G_1^s}{A^a} = \frac{G_1^s}{|\mathbf{Y_1^s}|}, \text{ if } \mathbf{y_{h,ab}} = \mathbf{y_{h,bc}} = \mathbf{y_{h,ca}} \tag{6.55}$$

from which it is clear that only the load's parameters affects the value of PF_1^a.

At last, equation (6.49) can be linearized for small VUF as mentioned before. So, the non-linear formula for PF_1^a can be linearized using the first two coefficients of its Taylor series, resulting in

$$PF_1^a \approx \frac{3G_1^s}{A^a} + \frac{3\,|\mathbf{Y_1^{au}}|}{A^a}\cos(\theta_1^- + \varphi_1^{au})\text{VUF} \tag{6.56}$$

where

$$\mathbf{Y_1^{au}} = \mathbf{Y_1^P} - \frac{G_1^s}{A^a}\left(\mathbf{y_a^u} + \mathbf{y_b^u} + \mathbf{y_c^u}\right) = |\mathbf{Y_1^{au}}|\underline{/\varphi_1^{au}} \tag{6.57}$$

$$\mathbf{y_a^u} = |\mathbf{y_{1,a}^+}|\left(1 + \frac{\mathbf{y_{1,a}^-}}{\mathbf{y_{1,a}^+}}\right) \tag{6.58}$$

$$\mathbf{y_b^u} = |\mathbf{y_{1,b}^+}|\boldsymbol{\alpha}^2\left(1 + \frac{\mathbf{y_{1,b}^-}}{\mathbf{y_{1,b}^+}}\right) \tag{6.59}$$

$$\mathbf{y_c^u} = |\mathbf{y_{1,c}^+}|\boldsymbol{\alpha}\left(1 + \frac{\mathbf{y_{1,c}^-}}{\mathbf{y_{1,c}^+}}\right). \tag{6.60}$$

Based on the this linearized equation (6.56), it can be observed a sinusoidal dependence with respect to the negative-sequence angle, having the VUF multiplying the sine amplitude. Therefore, (6.56) explains the results observed in the simulations and experimental tests.

Summarizing, when the source or the load are balanced, then PF_1^a depends exclusively on the load's admittances. When the voltages and the load are both unbalanced, it was shown that PF_1^a is a non-linear function of the VUF and the load's admittances. For small VUF values, PF_1^a is approximately sinusoidal, having the VUF as the sine amplitude and the negative-sequence voltage angle as the sine argument.

6.1.3 Fundamental Geometric Power Factor

The fundamental geometric PF can be computed by dividing the active power given in (6.38) by the fundamental geometric apparent power, which is the absolute value of (6.18). Computing the absolute value of (6.18) by adding the squares of the real and imaginary parts leads to

$$\begin{aligned}(S_1^g)^2 = 9|\mathbf{V_1^+}|^4\Big\{&|\mathbf{Y_1^s}|^2(1+\text{VUF}^2)^2 + \\ &2|\mathbf{Y_1^s}|(1+\text{VUF}^2)\text{VUF}\left[|\mathbf{Y_1^{+-}}|\cos(\varphi_1^{+-} + \theta_1^- - \varphi_1^e) + |\mathbf{Y_1^{-+}Y_1^s}|\cos(\varphi_1^{-+} - \theta_1^- - \varphi_1^e)\right] + \\ &\text{VUF}^2\left[|\mathbf{Y_1^{+-}}|^2 + |\mathbf{Y_1^{-+}}|^2 + 2|\mathbf{Y_1^{+-}}||\mathbf{Y_1^{-+}}|\cos(\varphi_1^{+-} - \varphi_1^{-+} + 2\theta_1^-)\right]\Big\}.\end{aligned} \tag{6.61}$$

Applying the trigonometric identity (I.1), the following simplification is obtained

$$S_1^g = 3|V^+|^2\sqrt{|\mathbf{Y_1^s}|^2(1+\text{VUF}^2)^2 + 2(1+\text{VUF}^2)|\mathbf{Y_1^c}|\text{VUF}\cos(\theta_1^- + \theta_1^c) + |\mathbf{Y_1^d}|^2\text{VUF}^2}, \tag{6.62}$$

where

$$\mathbf{Y_1^c} = \mathbf{Y_1^{+-}Y_1^{s*}} + \mathbf{Y_1^{-+*}Y_1^s} \tag{6.63}$$

and

$$\mathbf{Y_1^d} = \mathbf{Y_1^{+-}}\frac{\mathbf{V_1^-}}{|\mathbf{V_1^-}|} + \mathbf{Y_1^{-+}}\frac{\mathbf{V_1^{-*}}}{|\mathbf{V_1^-}|}. \tag{6.64}$$

Diving (6.38) by (6.62), the exact expression for the PF_1^g is obtained as

$$PF_1^g = \frac{G_1^s\left(1+\text{VUF}^2\right) + |\mathbf{Y_1^P}|\cos(\theta_1^- + \varphi_1^P)\text{VUF}}{\sqrt{|\mathbf{Y_1^s}|^2(1+\text{VUF}^2)^2 + 2(1+\text{VUF}^2)|\mathbf{Y_1^c}|\text{VUF}\cos(\theta_1^- + \theta_1^c) + |\mathbf{Y_1^d}|^2\text{VUF}^2}}. \tag{6.65}$$

If the load is purely resistive, then $\mathbf{Y_h^s} = G_h^s$, $\theta_h^s = 0$ and the fundamental reactive geometric power given by (6.39) is zero. So, the fundamental apparent power geometric power is simply given by the fundamental active power and PF_1^g is constant and equal to one. This explains the results obtained in the simulations and experimental tests. It is noteworthy that if the load is not purely resistive, then $B_h^s \neq 0$ and PF_1^g will be a non-linear function of the negative-sequence voltage angle and magnitude.

When the source is balanced, VUF = 0 and the fundamental geometric apparent power simplifies to

$$S_1^g = \left|\sum_{x\in[a,b,c]} \mathbf{S_{1,x}}\right| = 3|\mathbf{V_1^+}|^2|\mathbf{Y_1^s}|, \text{ if VUF} = 0. \tag{6.66}$$

In this case, the fundamental active power is given by (6.51) and it depends only on the equivalent conductance G_1^s and on the fundamental positive-sequence voltage V_1^+. These simplifications lead to

$$PF_1^g = \frac{G_1^s}{|\mathbf{Y_1^s}|}, \text{ if VUF} = 0, \tag{6.67}$$

which is valid for both balanced and unbalanced loads and it depends solely on the load's admittance and not on the voltages.

When the source is unbalanced and the load is balanced, then $V^- \neq 0$, $\mathbf{y_{h,ab}} = \mathbf{y_{h,bc}} = \mathbf{y_{h,ca}}$, $\mathbf{Y_h^{+-}} = \mathbf{Y_h^{-+}} = 0$, and $\mathbf{y_{h,a}^+} = \mathbf{y_{h,a}^-} = \mathbf{y_{h,b}^+} = \mathbf{y_{h,b}^-} = \mathbf{y_{h,c}^+} = \mathbf{y_{h,c}^-} = \mathbf{Y_h^s}$. Under these constraints, (6.38) simplifies to (6.53) and the fundamental geometric apparent power simplifies to

$$S_1^g = 3\left[|\mathbf{V_1^+}|^2 + |\mathbf{V_1^-}|^2\right]|\mathbf{Y_1^s}|, \text{ if } \mathbf{y_{h,ab}} = \mathbf{y_{h,bc}} = \mathbf{y_{h,ca}}, \tag{6.68}$$

and the fundamental geometric PF simplifies to (6.67) from which it is clear that only the load's parameters affects the value of PF_1^g.

At last, equation (6.65) can be linearized for small VUF as mentioned before. So, the non-linear formula for PF_1^g can be linearized using the first two coefficients of its Taylor series, resulting in

$$PF_1^g \approx \frac{G_1^s}{\mathbf{Y_1^s}} + \left|\frac{\mathbf{Y}^\tau}{\mathbf{Y_1^s}}\right|\cos(\theta_1^- + \tau)\text{VUF} \tag{6.69}$$

where

$$\mathbf{Y}^\tau = \mathbf{Y_1^P} - \frac{G_1^s}{|\mathbf{Y_1^s}|^2}Y^c. \tag{6.70}$$

Based on the this linearized equation (6.69), it can be observed a sinusoidal dependence with respect to the negative-sequence angle, having the VUF multiplying the sine amplitude. However, as mentioned before, if the load is purely resistive then $PF_1^g = 1$ because $\mathbf{Y_1^s} = G_1^s$ and $Y^c = \mathbf{Y_1^P} G_1^s$ leading to $\mathbf{Y}^\tau = 0$ and $PF_1^g = 1$.

Summarizing, when the source or the load are balanced, then PF_1^g depends exclusively on the load's admittances. When both the voltages and the load are unbalanced, it was shown that PF_1^g is a non-linear function of the VUF and the load's admittances.

6.1.4 Fundamental Positive-Sequence Power Factor

The fundamental positive-sequence complex power is given by

$$\mathbf{S_1^+} = 3\mathbf{V_1^+}(\mathbf{I_1^+})^*. \tag{6.71}$$

Considering that

$$\mathbf{I_1^+} = \mathbf{Y_1^s}\mathbf{V_1^+} + \mathbf{Y_1^{+-}}\mathbf{V_1^-}, \tag{6.72}$$

the complex power can be rewritten as

$$\mathbf{S_1^+} = 3\left[|\mathbf{V_1^+}|^2(\mathbf{Y_1^s})^* + \mathbf{V_1^+}(\mathbf{V_1^-}\mathbf{Y_1^{+-}})^*\right] \tag{6.73}$$

and the fundamental positive-sequence active power, given by the real part of $\mathbf{S}^+$, is

$$P_1^+ = 3\left[|\mathbf{V_1^+}|^2 G_1^s + \mathbf{V_1^+}\mathbf{V_1^-}|\mathbf{Y_1^{+-}}|\cos(\theta_1^- + \varphi_1^{+-})\right]. \tag{6.74}$$

The fundamental positive-sequence apparent power is given by the non-linear equation (6.75). So, the PF_1^+ can be computed as (6.76).

$$S_1^+ = 3|\mathbf{V_1^+}|^2\sqrt{\left[|\mathbf{Y_1^s}|^2 + 2\text{VUF}|\mathbf{Y_1^s}\mathbf{Y_1^{+-}}|\cos(\theta_1^- + \varphi_1^{+-} - \theta_1^s) + \text{VUF}^2|\mathbf{Y_1^{+-}}|^2\right]} \tag{6.75}$$

$$PF_1^+ = \frac{G_1^s + \text{VUF}|\mathbf{Y_1^{+-}}|\cos(\theta_1^- + \varphi_1^{+-}).}{\sqrt{\left[|\mathbf{Y_1^s}|^2 + 2\text{VUF}|\mathbf{Y_1^s}\mathbf{Y_1^{+-}}|\cos(\theta_1^- + \varphi_1^{+-} - \theta_1^s) + \text{VUF}^2|\mathbf{Y_1^{+-}}|^2\right]}} \tag{6.76}$$

When the source is balanced, the VUF is zero. In this case, the fundamental positive-sequence active power, given by (6.74) simplifies to

$$P_1^+ = 3|\mathbf{V_1^+}|^2 G_1^s \tag{6.77}$$

and it depends only on the equivalent conductance G_1^s and on the fundamental positive-sequence voltage V_1^+. The fundamental positive-sequence apparent power simplifies to

$$S_1^+ = |\mathbf{S_1^+}| = 3|\mathbf{V_1^+}|^2|\mathbf{Y_1^s}|. \tag{6.78}$$

These simplifications lead to

$$PF_1^+ = \frac{G_1^s}{|\mathbf{Y_1^s}|} \tag{6.79}$$

which is valid for both balanced and unbalanced loads and it depends solely on the load's admittance and not on the voltages.

When the source is unbalanced and the load is balanced, then $V^- \neq 0$, $\mathbf{y_{h,ab}} = \mathbf{y_{h,bc}} = \mathbf{y_{h,ca}}$, $\mathbf{Y_h^{+-}} = \mathbf{Y_h^{-+}} = 0$, and $\mathbf{y_{h,a}^+} = \mathbf{y_{h,a}^-} = \mathbf{y_{h,b}^+} = \mathbf{y_{h,b}^-} = \mathbf{y_{h,c}^+} = \mathbf{y_{h,c}^-} = \mathbf{Y_h^s}$. Under these constraints, (6.74) simplifies to (6.77) and the fundamental positive-sequence apparent power simplifies to (6.78) and the fundamental positive-sequence PF simplifies to (6.79) from which it is clear that only the load's parameters affects the value of PF_1^+.

At last, equation (6.76) can be linearized for small VUF as mentioned before. So, the non-linear formula for PF_1^+ can be linearized using the first two coefficients of its Taylor series, resulting in

$$PF_1^+ \approx \frac{G_1^s}{|\mathbf{Y_1^s}|} + \left|\frac{\mathbf{Y_1^p}}{\mathbf{Y_1^s}}\right| \cos(\theta_1^- + \theta_1^p)\text{VUF} \tag{6.80}$$

where

$$\mathbf{Y_1^p} = \mathbf{Y_1^{+-}}(1 - \frac{G_1^s}{\mathbf{Y_1^s}}).$$

Based on the this linearized equation (6.80), it can be observed a sinusoidal dependence with respect to the negative-sequence angle, having the VUF multiplying the sine amplitude. However, if the load is purely resistive then $\mathbf{Y_h^s} = G_h^s$ and $\mathbf{Y_1^p} = 0$ leading to $PF_1^g \approx 1$. It is noteworthy that this approximation is valid only for small VUF values unlike the PF_1^g which is always equal to one if the load is purely resistive.

Summarizing, when the source or the load are balanced, then PF_1^+ depends exclusively on the load's admittances. Additionally, (6.56) explains the results observed in Section 4.1.

6.1.5 Effective Power Factor

The effective PF is given by the ratio of the active power and the effective apparent power, both encompassing all frequency components. First, let us analyze the effective PF considering only sinusoidal voltages and currents.

The fundamental active power is rewritten as a function of the voltage and the load's admittances in the sequence domain in (6.38). According to the cosine law, the effective apparent power (2.73) considering only the fundamental component can be rewritten as

$$S_1^e = 3\sqrt{|\mathbf{V_1^+}|^2 + |\mathbf{V_1^-}|^2}\sqrt{|\mathbf{Y_1^s V_1^+} + \mathbf{Y_1^{+-}V_1^-}|^2 + |\mathbf{Y_1^s V_1^-} + \mathbf{Y_1^{-+}V_1^+}|^2}. \tag{6.81}$$

Considering the trigonometric identity 1 (shown in appendix I), equation (6.81) can be further simplified into

$$S_1^e = 3|\mathbf{V_1^+}|^2\sqrt{1+\text{VUF}^2}\sqrt{(|\mathbf{Y_1^s}|^2 + |\mathbf{Y_1^{-+}}|^2) + 2\text{VUF}|\mathbf{Y^u}|\cos(\theta_1^- + \varphi_1^u) + \text{VUF}^2(|\mathbf{Y_1^s}|^2 + |\mathbf{Y_1^{+-}}|^2)} \tag{6.82}$$

where $\mathbf{Y^u} = (\mathbf{Y_1^s})^*\mathbf{Y_1^{+-}} + \mathbf{Y_1^s}(\mathbf{Y_1^{-+}})^* = |\mathbf{Y^u}|\underline{/\varphi_1^u}$. Dividing the active power (6.38) by the effective apparent power (6.82), the effective power factor is given by

$$PF^e = \frac{G_1^s(1+\text{VUF}^2) + \text{VUF}|\mathbf{Y_1^P}|\cos(\theta_1^- + \varphi_1^P)}{\sqrt{1+\text{VUF}^2}\sqrt{(|\mathbf{Y_1^s}|^2 + |\mathbf{Y_1^{-+}}|^2) + 2\text{VUF}|Y_1^u|\cos(\theta_1^- + \varphi_1^u) + \text{VUF}^2(|\mathbf{Y_1^s}|^2 + |\mathbf{Y_1^{+-}}|^2)}}. \tag{6.83}$$

It can be observed that P and S^e are functions of $\mathbf{V_1^+}$ and $\mathbf{V_1^-}$. PF^e, on the other hand, is a function of the VUF, θ_1^- and $\mathbf{Y_1^s}$, $\mathbf{Y_1^{+-}}$, and $\mathbf{Y_1^{-+}}$.

When the source is balanced, the VUF is equal to zero. In this case, the active power, given by (6.51) depends only on the equivalent conductance G_1^s and on the positive-sequence voltage V^+. The effective apparent power simplifies to

$$S^e = 3|\mathbf{V_1^+}|^2\sqrt{|\mathbf{Y_1^s}|^2 + |\mathbf{Y_1^{-+}}|^2}, \text{ if VUF} = 0. \tag{6.84}$$

These simplifications lead to

$$PF^e = \frac{G_h^s}{\sqrt{|\mathbf{Y_1^s}|^2 + |\mathbf{Y_1^{+-}}|^2}}, \text{ if VUF} = 0 \tag{6.85}$$

which is valid for both balanced and unbalanced loads and it depends solely on the load's admittance and not on the voltages.

When the source is unbalanced and the load is balanced, then $V^- \neq 0$, $\mathbf{y_{h,ab}} = \mathbf{y_{h,bc}} = \mathbf{y_{h,ca}}$, $\mathbf{Y_h^{+-}} = \mathbf{Y_h^{-+}} = 0$, and $\mathbf{y_{h,a}^+} = \mathbf{y_{h,a}^-} = \mathbf{y_{h,b}^+} = \mathbf{y_{h,b}^-} = \mathbf{y_{h,c}^+} = \mathbf{y_{h,c}^-} = \mathbf{Y_h^s}$. Under these constraints, (6.38) simplifies to (6.53) and the effective apparent power simplifies to

$$S^e = 3\left[|\mathbf{V_1^+}|^2 + |\mathbf{V_1^-}|^2\right]|\mathbf{Y_1^s}|, \text{ if } \mathbf{y_{h,ab}} = \mathbf{y_{h,bc}} = \mathbf{y_{h,ca}} \tag{6.86}$$

and the effective PF simplifies to

$$PF^e = \frac{G_h^s}{|\mathbf{Y_1^s}|}, \text{ if } \mathbf{y_{h,ab}} = \mathbf{y_{h,bc}} = \mathbf{y_{h,ca}} \tag{6.87}$$

from which it is clear that only the load's parameters affects the value of PF^e.

At last, equation (6.83) can be linearized for small VUF as mentioned before. So, the non-linear formula for PF^e can be linearized using the first two coefficients of its Taylor series, resulting in

$$PF^e \approx \frac{G_h^s}{\sqrt{|\mathbf{Y_1^s}|^2 + |\mathbf{Y_1^{-+}}|^2}} + \frac{|\mathbf{Y^f}|\cos(\theta_1^- + \theta^f)}{\sqrt{|\mathbf{Y_1^s}|^2 + |\mathbf{Y_1^{-+}}|^2}}\text{VUF} \tag{6.88}$$

where

$$\mathbf{Y^f} = \mathbf{Y_h^P} - \frac{G_h^s Y^u}{|\mathbf{Y_1^s}|^2 + |\mathbf{Y_1^{-+}}|^2}$$

It can be observed that this linearized equation (6.88) is composed of a constant term, with respect to the VUF, that is equal to the PF value under balanced voltages and one term that is composed of a cosine function with amplitude proportional to the product of an admittance factor ($|\mathbf{Y^f}|/\sqrt{|\mathbf{Y^s}|^2 + |\mathbf{Y^{-+}}|^2}$) with the VUF. The argument of the cosine is a function of the negative-sequence angle and the angle of $\mathbf{Y^f}$. This function (6.88), therefore, indicates that PF^e grows or decreases with the VUF depending on the sign of $\cos(\theta^- + \varphi^f)$. For any fixed value for voltage unbalance, equation (6.88) presents sinusoidal behavior with respect to θ^-, which is consistent with the experimental result obtained in Section 5.1, more specifically in Figure 5.4.

Let us now consider the effect of harmonic components. The total active power is

$$P = \sum_{h \in H} P_h \tag{6.89}$$

where

$$P_h = 3\Big\{ \left[|\mathbf{V_h^+}|^2 + |\mathbf{V_h^-}|^2\right] G_h^s + |\mathbf{V_h^+}\mathbf{V_h^-}||\mathbf{Y_h^P}| \cos(\theta_h^- - \theta_h^+ + \varphi_h^P) \Big\}, \tag{6.90}$$

is the active power component at each frequency order h, $\mathbf{Y_h^P} = |\mathbf{Y_h^P}|\underline{/\varphi_h^P} = \mathbf{Y_h^s} + \mathbf{Y_h^{-+}}^*$, $\mathbf{Y_h^{+-}}$ and $\mathbf{Y_h^{-+}}$ are the components from the admittance matrix in the sequence domain at the harmonic order h. The effective apparent power given by (2.73) can be rewritten as

$$S^e = 3\sqrt{\sum_{h\in H}(V_h^+)^2 + (V_h^-)^2}\sqrt{\sum_{h\in H}(I_h^+)^2 + (I_h^-)^2}. \tag{6.91}$$

Considering the modified effective voltage and current at the harmonic order h,

$$V_h^e = \sqrt{(V_h^+)^2 + (V_h^-)^2} \tag{6.92}$$

$$I_h^e = \sqrt{(I_h^+)^2 + (I_h^-)^2}. \tag{6.93}$$

The effective power can be rewritten as

$$S^e = 3\sqrt{\sum_{h\in H}(V_h^e)^2}\sqrt{\sum_{h\in H}(I_h^e)^2}. \tag{6.94}$$

According to Cauchy–Schwarz inequality, it can be shown that

$$S^e \geq \sum_{h\in H} V_h^e I_h^e, \tag{6.95}$$

which implies that

$$PF^e \leq \frac{\sum_{h\in H} P_h}{\sum_{h\in H} 3V_h^e I_h^e} \leq \frac{P_1}{3V_1^e I_1^e}, \tag{6.96}$$

where the second inequality holds if

$$\frac{\sum_{h\in H\setminus\{1\}} P_h}{\sum_{h\in H\setminus\{1\}} 3V_h^e I_h^e} \leq \frac{P_1}{3V_1^e I_1^e}. \tag{6.97}$$

The first bound in (6.96) indicates that when harmonics are present, they contribute to both the total active power and the effective apparent power. Their contribution to the total active power is in terms of adding each harmonic active power component. For the effective apparent power, however, the contribution of the harmonics result in a higher effective apparent power than the simply addition of each frequency component. Therefore, accounting for the harmonic components will actually lead to a lower effective PF in most practical cases where the active power of the fundamental is predominant over the active power of the higher harmonics.

6.2 Interpretation of the PF expressions

Table 6.1 shows the findings of the analytical investigation. Each row represents a given PF definition and each column represents a condition of the load and the voltages. A comparison across columns allows to compare a given definition under different conditions, whereas a comparison across rows allows to compare

Table 6.1: Analytical expressions for PF definitions under different voltage and load conditions for a delta-connected constant impedance load.

	Balanced Load		Unbalanced Load	
	Balanced Voltages	Unbalanced Voltages	Balanced Voltages	Unbalanced Voltages
$PF_{1,a}$	$\frac{G^e}{\lvert Y^e\rvert}$	$\frac{G^e}{\lvert Y^e\rvert}$	$\frac{g^+}{\lvert y^+\rvert}$	(6.42)
PF_1^a	$\frac{G^e}{\lvert Y^e\rvert}$	$\frac{G^e}{\lvert Y^e\rvert}$	$\frac{3G^e}{\lvert y^+\rvert+\lvert y_b^+\rvert+\lvert y_c^+\rvert}$	(6.49)
PF_1^g	$\frac{G^e}{\lvert Y^e\rvert}$	$\frac{G^e}{\lvert Y^e\rvert}$	$\frac{G^e}{\lvert Y^e\rvert}$	(6.65)
PF_1^+	$\frac{G^e}{\lvert Y^e\rvert}$	$\frac{G^e}{\lvert Y^e\rvert}$	$\frac{G^e}{\lvert Y^e\rvert}$	(6.76)
PF^e	$\frac{G^e}{\lvert Y^e\rvert}$	$\frac{G^e}{\lvert Y^e\rvert}$	$\frac{G^e}{\sqrt{\lvert Y^e\rvert^2+\lvert Y^{-+}\rvert^2}}$	(6.83)

different definitions for a given condition. For conciseness, we refer to the first column as the first with mathematical expressions and likewise to the rows.

Based on the first three columns, it can be observed that if either the load or the voltages are balanced, then all investigated definitions can be rewritten solely in terms of the load's parameters. If both the load and the voltages are unbalanced (see the last column), then the expressions obtained are (non-linear, in case of the general expression) functions of the i) load's admittances, ii) VUF and iii) negative-sequence voltage angle. An exception occurs if the unbalanced load is purely resistive. In this case, PF_1^g is constant and equal to one and PF_1^+ is approximately equal to one.

Comparison of the first column with the third allows to verify what happens when the load becomes unbalanced under balanced voltage supply. It can be observed that the expressions for $PF_{1,a}$, PF_1^a, and PF^e are affected by the load unbalance since their formulas change between the two compared columns. As for PF_1^g and for PF_1^+, it can be observed that their expressions in the third column are equal to those in the first one (remember when the load is balanced $Y = Y^s$).

It is worth mentioning that, in the third column ("Unbalanced Load, Balanced Voltages"), the expressions for $PF_{1,a}$, PF_1^a, and PF^e account for the load unbalance by the presence of the terms $|\mathbf{Y_a^+}|$, $|\mathbf{Y_a^+}|+|\mathbf{Y_b^+}|+|\mathbf{Y_c^+}|$, and $|\mathbf{Y}^{-+}|$, respectively. It can be shown that $|\mathbf{Y}^{-+}|$ is zero when the load is balanced, thus being an indicator of the load unbalance. Although the other two terms are not necessarily zero when the load is balanced, they can be rewritten in order to clearly display their relation to the unbalance. Considering for example $\mathbf{Y_a^+}$ defined by (6.11), adding the null term $\mathbf{Y_{ca}}\boldsymbol{\beta}(1-1)$ and considering that $\boldsymbol{\beta}+\boldsymbol{\beta}^* = 3$ leads to

$$\mathbf{Y_a^+} = 3\mathbf{Y_{ca}} + (\mathbf{Y_{ab}} - \mathbf{Y_{ca}})\boldsymbol{\beta} \tag{6.98}$$

in which it is clear that $(\mathbf{Y_{ab}} - \mathbf{Y_{ca}})$ is always zero when the load is balanced, thus fulfilling the role of accounting (at least partially) for the load unbalance. The same approach can be applied for $|\mathbf{Y_b^+}|$, $|\mathbf{Y_c^+}|$, and then for $|\mathbf{Y_a^+}| + |\mathbf{Y_b^+}| + |\mathbf{Y_c^+}|$.

When the voltages are unbalanced, it is possible to evaluate the effects of the load unbalance in the PF definitions by comparing the second and fourth columns. For example, the effective PF expression changes

from the second to the fourth column, meaning that the effective PF is affected by the load unbalance when the voltages are unbalanced. This can also be confirmed in the last column ("Unbalanced Load, Unbalanced Voltages") since the terms $\mathbf{Y}^{-+}$ and Y^{+-} in (6.83) reflect the load unbalance (*i.e.* they are zero for balanced loads). It is noteworthy that when reduced to balanced voltage conditions, our results related to the effective PF are in agreement with previous results of the literature (see, e.g., [95]). For the general situation of a system with unbalanced voltages, our analysis shows the necessity of considering the extra parameter Y^{+-}, which relates the effect of the negative-sequence voltage in the positive-sequence current.

Still comparing the second and fourth columns, it is possible to verify that the equations in the fourth column for each definition (with the exception of PF_1^g for purely resistive loads) are not the same as in the second column. So, introducing the load unbalance when the voltages are already unbalanced changes the PF expressions computed with each of these five definitions, which is equivalent to say that they account in a way for the load unbalance. This can also be observed in the fourth column ("Unbalanced Load, Unbalanced Voltages") by the presence of the terms $\mathbf{y_a^u}$, $\mathbf{Y^{au}}$, $\mathbf{Y}^{\tau}$, $\mathbf{Y^{ps}}$, and $\mathbf{Y^f}$ related specifically to the load unbalance (as they are zero when the load is balanced).

At last, it should be noted that the voltage unbalance is accounted for by the presence of the VUF in the equations of the column "Unbalanced Load, Unbalanced Voltages". All power factor definitions in this column show that the load unbalance and the VUF are intrinsically combined within each PF definition. As a consequence, an increase of the load unbalance or of the VUF may increase or lower the PF value depending on the negative-sequence voltage angle. Consider, for example, the linearized effective PF (6.88). The term $|\mathbf{Y^f}|/\sqrt{|\mathbf{Y^s}|^2 + |\mathbf{Y}^{-+}|^2}$ increases with the load unbalance. If the sign of $\cos(\phi^- + \varphi^f)$ is negative, then an increase of the load unbalance or the VUF will reduce the effective PF. On the other hand, if $\cos(\phi^- + \varphi^f)$ is positive, then an increase of the load unbalance or the VUF will increase the effective PF, contrary to the common sense of an expected decrease of its value.

Furthermore, the presence of the cosine (which is a function of the negative-sequence angle and an angle due to the load unbalance) term multiplying the VUF in the linearized expressions indicates that the influence of the voltage and load unbalance on the PF value cannot be separated in general even for small values of VUF. In fact, if the VUF and the load unbalance terms appeared in two separate terms adding each other, then it would be possible to segregate and isolate the influence of each component. As this is not the case, the VUF and the load unbalance contributions get inseparably mixed. Considering that the VUF is under the responsibility of the source supplier and that the customer is responsible for the unbalance in the load, one can conclude that none of the investigated definitions allows a clear assignment of the responsibilities for an eventual low PF value when unbalances are present on both the voltages and the load.

Considering the physical meaning of the effective PF as the ratio of the actual power to the maximum power that could be transmitted while keeping the line power loss and the load voltage constant [31, 33, 44, 45, 97], the second term of the linearized equation (6.88) indicates the shared contribution between the customer and the source supplier regarding the increase of transmission losses due to unbalances in the load and voltages. Nonetheless, the individual contributions cannot be easily separated using the effective PF.

6.2.1 Modified PF definitions

Based on the preceding discussion, it can be concluded that any proposition for billing purposes should correctly assign responsibilities, which is not the case with the evaluated definitions. In this sense, we propose that corrected/modified PF definitions should be equal to the first terms of the linearized expressions (6.46), (6.56), (6.69), (6.80), and (6.88). In other words, they should be equal to the following admittance factor (AF) definitions (valid for delta-connected loads).

$$AF_{1,a} = \frac{G_a^+}{|\mathbf{Y_a^+}|} \tag{6.99}$$

$$AF_1^{\mathbf{a}} = \frac{3G^s}{|\mathbf{Y_a^+}| + |\mathbf{Y_b^+}| + |\mathbf{Y_c^+}|} \tag{6.100}$$

$$AF_1^{\mathbf{g}} = AF_1^+ = \frac{G^s}{|\mathbf{Y^s}|} \tag{6.101}$$

$$AF^{\mathbf{e}} = \frac{G^s}{\sqrt{|\mathbf{Y^s}|^2 + |\mathbf{Y^{-+}}|^2}} \tag{6.102}$$

These AFs depend solely on the load's admittances and not on the voltages, thus eliminating the influence of the source quality over the customer's AF. It is worth mentioning that $AF_1^{\mathbf{g}}$ and AF_1^+ account only for the effects of the load's susceptance on the transmission of power, whereas $AF^{\mathbf{e}}$ accounts also for the effects of the load unbalance.

Considering that the loads change over time, one can meter these AFs with the aid of impedance estimation algorithms, such as those proposed in [139, 140]. So, the proposed definitions can be measured and they allow to charge customers based on their sole responsibility.

6.3 Graphical Analysis and Comparison with the Simulation and Experimental Results

We also implemented the obtained general and linearized PF expressions in a computational program to compare the results with those obtained with the simulation and experimental data.

6.3.1 Balanced Constant Impedance Loads

In Section 4.1, after running the computational simulations of 35280 voltage conditions for the balanced constant impedance load, it was observed that all definitions have the same reference value of 1 and they are not affected by the voltage unbalance, that is $PF_{1,a} = PF_1^{\mathbf{g}} = PF_1^{\mathbf{e}} = PF_1^{\mathbf{a}} = PF_1^+ = PF_{\text{ref}} = 1$. Using the expressions obtained from the analytical investigation in Section 6.1, the equivalent admittance is equal to $Y^s = G^s = 0.0556$. Substituting these values in the expression, all PF definitions yield the same value of 1. So, the results of the analytical investigation are in agreement with the results from Section 4.1.

6.3.2 Unbalanced Constant Impedance Loads

For the unbalanced load employed in this work, the following admittance values were obtained

$$\mathbf{Y_a^+} = (\mathbf{Y_b^+})^* = 0.0268 + j0.0155,$$
$$\mathbf{Y^s} = 0.0179,$$
$$\mathbf{Y^{-+}} = (\mathbf{Y^{+-}})^* = 0.0089 + j0.0155.$$

Employing these admittance values, the PF values obtained with the linearized expression of each definition are shown in Table 6.2. As discussed in the analytical development, the variations of the PF when both the load and the source are unbalanced are due to the negative-sequence voltage angle and magnitude. Since the PF definitions are shown to be a function of the VUF and of the cosine of the negative-sequence voltage angle, they have a periodic behavior.

Table 6.2: Summary of the simulation results.

	Balanced Load		Unbalanced Load	
	Balanced Voltages	Unbalanced Voltages	Balanced Voltages	Unbalanced Voltages
$PF_{1,a}$	1	1	0.8660	$[0.8510, 0.8810]$
$PF_1^{\mathbf{a}}$	1	1	0.8660	$[0.8530, 0.8790]$
$PF_1^{\mathbf{g}}$	1	1	1	1
PF_1^{+}	1	1	1	1
$PF^{\mathbf{e}}$	1	1	0.7071	$[0.6859, 0.7283]$

Also using the linearized expressions, it possible to plot the effective PF as function of the negative-sequence voltage magnitude and angle as shown in Figure 6.1. Comparing Figure 6.1 with Figures 6.1 and 5.4, it can be concluded that the linearized equation matches the observed sinusoidal behavior of the simulations and the experimental tests. Additionally, the same behavior is observed for the remaining PF definitions with the exception of $PF_1^{\mathbf{g}}$ and PF_1^{+} when the load is purely resistive.

The linearized equations are also compared with the results obtained from the experimental tests. The mean squared error obtained for the effective PF is approximately 7.64×10^{-7}.

In order to verify the effects of the harmonics on the effective PF, the signed error with respect to the expression 2.72 is computed considering the same unbalanced voltage conditions with and without the harmonics. Figure 6.2 shows the obtained results as a function of the VUF side-by-side. It was observed that without harmonics in the voltage signal, the error is zero when the VUF is zero. As the VUF increases, the signed error decreases, meaning that the actual effective PF is lower than that obtained with the linearized expression. For a VUF equal to 3%, the signed error is close to -3.3×10^{-4}. It is worth mentioning that in many PF billing policies [9, 11, 94] the PF thresholds are defined using only two decimals. So, an error in the order of 10^{-4} should not be very significantly for PF billing purposes. Considering now the case with harmonics, it can be observed that the signed error is worse than it was without harmonics. This means that the harmonics

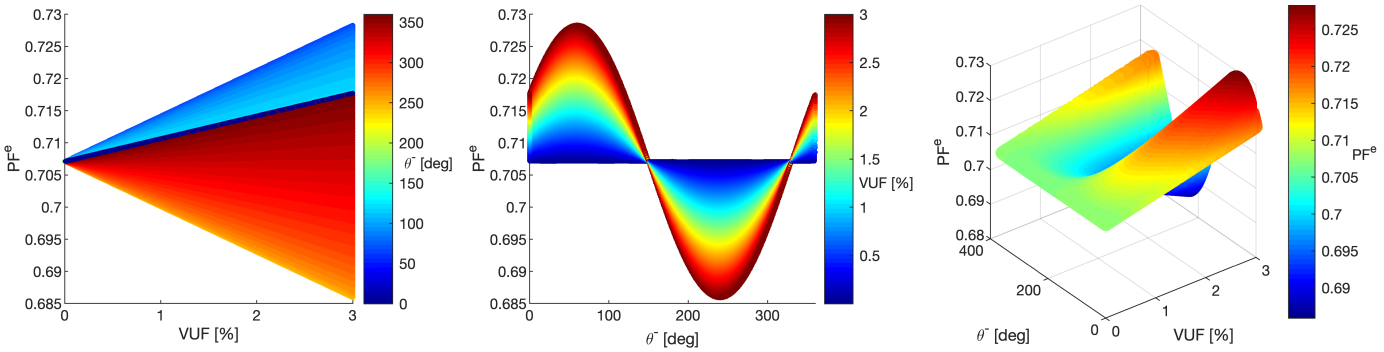

(a) (b) (c)

Figure 6.1: $PF^{\mathbf{e}}$ of the unbalanced resistive load computed by the linearized equation (6.88). (a) 2D plot of $PF^{\mathbf{e}}$ as a function of VUF with the θ^{-} as the colorbar. (b) 2D plot of $PF^{\mathbf{e}}$ as a function of θ^{-} with the VUF as the colorbar. (c) 3D plot of $PF^{\mathbf{e}}$ as a function of VUF and θ^{-} with $PF^{\mathbf{e}}$ as the colorbar.

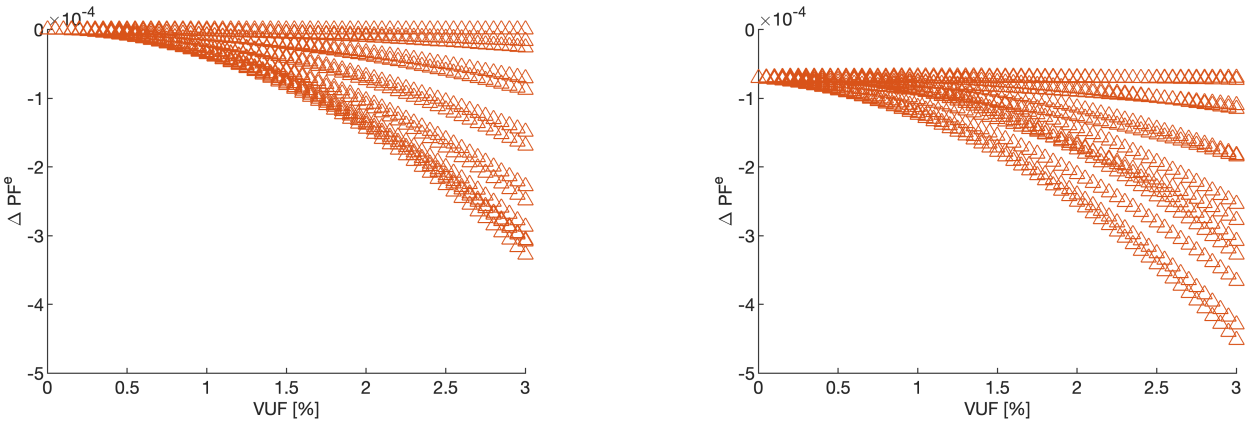

(a) Without harmonics in the voltage signal (THD= 0).

(b) With harmonics in the voltage signal (THD≈ 3.74%).

Figure 6.2: Signed errors of the Taylor series approximation for the effective PF as a function of the VUF.

contribute to lowering the actual effective PF, as the major power flow occurs at the fundamental frequency thus leading to the upper bound shown in (6.96). When the VUF is zero, a signed error of -0.7×10^{-4} is shown. When the VUF is 3%, the signed error is close to -4.5×10^{-4}. Comparing the errors for VUFs of 0% and 3% with and without harmonics, it can also be observed that the harmonics contribute more to the reduction of the signed error when the VUF increases. Nonetheless, the errors are still within the order of 10^{-4}.

Figure 6.3 shows the approximation errors obtained using the linearized equations for all definitions. Comparing the linearized expressions with the general expressions using data from the simulations, it was observed that the highest error (approximately 8×10^{-4}) occurred for $PF_{1,a}$ with the VUF equal to 3%. The second highest error occurred for PF_1^{+} and $PF^{\mathbf{e}}$, followed by $PF_1^{\mathbf{a}}$. The error for $PF_1^{\mathbf{g}}$ was zero since the load is purely resistive. In this condition, the complete and the linearized expressions are both constant and equal to one.

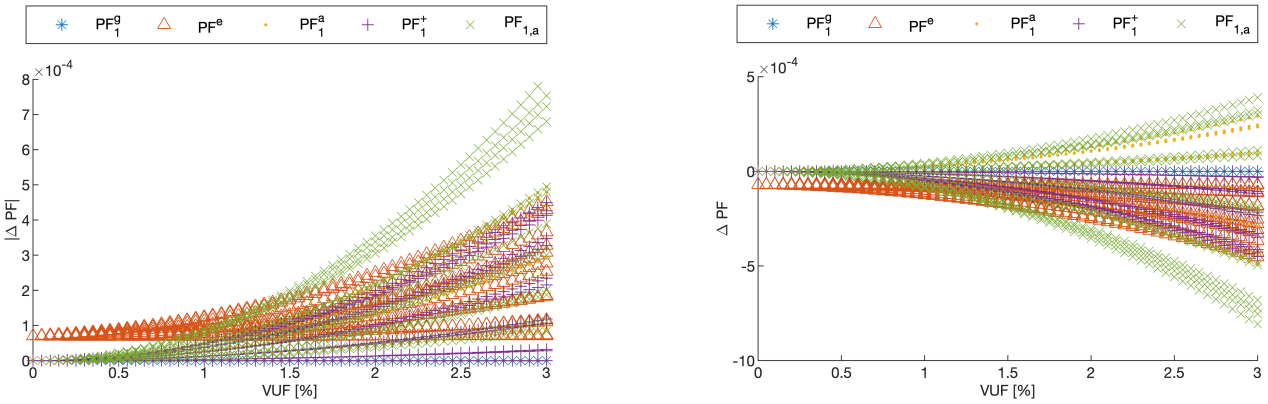

(a) Absolute error.

(b) Signed error.

Figure 6.3: Errors of the Taylor series approximation for each PF definition as a function of the VUF, with THD $\approx 3.74\%$.

6.4 Chapter Remarks

This chapter has evaluated different PF definitions applied to constant impedance loads (balanced and unbalanced) under several unbalanced nonsinusoidal voltage conditions by means of digital simulations and experimental tests. It also presented analytical expressions for each PF definition as a function of the load's admittances and the VUF.

The simulations and experimental tests revealed that, when applied to a balanced constant impedance load, none of the investigated PF definitions are affected by the voltage unbalance. On the other hand, when the load is unbalanced, the fundamental per-phase PF, the fundamental arithmetic PF and the effective PF are significantly affected by the unbalances present in the voltage supply. Only the fundamental geometric and the fundamental positive-sequence PFs were independent of the VUF for the unbalanced resistive load.

The analytical development revealed that actually all investigated PF definitions are non-linear functions of the VUF, the negative-sequence voltage angle (θ^-), and the load's admittances. An exception occurs when the load is purely resistive. In this case the fundamental geometric PF is constant and equal to 1 and the fundamental positive-sequence PF is approximately equal to 1. The non-linear functions were also linearized considering the first two terms of their Taylor's Series. The linearization errors were lower than 8×10^{-4}. The second term of each PF definition approximation also revealed that the contributions of the unbalances in the voltages and loads are intricately connected. They may increase or lower the reference PF (measured under balanced sinusoidal nominal voltages) based on a combination of the negative-sequence voltage angle and the load's parameters. Lastly, we indicated that PF definitions for billing purposes should depend solely on the customer's load, and for this reason we proposed admittance factors that can be employed for billing purposes in substitution to the actual PF definitions.

CHAPTER 7

Conclusions

This work evaluates several PF definitions and their applicable measurement algorithms under several unbalanced and nonsinusoidal voltage conditions, considering the fairness perspective for billing purposes employing computational simulations, experimental tests and analytical developments. Here, the fairness notion is in the sense that the meter (built based on a particular definition and measurement method) under a nonideal supply should lead to very close values as if it was submitted to an ideal balanced sinusoidal nominal supply.

The simulations were performed with Matlab, and they consisted of applying unbalanced nonsinusoidal voltages at the point of connection of the loads represented by their electrical models. This work has evaluated a balanced constant impedance load, an unbalanced constant impedance load, a three-phase induction motor, and an unbalanced non-linear load consisting of a set of light-emitting diode (LED) lamps. The resulting current was applied in the calculation of different PF definitions. Then, a time-domain simulation was performed to assess the accuracy of the PF measurement methods with noiseless and noisy voltage and current signals. Also, experimental tests were executed with a controlled voltage source, a adjustable constant impedance load, a three-phase induction motor, a mechanical load (DC generator and a variable resistor), a computer, and a speed sensor.

Simulations with the balanced constant impedance load showed that all investigated PF definitions (per phase and three-phase) and measurement algorithms yielded fair PF values. On the other hand, simulations with the unbalanced constant impedance load, the induction motor, and the unbalanced non-linear load showed that the values of the per phase and some three-phase PF definitions are significantly affected by unbalanced nonsinusoidal voltages. Therefore, the behavior of each PF definition with respect to voltage variations also depends on the evaluated load.

For the unbalanced constant impedance load, simulations revealed that the fundamental per-phase PF, the fundamental arithmetic PF (PF_1^a), and the effective PF (PF^e) were sensitive to voltage unbalance. Depending

on the negative-sequence voltage angle, the values of the fundamental per-phase PF, PF_1^a, and PF^e were higher or lower than their respective reference values, leading to unfair situations for the utility or the customer, respectively. Additionally, the PF^e was also affected by the voltage harmonic distortion. It was shown that only the fundamental geometric PF (PF_1^g) and the fundamental positive-sequence PF (PF_1^+) had constant values regardless of the voltages and they have the property of being accurately measurable even with simple methods and considering an approximately 14 dB of SNR in the voltage and current signals.

For the motor, at least one of the phases had the fundamental per phase PF lower than the commonly accepted value of 0.92 when the VUF was equal to or greater than 1.5%. It is worth recalling that the European Standard EN 51060 establishes 2% as the upper limit for the VUF. So, if a fundamental per phase PF charging is applied and the VUF is between 1.5% and 2%, customers may be penalized while the utility has no obligation to improve the supply quality. The PF_1^a and the PF^e were also sensitive to voltage unbalance, decreasing with respect to their reference values as the VUF increased. This leads to unfair charges for the customer when the VUF was greater than 2.5%. Only the PF_1^g and the PF_1^+ had stable values for the motor supplied by poor quality voltages and they have the property of being accurately measurable even with simple methods and considering an approximately 14 dB of SNR in the voltage and current signals. It is noteworthy that, since the motor was balanced, linear, and kept constant throughout the simulations, the customer is not responsible for the voltage unbalance and harmonic distortion. In fact, the application of the fundamental per phase PF, or PF_1^a or PF^e for billing purposes can penalize the customer in addition to the issues already caused to the motor by the presence of the voltage unbalance and harmonic distortion.

It was observed that, for the LED lamps, all investigated definitions were affected by V^z, V^+, and V^- in the simulations. Voltage levels (V^+) higher or lower than the nominal may increase or reduce their values with respect to their references. The sensitivity to V^z also implies that they are affected by the choice of the measurement point. It was also shown that the fundamental per-phase PF was the most sensitive, whereas the fundamental geometric and fundamental arithmetic PFs were the least. Nonetheless, none of them are recommended for billing purposes as they may lead to unfair billing scenarios for the utility and the customer.

After analyzing the three different types of loads (constant impedance, three-phase induction motor and LED lamps), the simulations indicate that none of the PF definitions were totally independent of the voltages for all loads. Although the fundamental geometric PF presented the least sensitivity to the voltages in all cases, it does not represent the load unbalance. The fundamental per-phase PF, the fundamental arithmetic and effective PFs accounted for the load unbalance. However, their application to the unbalanced constant impedance load or the unbalanced set of LED lamps may lead to unfair billing scenarios for both the utility and the customer, while their application to the TIM may lead to unfair billing scenarios for the customer.

The experimental results obtained in this work ratified the simulations' results. They showed that the voltage unbalance can reduce the customer's $PF_{1,a}$, PF_1^a, and PF^e to values below the acceptable limits. Therefore, the PF^e definition is not adequate for the scenarios investigated in this work even though it is recommended by IEEE Standard 1459-2010.

At last, Chapter 6 provided, for the delta-connected constant impedance load, the analytical expressions for each PF definition as a function of the load's admittances and the VUF. The obtained equations revealed that actually all investigated PF definitions are non-linear functions of the VUF, the negative-sequence voltage angle (θ^-), and the load's admittances. An exception occurs when the load is purely resistive. In this case

the PF_1^g is constant and equal to 1 and the PF_1^+ is approximately equal to 1. The non-linear functions were also linearized considering the first two terms of their Taylor's Series, resulting in linearization errors were lower than 8×10^{-4}. The first term of each PF approximation is the reference value (also named as the admittance factor) of that definition, depending solely on the load's admittances. The second term revealed that the contributions of the unbalances in the voltages and loads are intricately connected since the factors representing the unbalances appear multiplying each other. If these factors appeared in two separate terms adding up to the PF value, it would be possible to quantify the additive contributions from the load and the source to the variations of that PF. They may increase or lower the reference PF based on a combination of the negative-sequence voltage angle and the load's parameters. As a result, their usage may lead to unfair billing scenarios for both the utility and the customer. Lastly, it is indicated that PF definitions for billing purposes should depend solely on the customer's load, and for this reason it is proposed admittance factors that can be employed for billing purposes in substitution to the actual PF definitions.

This work demonstrated that the behavior of each PF definition depends on the evaluated load. For the delta-connected constant impedance, it was proved that, in general, none of the actual PF definitions are independent of the voltages. The application of these definitions for billing under unbalanced voltage conditions may result in unpredictable and potentially unfair situations for utilities or customers. It is also emphasized that, considering the actual levels and the expected worsening of voltage unbalance and harmonic distortion, there is a pressing need for regulatory agencies to thoroughly investigate and discuss PF definitions and measurement methods. In this sense, it is the author's opinion that the actual use of current PF definitions for billing purposes should be reviewed. The use of the proposed admittance factors (AF) represents a step towards finding the fairest billing index; however, it does not represent a final solution as other types of loads and the effects of the harmonics still require further studies. Given the impracticality of extensively evaluating all the possible loads or considering all different combinations of harmonics, we believe that the study of PF definitions for billing purposes should also be accompanied by the identification of the main loads subjected to PF billing and the most common harmonics presently at the grid.

7.1 Future works

We have discussed the PF billing of a balanced constant impedance load, an unbalanced constant impedance load, an induction motor, and an unbalanced set of light-emitting diode (LED) lamps supplied by unbalanced nonsinusoidal voltages. Simulation and in-laboratory experiments showed that the voltage supply could significantly impact the values of the measured PF depending on the definition used, even if the load remains constant. Additionally, this work presented evidence that a PF definition that leads to fair billing for a given type of load may not provide fair billing for other types. This work did not quantify the customer's influence on the VUF but instead identified the impact of the VUF on PF definitions. It is shown that PF definitions mix the contributions of the customer and the source to the total unbalance without being able to correctly assign responsibilities. For this reason, they are not recommended for studies aiming to pinpoint the customer's influence on the VUF.

A natural continuation of the work is to extend the analytical findings considering other topologies and considering the special case of the TIM with constant speed. The application of the proposed admittance

factors with a method for estimating the load's admittances is also suggested for future works with the TIM, the LED, and other types of loads. The evaluation of PF measurements to systems with different unbalanced nonlinear loads supplied by unbalanced nonsinusoidal voltages is also a possible continuation of this work. Some nonlinear loads, such as the LED, have electric models available in the literature. However, there are some loads which may not have electric models available at the time of evaluation. In this case, it is necessary to conduct experimental tests in order to evaluate the application of PF definitions under different supply conditions.

Bibliography

[1] IEEE. *IEEE Standard 1459-2010 - Definitions for the Measurement of Electric Power Quantities Under Sinusoidal, Nonsinusoidal, Balanced, or Unbalanced Conditions*. 2010. 1–50 p.

[2] IEA. Renewables 2019-Analysis and forecast to 2024. *Int. Energy Agency*, p. 204, 2019. Available from Internet: <https://www.iea.org/reports/renewables-2019>.

[3] IEA. Renewables 2021. *Int. Energy Agency Publ. Int.*, p. 167, 2021. Available from Internet: <www.iea.org/t&c/%0Ahttps://webstore.iea.org/download/direct/4329>.

[4] IEA. Global EV Outlook 2022 Securing supplies for an electric future. 2022. Available from Internet: <www.iea.org/t&c/>.

[5] DULAU, L. I.; BICA, D. Effects of electric vehicles on power networks. *Procedia Manuf.*, IEEE, vol. 46, p. 370–377, 2020. ISSN 23519789.

[6] BALAMURUGAN, K.; SRINIVASAN, D.; REINDL, T. Impact of distributed generation on power distribution systems. *Energy Procedia*, vol. 25, p. 93–100, 2012. ISSN 18766102.

[7] KARIMI, M. et al. Photovoltaic penetration issues and impacts in distribution network - A review. *Renew. Sustain. Energy Rev.*, Elsevier, vol. 53, p. 594–605, 2016. ISSN 18790690.

[8] BAJAJ, M.; SINGH, A. K. Grid integrated renewable DG systems: A review of power quality challenges and state-of-the-art mitigation techniques. *Int. J. Energy Res.*, vol. 44, no. 1, p. 26–69, 2020. ISSN 1099114X.

[9] BRASIL, V. P.; ISHIHARA, J. A. Y.; Ferreira Filho, A. d. L. Fair Power Factor Billing Under Unbalanced and Nonsinusoidal Voltage Supply. *IEEE Access*, vol. 10, p. 19301–19311, 2022. ISSN 2169-3536.

[10] CZARNECKI, L. S. Why the power theory has a limited contribution to studies on the supply and loading quality? In *Int. Conf. Harmon. Qual. Power*. [S.l.: s.n.], 2018. vol. 2018-May, p. 1–6. ISBN 9781538605172. ISSN 21640610.

[11] VIEIRA, D.; SHAYANI, R. A.; OLIVEIRA, M. A. G. de. Reactive Power Billing Under Nonsinusoidal Conditions for Low-Voltage Systems. *IEEE Trans. Instrum. Meas.*, vol. 66, no. 8, p. 2004–2011, aug 2017. ISSN 0018-9456.

[12] CZARNECKI, L. S. What is wrong with the conservative power theory (CPT). *2016 Int. Conf. Appl. Theor. Electr. ICATE 2016 - Proc.*, IEEE, p. 1–6, 2016.

[13] CZARNECKI, L. S.; HALEY, P. M. Power Properties of Four-Wire Systems at Nonsinusoidal Supply Voltage. *IEEE Trans. Power Deliv.*, IEEE, vol. 31, no. 2, p. 513–521, 2016. ISSN 08858977.

[14] CZARNECKI, L. S.; HALEY, P. M. Unbalanced power in four-wire systems and its reactive compensation. *IEEE Trans. Power Deliv.*, vol. 30, no. 1, p. 53–63, 2015. ISSN 08858977.

[15] PETROIANU, A. I. Mathematical representations of electrical power: Vector or complex number? Neither! *Proc. - 2014 Electr. Power Energy Conf. EPEC 2014*, p. 170–177, 2014.

[16] CASTRO-NÚÑEZ, M.; CASTRO-PUCHE, R. Advantages of geometric algebra over complex numbers in the analysis of networks with nonsinusoidal sources and linear loads. *IEEE Trans. Circuits Syst. I Regul. Pap.*, vol. 59, no. 9, p. 2056–2064, 2012. ISSN 15498328.

[17] CASTRO-NÚÑEZ, M.; CASTRO-PUCHE, R. The IEEE standard 1459, the CPC power theory, and geometric algebra in circuits with nonsinusoidal sources and linear loads. *IEEE Trans. Circuits Syst. I Regul. Pap.*, vol. 59, no. 12, p. 2980–2990, 2012. ISSN 15498328.

[18] CZARNECKI, L. S. Working, reflected and detrimental active powers. *IET Gener. Transm. Distrib.*, vol. 6, no. 3, p. 233, 2012. ISSN 17518687.

[19] BERRISFORD, A. J. Smart Meters should be smarter. In *2012 IEEE Power Energy Soc. Gen. Meet.* [S.l.]: IEEE, 2012. p. 1–6. ISBN 978-1-4673-2729-9. ISSN 19449925.

[20] TENTI, P.; PAREDES, H. K. M.; MATTAVELLI, P. Conservative power theory, a framework to approach control and accountability issues in smart microgrids. *IEEE Trans. Power Electron.*, IEEE, vol. 26, no. 3, p. 664–673, 2011. ISSN 08858993.

[21] WILLEMS, J. L. Budeanu's reactive power and related concepts revisited. *IEEE Trans. Instrum. Meas.*, vol. 60, no. 4, p. 1182–1186, 2011. ISSN 00189456.

[22] ORTS-GRAU, S. et al. New resolution of the unbalance power according to Std. 1459. *IEEE Trans. Power Deliv.*, vol. 25, no. 1, p. 341–350, 2010. ISSN 08858977.

[23] PAJIC, S.; EMANUEL, A. E. Effect of neutral path power losses on the apparent power definitions: A preliminary study. *IEEE Trans. Power Deliv.*, vol. 24, no. 2, p. 517–523, 2009. ISSN 08858977.

[24] SALMERÓN, P.; HERRERA, R. S. Instantaneous reactive power theory—A general approach to polyphase systems. *Electr. Power Syst. Res.*, Elsevier, vol. 79, no. 9, p. 1263–1270, 2009.

[25] LEV-ARI, H.; STANKOVIĆ, A. M. Instantaneous power quantities in polyphase systems - A geometric algebra approach. *2009 IEEE Energy Convers. Congr. Expo. ECCE 2009*, p. 592–596, 2009.

[26] MORSI, W. G.; EL-HAWARY, M. E. A New Fuzzy-Based Representative Quality Power Factor for Nonsinusoidal Situations. *IEEE Trans. Power Deliv.*, vol. 23, no. 2, p. 1007–1014, 2008.

[27] MORSI, W. G.; EL-HAWARY, M. E. A new fuzzy-based representative quality power factor for unbalanced three-phase systems with nonsinusoidal situations. *IEEE Trans. Power Deliv.*, vol. 23, no. 4, p. 2426–2438, 2008. ISSN 08858977.

[28] CASTILLA, M. et al. Clifford theory: A geometrical interpretation of multivectorial apparent power. *IEEE Trans. Circuits Syst. I Regul. Pap.*, vol. 55, no. 10, p. 3358–3367, 2008. ISSN 10577122.

[29] MENTI, A.; ZACHARIAS, T.; MILIAS-ARGITIS, J. Geometric algebra: A powerful tool for representing power under nonsinusoidal conditions. *IEEE Trans. Circuits Syst. I Regul. Pap.*, vol. 54, no. 3, p. 601–609, 2007. ISSN 10577122.

[30] AKAGI, H.; WATANABE, E. H.; AREDES, M. *Instantaneous Power Theory and Applications to Power Conditioning*. Hoboken, NJ, USA: John Wiley & Sons, Inc., 2007. 41–107 p. ISBN 9780470118931. Available from Internet: <http://doi.wiley.com/10.1002/9781119307181.ch2 http://dx.doi.org/10.1002/9780470118931.ch3>.

[31] PAJIC, S.; EMANUEL, A. E. Modern Apparent Power Definitions: Theoretical Versus Practical Approach—The General Case. *IEEE Trans. Power Deliv.*, vol. 21, no. 4, p. 1787–1792, oct 2006. ISSN 0885-8977.

[32] JEON, S. J. Definitions of apparent power and power factor in a power system having transmission lines with unequal resistances. *IEEE Trans. Power Deliv.*, vol. 20, no. 3, p. 1806–1811, 2005. ISSN 08858977.

[33] WILLEMS, J. L.; GHIJSELEN, J. A.; EMANUEL, A. E. The apparent power concept and the IEEE standard 1459-2000. *IEEE Trans. Power Deliv.*, vol. 20, no. 2 I, p. 876–884, 2005. ISSN 08858977.

[34] DAI, X.; LIU, G.; GRETSCH, R. Generalized theory of instantaneous reactive quantity for multiphase power system. *IEEE Trans. Power Deliv.*, IEEE, vol. 19, no. 3, p. 965–972, 2004. ISSN 08858977.

[35] WILLEMS, J. L. Reflections on apparent power and power factor in nonsinusoidal and polyphase situations. *IEEE Trans. Power Deliv.*, vol. 19, no. 2, p. 835–840, 2004. ISSN 08858977.

[36] CZARNECKI, L. S. On Some Misinterpretations of the Instantaneous Reactive Power p - q Theory. *IEEE Trans. POWER Electron.*, vol. 19, no. 3, p. 828–836, 2004.

[37] EMANUEL, A. E. Summary of IEEE Standard 1459: Definitions for the Measurement of Electric Power Quantities Under Sinusoidal, Nonsinusoidal, Balanced, or Unbalanced Conditions. *IEEE Trans. Ind. Appl.*, vol. 40, no. 3, p. 869–876, 2004. ISSN 0093-9994.

[38] CZARNECKI, L. S. Comparison of instantaneous reactive power p-q theory with theory of the current's physical components. *Electr. Eng.*, vol. 85, no. 1, p. 21–28, 2003. ISSN 09487921.

[39] HUGHES, M. Electric power measurements-a utility's perspective. In *IEEE Power Eng. Soc. Summer Meet.* [S.l.]: IEEE, 2003. vol. 3, no. 1, p. 1680–1681. ISBN 0-7803-7518-1.

[40] WILLEMS, J. L.; GHIJSELEN, J. A. Apparent power and power factor concepts in unbalanced and nonsinusoidal situations. *2003 IEEE Bol. PowerTech - Conf. Proc.*, vol. 3, no. 3, p. 412–418, 2003.

[41] WU, C. J. et al. Power Factor Definitions and Effect on Revenue of Electric Arc Furnace Load. In *Int. Conf. Power Syst. Technol.* [S.l.: s.n.], 2002. p. 93–97. ISBN 0780374592.

[42] YOON, W.-k. K.; DEVANEY, M. J. Reactive Power Measurement Using the Wavelet Transform. *IEEE Trans. Instrum. Meas.*, vol. 49, no. 2, p. 246–252, 2000. ISSN 00189456.

[43] CZARNECKI, L. S. Energy flow and power phenomena in electrical circuits: Illusions and reality. *Electr. Eng.*, vol. 82, no. 3, p. 119–126, 2000. ISSN 09487921.

[44] EMANUEL, A. E. Apparent power definitions for three-phase systems. *IEEE Trans. Power Deliv.*, vol. 14, no. 3, p. 767–772, 1999. ISSN 08858977.

[45] EMANUEL, A. E. The Buchholz-Goodhue apparent power definition: The practical approach for nonsinusoidal and unbalanced systems. *IEEE Trans. Power Deliv.*, vol. 13, no. 2, p. 344–348, 1998. ISSN 08858977.

[46] YOON, W. K.; DEVANEY, M. J. Power Measurement Using the Wavelet Transform. *IEEE Trans. Instrum. Meas.*, vol. 49, no. 2, p. 246–252, 1998. ISSN 00189456.

[47] VLADIMIRTERZIJA, V.; LAZAREVIC, Z.; POPOV, M. Active and reactive power metering in nonsinusoidal conditions using newton type algorithm. *Int. Conf. . . .*, vol. 1, no. 1, p. 2–6, 1997. Available from Internet: <http://www.icrepq.com/full-paper-icrep/265-terzija.pdf>.

[48] CRISTALDI, L.; FERRERO, A. Mathematical foundations of the instantaneous power concepts: An Algebraic Approach. *Eur. Trans. Electr. Power*, vol. 6, no. 5, p. 305–309, 1996. ISSN 1430144X. Available from Internet: <http://doi.wiley.com/10.1002/etep.4450060503>.

[49] SHARON, D. Power factor definitions and power transfer quality in nonsinusoidal situations. *IEEE Trans. Instrum. Meas.*, IEEE, vol. 45, no. 3, p. 728–733, jun 1996. ISSN 00189456. Available from Internet: <http://ieeexplore.ieee.org/document/494589/>.

[50] PENG, F. Z.; LAI, J.-S. Generalized instantaneous reactive power theory for three-phase power systems. *IEEE Trans. Instrum. Meas.*, IEEE, vol. 45, no. 1, p. 293–297, 1996.

[51] DEPENBROCK, M. The FBD-Method, a generally applicable tool for analyzing power relations. *IEEE Trans. Power Syst.*, vol. 8, no. 2, p. 381–387, 1993. ISSN 15580679.

[52] EMANUEL, A. E. On the definition of power factor and apparent power in unbalanced polyphase circuits with sinusoidal voltage and currents. *IEEE Trans. Power Deliv.*, vol. 8, no. 3, p. 841–852, 1993. ISSN 19374208.

[53] WILLEMS, J. L. A new interpretation of the Akagi-Nabae power components for nonsinusoidal three-phase situations. *IEEE Trans. Instrum. Meas.*, IEEE, vol. 41, no. 4, p. 523–527, 1992.

[54] CZARNECKI, L. S. Scattered and Reactive Current, Voltage, and Power in Circuits with Nonsinusoidal Waveforms and Their Compensation. *IEEE Trans. Instrum. Meas.*, vol. 40, no. 3, p. 563–574, 1991. ISSN 15579662.

[55] CZARNECKI, L. S.; SWIETLICKI, T. Powers in Nonsinusoidal Networks : Their Interpretation, Analysis, and Measurement. *IEEE Trans. Instrum. Meas.*, vol. 39, no. 2, p. 340–345, 1990.

[56] CZARNECKI, L. S. Orthogonal decomposition of the currents in a 3-phase nonlinear asymmetrical circuit with a nonsinusoidal voltage source. *IEEE Trans. Instrum. Meas.*, IEEE, vol. 37, no. 1, p. 30–34, 1988.

[57] CZARNECKI, L. S. What is Wrong with the Budeanu Concept of Reactive and Distortion Power and Why It Should be Abandoned. *IEEE Trans. Instrum. Meas.*, IEEE, IM-36, no. 3, p. 834–837, 1987. ISSN 15579662.

[58] DAI, X.; TANG, T. Definition and Properties of Reactive Quantity in Non Sinusoidal Non Linear Systems. In *Proc. 2nd Int. Conf. Harmon. Power Syst. Winnipeg, MB, Canada.* [S.l.: s.n.], 1986. p. 381–388.

[59] CZARNECKI, L. S. Considerations on the Reactive Power in Nonsinusoidal Situations. *IEEE Trans. Instrum. Meas.*, IEEE, vol. 34, no. 3, p. 399–404, sep 1985. ISSN 15579662.

[60] AKAGI, H.; KANAZAWA, Y.; NABAE, A. Instantaneous reactive power compensators comprising switching devices without energy storage components. *IEEE Trans. Ind. Appl.*, IEEE, no. 3, p. 625–630, 1984.

[61] KUSTERS, N.; MOORE, W. On the Definition of Reactive Power Under Non-Sinusoidal Conditions. *IEEE Trans. Power Appar. Syst.*, IEEE, PAS-99, no. 5, p. 1845–1854, sep 1980. ISSN 0018-9510.

[62] PAGE, C. H. Reactive Power in Nonsinusoidal Situations. *IEEE Trans. Instrum. Meas.*, vol. 29, no. 4, p. 420–423, dec 1980. ISSN 0018-9456.

[63] EMANUEL, A. E. et al. Suggested definition of reactive power in nonsinusoidal systems and Reactive-power definitions and power-factor improvement in nonlinear systems. *Proc. Inst. Electr. Eng.*, The Institution of Electrical Engineers, vol. 121, no. 7, p. 705, jul 1974. ISSN 00203270.

[64] NEDELCU, V.; SHEPHERD, W.; ZAKIKHANI, P. Suggested definition of reactive power for nonsinusoidal systems - Discussion. *Proc. Inst. Electr. Eng.*, The Institution of Electrical Engineers, vol. 121, no. 5, p. 389, may 1974. ISSN 00203270.

[65] SHARON, D. Reactive-power definitions and power-factor improvement in nonlinear systems. *Proc. Inst. Electr. Eng.*, The Institution of Electrical Engineers, vol. 120, no. 6, p. 704–706, jun 1973. ISSN 00203270.

[66] MICU, E.; SHEPHERD, W.; ZAKIKHANI, P. Suggested definition of reactive power for nonsinusoidal systems - Discussion. *Proc. Inst. Electr. Eng.*, The Institution of Electrical Engineers, vol. 120, no. 7, p. 796–798, jul 1973. ISSN 00203270.

[67] SHARON, D.; SHEPHERD, W.; ZAKIKHANI, P. Suggested definition of reactive power for nonsinusoidal systems - Discussion. *Proc. Inst. Electr. Eng.*, The Institution of Electrical Engineers, vol. 120, no. 1, p. 108, jan 1973. ISSN 00203270.

[68] SHEPHERD, W.; ZAKIKHANI, P. Suggested definition of reactive power for nonsinusoidal systems. *Proc. Inst. Electr. Eng.*, The Institution of Electrical Engineers, vol. 119, no. 9, p. 1361–1362, sep 1972. ISSN 00203270.

[69] FRYZE, S. Active reactive and apparent power in circuits with nonsinusoidal voltage and current. *Elektrotechnische Zeitschrift*, vol. 53, no. 25, p. 596–599, 1932.

[70] BUCHHOLZ, F. Die drehstrom-scheinleistung bei ungleichmassiger belastung der drei zweige. *Licht und Kraft*, vol. 2, p. 9–11, 1922.

[71] WALLAU, H. L. Polyphase Power Factor. *Trans. Am. Inst. Electr. Eng.*, XXXIX, no. 2, p. 1475–1476, jul 1920. ISSN 0096-3860.

[72] Special Joint Committee. Power Factor in Polyphase Circuits. *Trans. Am. Inst. Electr. Eng.*, XXXIX, no. 2, p. 1449–1450, jul 1920. ISSN 0096-3860.

[73] LINCOLN, P. M. Polyphase Power Factor. *Trans. Am. Inst. Electr. Eng.*, XXXIX, no. 2, p. 1477–1479, jul 1920. ISSN 0096-3860.

[74] HOLTZ, F. C. Polyphase Power Factor. *Trans. Am. Inst. Electr. Eng.*, XXXIX, no. 2, p. 1451–1455, jul 1920. ISSN 0096-3860.

[75] SILSBEE, F. B. Power Factor in Polyphase Systems. *Trans. Am. Inst. Electr. Eng.*, XXXIX, no. 2, p. 1465–1467, jul 1920. ISSN 0096-3860.

[76] TORCHIO, P. Polyphase Power Factor and Unbalanced Loads. *Trans. Am. Inst. Electr. Eng.*, XXXIX, no. 2, p. 1489–1490, jul 1920. ISSN 0096-3860.

[77] FORTESCUE, C. L. Polyphase Power Representation by Means of Symmetrical Coordinates. *Trans. Am. Inst. Electr. Eng.*, XXXIX, no. 2, p. 1481–1484, jul 1920. ISSN 0096-3860. Available from Internet: <http://ieeexplore.ieee.org/document/4765340/>.

[78] EVANS, R. D. Measurement of Power Factor on Unbalanced Polyphase Circuits. *Trans. Am. Inst. Electr. Eng.*, XXXIX, no. 2, p. 1485–1487, jul 1920. ISSN 0096-3860.

[79] BURT, A. Three-Phase Power-Factor. In *25th Annu. Conv. Am. Inst. Electr. Eng.* [S.l.: s.n.], 1908. p. 801–814.

[80] STEINMETZ, C. P. *theory calculation of alternating current phenomena.* 3rd. ed. [S.l.]: Electrical World and Engineer, 1900. 547 p.

[81] STEINMETZ, C. P.; KAISER, G. Does phase displacement occur in the current of electric arcs? (Translation by G. Kaiser). *ETZ*, vol. 587, p. 1–3, 1892. Available from Internet: <http://arxiv.org/abs/1602.06868>.

[82] SILVA, R. P. B. da. *Analysis of electronic loads on electrical measurements, power quality and billing.* 194 p. Tese (Doctoral Thesis) — Unicamp em cotutela com a SDU, 2012.

[83] GNACINSKI, P. Windings temperature and loss of life of an induction machine under voltage unbalance combined with over-or undervoltages. *IEEE Trans. Energy Convers.*, vol. 23, no. 2, p. 363–371, 2008. ISSN 0885-8969.

[84] WANG, Y.-J. Analysis of effects of three-phase voltage unbalance on induction motors with emphasis on the angle of the complex voltage unbalance factor. *IEEE Trans. Energy Convers.*, vol. 16, no. 3, p. 270–275, 2001. ISSN 08858969.

[85] KERSTING, W. H.; PHILLIPS, W. H. Phase frame analysis of the effects of voltage unbalance on induction machines. *IEEE Trans. Ind. Appl.*, vol. 33, no. 2, p. 415–420, 1997. ISSN 00939994.

[86] FAIZ, J.; EBRAHIMPOUR, H.; PILLAY, P. Influence of unbalanced voltage on the steady-state performance of a three-phase squirrel-cage induction motor. *IEEE Trans. Energy Convers.*, vol. 19, no. 4, p. 657–662, 2004. ISSN 08858969.

[87] DONOLO, P. et al. Voltage unbalance and harmonic distortion effects on induction motor power, torque and vibrations. *Electr. Power Syst. Res.*, vol. 140, p. 866–873, 2016. ISSN 03787796.

[88] SINGH, G. K. A research survey of induction motor operation with non-sinusoidal supply wave forms. *Electr. Power Syst. Res.*, vol. 75, no. 2-3, p. 200–213, 2005. ISSN 03787796.

[89] FORTESCUE, C. L. Power , Reactive Volt-Amperes , Power Factor. In *North East. Dist. Meet. A.I.E.E.* Schenectady, N. Y.: [s.n.], 1933. p. 5.

[90] CURTIS, H. L.; SILSBEE, F. B. Definitions of Power and Related Quantities. *Trans. Am. Inst. Electr. Eng.*, vol. 54, no. 4, p. 394–404, apr 1935. ISSN 0096-3860.

[91] EMANUEL, A. E. Powers in nonsinusoidal situations-a review of definitions and physical meaning. *IEEE Trans. Power Deliv.*, vol. 5, no. 3, p. 1377–1389, jul 1990. ISSN 08858977.

[92] FILIPSKI, P. Polyphase apparent power and power factor under distorted waveform conditions. *IEEE Trans. Power Deliv.*, IEEE, vol. 6, no. 3, p. 1161–1165, jul 1991.

[93] SASDELLI, R.; MENCHETTI, A.; MONTANARI, G. C. Power definitions for power-factor correction under nonsinusoidal conditions. *Measurement*, vol. 13, no. 4, p. 289–296, 1994. ISSN 02632241.

[94] AZIZ, M. M. A.; EL-ZAHAB, E. E. A.; ZOBAA, A. F. Power factor and your electrical utility bill in Egypt. *IEEE Trans. Power Deliv.*, vol. 18, no. 4, p. 1567–1568, 2003. ISSN 0885-8977. Available from Internet: <https://ieeexplore.ieee.org/document/1234721>.

[95] CZARNECKI, L. S. Power related phenomena in three-phase unbalanced systems. *IEEE Trans. Power Deliv.*, vol. 10, no. 3, p. 1168–1176, 1995. ISSN 19374208.

[96] JEON, S. J. Considerations on a reactive power concept in a multiline system. *IEEE Trans. Power Deliv.*, vol. 21, no. 2, p. 551–559, 2006. ISSN 08858977.

[97] EMANUEL, A. E. Apparent and reactive powers in three-phase systems: In search of a physical meaning and a better resolution. *Eur. Trans. Electr. Power*, Wiley-Blackwell, vol. 3, no. 1, p. 7–14, sep 2007. ISSN 1430144X. Available from Internet: <http://doi.wiley.com/10.1002/etep.4450030103>.

[98] FACCIO, M.; GAMBERI, M. Energy saving in case of intermittent production by retrofitting service plant systems through inverter technology: A feasibility study. *Int. J. Prod. Res.*, Taylor & Francis, vol. 52, no. 2, p. 462–481, jan 2014. ISSN 00207543. Available from Internet: <http://www.tandfonline.com/doi/abs/10.1080/00207543.2013.832840>.

[99] MBULI, N.; PRETORIUS, J. H. Some considerations for designing a reactive power charge. *Asia-Pacific Power Energy Eng. Conf. APPEEC*, IEEE, p. 1–4, 2012. ISSN 21574839.

[100] HYDRO, B. C.; AUTHORITY, P.; BC-HYDRO. Electric Tariff. p. 184, 2017. Available from Internet: <http://www.bchydro.com/electric_tariff>.

[101] HYDRO-QUEBEC. *Electricity Rates*. 2019. 180 p.

[102] Essential Servicces Commission. *Victorian Electricity Distribution Code*. Melbourne, Australia: [s.n.], 2018. 1–47 p. Available from Internet: <https://www.esc.vic.gov.au/electricity-and-gas/codes-guidelines-policies-and-manuals/electricity-distribution-code>.

[103] Ergon Energy. *Network Tariff Guide*. 2019. 61 p. Available from Internet: <https://www.ergon.com.au/__data/assets/pdf_file/0011/757874/EE-Network-Tariff-Guide-2019-20.pdf>.

[104] State of Queensland. *Queensland Electricity Regulation*. 2006. 127 p. Available from Internet: <https://www.commerce.wa.gov.au/sites/default/files/atoms/files/waer_july_2008.pdf>.

[105] SYNERGY. *Standard Electricity Prices and Charges*. 2019. 16 p. Available from Internet: <https://www.synergy.net.au/-/media/Files/PDF-Library/Standard_Electricity_Prices_Charges_brochure.pdf>.

[106] Government of Western Australia; SAFETY, D. o. C. E. *Western Australia Electrical Requirements*. 2008. 72 p. Available from Internet: <https://www.commerce.wa.gov.au/sites/default/files/atoms/files/waer_july_2008.pdf>.

[107] Southern Electric Power Distribution plc. *SEPD DUoS Charging Statements 2020/21*. 2020. 67 p. Available from Internet: <https://www.ssen.co.uk/Library/ChargingStatements/SEPD/>.

[108] Southern Electric Power Distribution plc. *Statement of methodology and charges for connection to Southern Electric Power Distribution plc's electricity distribution system*. 2019. 137 p. Available from Internet: <https://www.ssen.co.uk/Library/ChargingStatements/SEPD/>.

[109] Office of Gas and Electricity Markets. *The Distribution Code of Licensed Distributions Network Operators of Great Britain*. 2019. 177 p. Available from Internet: <http://www.dcode.org.uk/http://www.dcode.org.uk/assets/files/dcode-pdfs/DCode_v42_01092019.pdf>.

[110] Scottish Power Energy Networks. *Use of System Charging Statement*. 2020. 51 p. Available from Internet: <https://www.scottishpower.com/userfiles/file/SPD_LC14_Statement_2020.pdf>.

[111] Scottish Power Energy Networks. *Methodology Statement Detailing The Basis of SP Distribution's Use of System Charges*. 2007. 28 p. Available from Internet: <https://www.scottishpower.com/userfiles/document_library/C4StatementUoSMethodologySPDistributionApril200

[112] ANEEL, A. N. d. E. E. *PRODIST MÓDULO 1*. 2018.

[113] Agência Nacional de Energia Elétrica. *Resolução Normativa Nº 414/2010*. 2010. 205 p.

[114] Agência Nacional de Energia Elétrica. *Manual de Controle Patrimonial do Setor Elétrico (MCPSE)*. 2015. 219 p.

[115] PAREDES, H. K. M. *Teoria de potência conservativa: uma nova abordagem para o controle cooperativo de condicionadores de energia e considerações sobre a atribuição de responsabilidades*. Tese (Doctoral thesis) — Universidade Estadual de Campinas, Campinas, SP, mar 2011. Available from Internet: <https://repositorio.unicamp.br/Busca/Download?codigoArquivo=467571>.

[116] KUKAČKA, L. et al. Review of AC power theories under stationary and non-stationary, clean and distorted conditions. *IET Gener. Transm. Distrib.*, vol. 10, no. 1, p. 221–231, 2016. ISSN 17518687.

[117] STEINMETZ, C. P.; KAISER, G. Does a phase shift occur in an AC arc? p. 1–3, 2018. Available from Internet: <http://arxiv.org/abs/1602.06868>.

[118] BUDEANU, C. I. Puissances réactives et fictives. Institut Romain de I'Energte. Bucharest. *Romania*, 1927.

[119] CZARNECKI, L. S. Measurement Principle of a Reactive Power Meter for Nonsinusoidal Systems. *IEEE Trans. Instrum. Meas.*, IEEE, IM-30, no. 3, p. 209–212, 1981. ISSN 15579662.

[120] FILIPSKI, P.; LABAJ, P. Evaluation of reactive power meters in the presence of high harmonic distortion. *IEEE Trans. Power Deliv.*, vol. 7, no. 4, p. 1793–1799, oct 1992. ISSN 08858977.

[121] FILIPSKI, P. The Measurement of Distortion Current and Distortion Power. *IEEE Trans. Instrum. Meas.*, vol. 33, no. 1, p. 36–40, 1984. ISSN 15579662.

[122] BUCHHOLZ, F. *Das Begriffssystem Rechtleistung, Wirkleistung, totale Blindleistung*. [S.l.]: Selbstverl.;[Lachner in Komm], 1950.

[123] DEPENBROCK, M. *Investigations of the voltage and power conditions at converters without Energy Storage*. Tese (Doutorado) — Phd thesis, Thecnical University of Hannover, Hannover, Germany, 1962.

[124] NICOLAE, P. M.; NICOLAE, I. D.; NICOLAE, M. S. Powers and Power Factor in Non-Sinusoidal and Non-Symmetrical Regimes in Three-Phase Systems. *Energies*, vol. 15, no. 14, 2022. ISSN 19961073.

[125] FORTESCUE, C. L. Method of symmetrical co-ordinates applied to the solution of polyphase networks. *Trans. Am. Inst. Electr. Eng.*, vol. 37, p. 1027–1140, 1918. ISSN 00963860.

[126] CATALIOTTI, A.; COSENTINO, V.; NUCCIO, S. The measurement of reactive energy in polluted distribution power systems: An analysis of the performance of commercial static meters. *IEEE Trans. Power Deliv.*, vol. 23, no. 3, p. 1296–1301, 2008. ISSN 08858977.

[127] HART, D. G.; NOVOSEL, D.; SMITH, R. A. *MODIFIED COSINE FILTERS*. 2000. 12 p.

[128] LANGELLA, R.; TESTA, A. A new algorithm for energy measurement at positive sequence of fundamental power frequency, under unbalanced non-sinusoidal conditions. In *2007 IEEE Lausanne POWERTECH, Proc.* [S.l.: s.n.], 2007. p. 1558–1563. ISBN 9781424421909.

[129] CATALIOTTI, A.; COSENTINO, V. A time-domain strategy for the measurement of IEEE standard 1459-2000 power quantities in nonsinusoidal three-phase and single-phase systems. *IEEE Trans. Power Deliv.*, vol. 23, no. 4, p. 2113–2123, 2008. ISSN 08858977.

[130] CATALIOTTI, A.; COSENTINO, V.; NUCCIO, S. A Virtual Instrument for the Measurement of IEEE Std. 1459-2000 Power Quantities. *IEEE Trans. Instrum. Meas.*, vol. 57, no. 1, p. 85–94, 2008.

[131] IRAVANI, M. R.; KARIMI-GHARTEMANI, M. Online estimation of steady state and instantaneous symmetrical components. *IEE Proc. - Gener. Transm. Distrib.*, vol. 1, no. 5, 2003.

[132] The Math Works Inc. Natick, M. A. . *MATLAB R2017a Student License*. [S.l.].

[133] GONZALEZ-CORDOBA, J. L. et al. Correlation Model between Voltage Unbalance and Mechanical Overload Based on Thermal Effect at the Induction Motor Stator. *IEEE Trans. Energy Convers.*, vol. 32, no. 4, p. 1602–1610, 2017. ISSN 08858969.

[134] TOLIYAT, H. A.; KLIMAN, G. B. *Handbook of Electrical Motors*. Second. [S.l.]: Taylor \& Francis Group, LCC, 2004. 791 p. ISBN 9780824741051.

[135] MOLINA, J. et al. LED lamp modelling for harmonic studies in distribution systems. *IET Gener. Transm. Distrib.*, vol. 11, no. 4, p. 1063–1071, 2017. ISSN 17518687.

[136] ZAIDI, S. K. A. et al. Design and implementation of low cost electronic prepaid energy meter. *IEEE INMIC 2008 12th IEEE Int. Multitopic Conf. - Conf. Proc.*, IEEE, p. 548–552, 2008.

[137] KUSLJEVIC, M. D. A simultaneous estimation of frequency, magnitude, and active and reactive power by using decoupled modules. *IEEE Trans. Instrum. Meas.*, IEEE, vol. 59, no. 7, p. 1866–1873, 2010. ISSN 00189456.

[138] BAZRAFSHAN, M.; GATSIS, N. Comprehensive Modeling of Three-Phase Distribution Systems via the Bus Admittance Matrix. *IEEE Trans. Power Syst.*, IEEE, vol. 33, no. 2, p. 2015–2029, 2018. ISSN 08858950.

[139] WU, T. F. et al. Load impedance estimation and iterative-learning control for a three-phase four-wire inverter. *2013 IEEE ECCE Asia Downunder - 5th IEEE Annu. Int. Energy Convers. Congr. Exhib. IEEE ECCE Asia 2013*, no. 3, p. 1275–1281, 2013.

[140] WU, T. F. et al. Three-phase four-leg voltage source inverter with load impedance estimation and D-Σ digital control. *2017 IEEE 3rd Int. Futur. Energy Electron. Conf. ECCE Asia, IFEEC - ECCE Asia 2017*, p. 1106–1113, 2017.

APPENDIX

I.0. TRIGONOMETRIC IDENTITIES

Identity 1 *[Sum of cosines]*

Consider the following complex numbers

$$\begin{aligned}\mathbf{a} &= |a|\underline{\angle\alpha} \\ \mathbf{b} &= |b|\underline{\angle\beta} \\ \mathbf{c} = \mathbf{a} + \mathbf{b} &= |c|\underline{\angle\chi}.\end{aligned}$$

It can be shown that

$$|a|\cos(x+\alpha) + |b|\cos(x+\beta) = |c|\cos(x+\chi) \tag{I.1}$$

where x is any given angle. It can also be shown that if

$$\mathbf{d} = \mathbf{a} + \mathbf{b}^* = |d|\underline{\angle\delta}$$

then

$$|a|\cos(x+\alpha) + |b|\cos(x-\beta) = |d|\cos(x+\delta).$$

Identity 2 *[Sum of sines]*

Consider the following complex numbers

$$\begin{aligned}\mathbf{a} &= |a|\underline{\angle\alpha} \\ \mathbf{b} &= |b|\underline{\angle\beta} \\ \mathbf{c} = \mathbf{a} + \mathbf{b} &= |c|\underline{\angle\chi}.\end{aligned}$$

It can be shown that

$$|a|\sin(x+\alpha) + |b|\sin(x+\beta) = |c|\sin(x+\chi) \tag{I.2}$$

where x is any given angle.

II.0. DESCRIPTION OF SOME POWER THEORIES

II.1 Fryze's Definitions

Seeking to define power components under nonsinusoidal conditions, Fryze proposed in [69] that the current drawn from the load can be decomposed as

$$i(t) = i_A(t) + i_N(t) \tag{II.1}$$

where

$$i_A(t) = Gv(t) \tag{II.2}$$

is the active current, G is a conductance and

$$i_N(t) = i(t) - i_A(t) \tag{II.3}$$

is the nonactive or *wattless* current (or *Blindstrom*, in German, hence the usage of the subscript "b" in some papers). Notice that $i_A(t)$ is parallel to the voltage $v(t)$. The term parallel here regards the function space. In this sense, it means the current is equal to the voltage multiplied by a scaling factor. Since $i_N(t)$ is the compliment of $i_A(t)$, it is orthogonal to the voltage and does not contribute to the active power. The orthogonality of $i_N(t)$ and $v(t)$ implies that their inner product

$$< i_N(t), v(t) >= \int i_N(t)v(t)dt \tag{II.4}$$

is equal to zero. So, the active power can be simply computed by

$$P = \frac{1}{kT}\int_{\tau}^{\tau+kT} i_A(t)v(t)dt \tag{II.5}$$

or, in terms of RMS values,

$$P = VI_A. \tag{II.6}$$

Fryze noticed that since the active and nonactive currents are orthogonal to each other, the current RMS value can be rewritten as

$$I^2 = I_A^2 + I_N^2 \tag{II.7}$$

where I_A is the RMS value of the active current and I_N is the RMS value of the nonactive current.

In order to define the reactive power, Fryze employed the apparent power (S_N) given by

$$S_N = VI. \tag{II.8}$$

Applying (II.7) in (II.8) and taking the squared values yields

$$S_N^2 = P^2 + Q_N^2 \tag{II.9}$$

in which P is the active power, and

$$Q_N = VI_N \tag{II.10}$$

is Fryze's reactive power, which sometimes can be called nonactive power (N). It is noteworthy that this generalization of the reactive power does not account only for the phase shift between voltage and current but also for all phenomena that increase V or I without increasing P. As a result, Q_n does not provide much information about which phenomena are at play, hindering the job of compensating Q_n.

It is important to notice that Fryze's works focused on defining active and reactive powers, while the PF was not directly addressed. As a result, the term "Fryze's power factor" is not very common in literature. Nevertheless, this definition is found on commercial meters [19]. Fryze's power factor PF_R is given by

$$PF_R = \frac{P}{S_N}. \tag{II.11}$$

II.2 Budeanu's Power Theory

Budeanu's power theory also adopts the same definition for apparent power as Fryze, but tries to decompose S_N into components associated with distinct phenomena aiming to facilitate the compensation of S_N. Here, the set H is restricted to ν integers that represent the fundamental and the harmonic components of voltage and current. Taking into account the trigonometric identity $\cos(\alpha)^2 + \sin(\alpha)^2 = 1$, the squared RMS value of the current $i_h(t)$ can be rewritten as

$$I_h^2 = [I_h \cos(\theta_h)]^2 + [I_h \sin(\theta_h)]^2 \tag{II.12}$$

in which θ_h is the current and voltage phase shift in the h^{th} order. Applying (II.12) in (2.10), the squared RMS current can be rewritten as

$$I^2 = \sum_{h=1}^{\nu} [I_h \cos(\theta_h)]^2 + [I_h \sin(\theta_h)]^2 . \tag{II.13}$$

The squared apparent power is given by

$$S_N^2 = \sum_{h=1}^{\nu} V_h^2 \left\{ \sum_{h=1}^{\nu} [I_h \cos(\theta_h)]^2 + [I_h \sin(\theta_h)]^2 \right\}, \tag{II.14}$$

and can be regrouped as

$$S_N^2 = \sum_{h=1}^{\nu} V_h^2 \sum_{h=1}^{\nu} [I_h \cos(\theta_h)]^2 + \sum_{h=1}^{\nu} V_h^2 \sum_{h=1}^{\nu} [I_h \sin(\theta_h)]^2 . \tag{II.15}$$

Considering Lagrange's identity

$$\sum_{h=1}^{\nu} A_h^2 \sum_{h=1}^{\nu} B_h^2 = \left(\sum_{h=1}^{\nu} A_h B_h \right)^2 + \sum_{m=1}^{\nu-1} \sum_{n=m+1}^{\nu} (A_m B_n - A_n B_m)^2 , \tag{II.16}$$

the apparent power results in

$$\begin{aligned} S_N^2 = &\left[\sum_{h=1}^{\nu} V_h I_h \cos(\theta_h) \right]^2 + \left[\sum_{h=1}^{\nu} V_h I_h \sin(\theta_h) \right]^2 \\ &+ \sum_{m=1}^{\nu-1} \sum_{n=m+1}^{\nu} \left\{ [V_m I_n \cos(\theta_n) - V_n I_m \cos(\theta_m)]^2 + [V_m I_n \sin(\theta_n) - V_n I_m \sin(\theta_m)]^2 \right\}. \end{aligned} \tag{II.17}$$

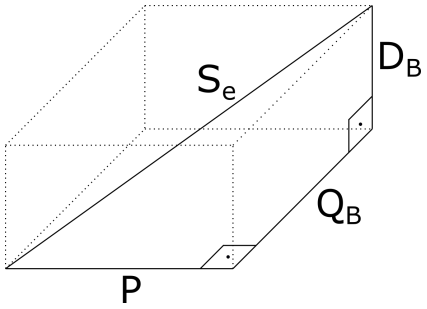

Figure II.1: Budeanu's PT parallelepiped

The last term can be further simplified using the following trigonometric identities

$$[V_m I_n \cos(\theta_n)]^2 + [V_m I_n \sin(\theta_n)]^2 = (V_m I_n)^2 \tag{II.18}$$

$$V_m V_n I_m I_n [\cos(\theta_n)\cos(\theta_m) + \sin(\theta_n)\sin(\theta_m)] = V_m V_n I_m I_n \cos(\theta_m - \theta_n). \tag{II.19}$$

Therefore, the final expression for the squared apparent power is

$$S_N^2 = P^2 + Q_B^2 + D_B^2, \tag{II.20}$$

in which P is the active power,

$$Q_B = \sum_{h=1}^{\nu} V_h I_h \sin(\theta_h) \tag{II.21}$$

is Budeanu's reactive power, and

$$D_B = \sum_{m=1}^{\nu-1} \sum_{n=m+1}^{\nu} \left[(V_m I_n)^2 + (V_n I_m)^2 - 2 V_m V_n I_m I_n \cos(\theta_m - \theta_n) \right] \tag{II.22}$$

is Budeanu's distortion power.

It is noteworthy that P, Q_B, and D_B are orthogonal, allowing the construction of a parallelepiped to represent the components of Budeanu's power theory (PT), as shown in Figure II.1.

Similarly to the works of Fryze, Budeanu focused on defining active and reactive powers, while the PF was not directly addressed. However, it is possible to define the PF based on Budeanu's power theory as

$$PF_B = \frac{P}{\sqrt{P^2 + Q_B^2}}. \tag{II.23}$$

Although the term 'Budeanu's power factor" is not very common in literature, some commercial meters employ PF_B [19].

Notice that Fryze's power factor, given in (II.11), can also be rewritten in terms of Q_B and D_B as

$$PF_R = \frac{P}{\sqrt{P^2 + Q_B^2 + D_B^2}}. \tag{II.24}$$

II.3 Shepherd Power Theory

reference [68] proposes a new decomposition of the apparent power in which

$$S_R = \sqrt{\sum_{n\in N} E_n^2 \sum_{n\in N} I_n^2 \cos^2\phi_n} \neq P^2 \tag{II.25}$$

is the active apparent power,

$$S_X = \sqrt{\sum_{n\in N} E_n^2 \sum_{n\in N} I_n^2 \sin^2\phi_n} \tag{II.26}$$

is the true reactive apparent power, and

$$S_D = \sqrt{\sum_{n\in N} E_n^2 \sum_{p\in P} I_p^2 + \sum_{m\in M} E_m^2 \left(\sum_{n\in N} I_n^2 + \sum_{p\in P} I_p^2\right)} \tag{II.27}$$

is the distortion power. N, M, and P are the sets of frequency components present in both the current and voltage signals, in the voltage signal only, and in the current signal only, respectively. In other words, the voltage and current can be rewritten as

$$e(t) = \sum_{n\in N} \sqrt{2}E_n \sin\left(n\omega t + \alpha_n\right) + \sum_{m\in M} \sqrt{2}E_m \sin\left(m\omega t + \alpha_m\right) \tag{II.28}$$

$$i(t) = \sum_{n\in N} \sqrt{2}I_n \sin\left(n\omega t + \alpha_n + \phi_n\right) + \sum_{p\in P} \sqrt{2}I_p \sin\left(p\omega t + \alpha_p + \phi_p\right). \tag{II.29}$$

The authors also discuss the components of apparent power drawn by the loads, whether S_X can be completely compensated with passive elements, the maximum power factor for the minimum S_X realizable with passive elements and the power theoretical value if S_X is zero. The discussion accounts for all possible combinations of sinusoidal and nonsinusoidal voltage supply with linear and nonlinear loads.

It is worth mentioning that publication of [68] was followed by three discussion papers criticizing that S_R, S_X, and S_D are mathematical quantities without any physical meaning [64,66,67]. Additionally, reference [67] points out that minimization of S_X leads to the maximum power factor realizable if the compensation is done with **only** passive linear energy-storage devices. According to [67], compensation of the power factor to unit is possible with nonlinear and/or active circuits. Reference [66] emphasizes the importance of correctly measuring the proposed quantities, which in that time was not possible. The practical importance of power definitions is subject to the creation of accurate measurement methods, according to [66]. Shepherd and Zakikhani in response to Micu [66] stated that "In particular, if a customer has a lagging-power-factor load and distorted supply voltage, the calculation of tariff based on the arbitrary value Q" [Budeanu's reactive power] "results in that customer receiving a free portion of his reactive-power consumption". At last, in [64] it is highlighted that [68] is restricted to balanced (or single-phase) systems, lacking a generalization to unbalanced three-phase systems.

II.4 Sharon Power Theory

In 1973, Sharon examined the "true reactive apparent power" (S_X) as defined by [68]. He showed that capacitor compensation may lead to an increase of S_X instead of reducing it because the harmonics that were

originally restricted to the voltage signal (belonging to the set M) now appear in the current signal as a result of their flow through the shunt impedance (belonging now to the set N). To address the impacts of new harmonics, reference [65] proposed

$$S_Q = V_{\text{RMS}} \sqrt{\sum_{n \in N} I_n^2 \sin^2 \phi_n} \tag{II.30}$$

as the definition for reactive power, accounting for all voltage harmonics (sets N and M) instead of only those present in both voltage and current signals (set N). The authors also propose a "complimentary reactive power" (S_C) that accounts for the cross-frequency reactive effects of the in-phase components of the harmonic currents in the N group, and the harmonic currents in the P group. It is shown that shunt compensation leads to the minimization of S_Q while not affecting the active power P and S_C; leading therefore to a better power factor. At last, the authors comment that defining reactive power is not indispensable for power factor improvement, since the value of the capacitor (C) for shunt compensation can be obtained through the minimization of the apparent power with respect to C. It is worth mentioning that the paper is restricted to balanced (or single-phase) systems.

II.5 Kusters and Moore Power Theory

In [61], the authors present a measurement instrument and claim that the proposed definitions "provide the operator with a direct indication of whether the reactive power can be reduced, by what means, and by how much." These definitions are based on the decomposition of the current into four likewise components, having the source voltage as a reference. The inductive/capacitive reactive current (I_{QL}/I_{QC}) component is an equivalent current that would flow through an inductor/capacitor submitted to the reference voltage. The residual inductive/capacitive reactive current (I_{QLr}/I_{QCr}) is the component that remains of the current after the active current and I_{QL}/I_{QC} components have been extracted. The paper also proposes an inductive frequency ω_L and a capacitive frequency ω_C. These fictitious frequencies allow representing the system by means of the equivalent impedances $Z_{\text{eq},L} = \omega_L L$ or $Z_{\text{eq},C} = 1/\omega_C C$. The proposed definitions are employed in three examples to identify whether the current RMS value can be reduced, by what means, and by how much. In the first, an inductor is supplied by nonsinusoidal voltages. The second and third examples consider a semi-conductor switched (thyristor-based) resistive load. Sinusoidal voltages are considered in the second examples, whereas nonsinusoidal voltages are considered in the third example Considering that in weak grids (with source impedance not equal to zero), nonlinear loads produce nonsinusoidal currents which in turn cause nonsinusoidal voltages in the system, the choice of the nonsinusoidal voltage as a reference to propose decompositions may not be the best choice. Whether the fundamental voltage is a better choice remains to be investigated. The effects of the source impedance should also be addressed.

II.6 Czarnecki's Current Physical Components (CPC) Power Theory

Reference [59] examines existing power definitions, such as those proposed in [61, 62, 68]. The author proposes the scattering power (D_S) and the Czanercki's reactive power (Q_Z) to decompose the apparent power. Additionally, the author shows that D_s establishes a link between the proposed definitions and those

proposed by Fryze [69] and Shepherd [68]. Mathematically,

$$D_S = \sqrt{\sum_{n\in N} V_n^2}\sqrt{\sum_{n\in N} (G_n - G_e)^2 V_n^2}, \tag{II.31}$$

$$Q_Z = \sqrt{\sum_{n\in N} V_n^2}\sqrt{\sum_{n\in N} B_n^2 V_n^2}, \tag{II.32}$$

where V_n, G_n, and B_n are the voltage RMS value, the load conductance and the load susceptance at frequency order n, respectively. G_e is the load "equivalent" conductance. In the proposed decomposition, the scattering power refers to the part of the apparent power caused by the difference between the load's "equivalent" conductance (G_e) and the actual harmonic conductance (G_n) at the harmonic order n. This power cannot be compensated by passive devices. Czarnecki's reactive power on the other hand, refers to the apparent power component caused by the phase shift between voltage and current at each harmonic order. This component can be compensated by passive devices.